10-2003

Identification of dynamic properties of materials for the Nuclear Waste Package

Brendan O'Toole
University of Nevada, Las Vegas, brendan.otoole@unlv.edu

Mohamed Trabia
University of Nevada, Las Vegas, mbt@me.unlv.edu

Amy J. Smiecinski
University of Nevada, Las Vegas, smiecins@unlv.nevada.edu

TECHNICAL REPORT

IDENTIFICATION OF DYNAMIC PROPERTIES OF MATERIALS FOR THE NUCLEAR WASTE PACKAGE

Prepared for the U.S. DOE/UCCSN Cooperative Agreement
Number: DE-FC08-98NV12081

Task 24

Document ID: TR-02-007
Revision: 0

Originator: [redacted] 9/30/03
Dr. Brendan O'Toole, Investigator, Mechanical Engineering Department

Approvals:

[redacted]
Dr. Mohamed Trabia, Principal Investigator — 9/30/03 Date

[redacted]
Dr. Mohamed Trabia, Technical Reviewer — 9/30/03 Date

[redacted]
Amy Smiecinski, QA Manager, UCCSN — 10-1-03 Date

TABLE OF CONTENTS

LIST OF TABLES

LIST OF FIGURES

ABSTRACT

Stainless steel 316L, titanium alloy grade 7, and alloy C22 are currently under consideration as candidate materials for use in various components associated with the spent nuclear fuel package, which must be designed to withstand structural deformation caused by static, thermal, and handling loads. In addition, it has to maintain its integrity in case of accidents, where it may be subjected to high loads over a very short period of time. Mechanical characteristics of these three materials under dynamic loading are not well documented. This paper describes the procedures and results obtained from experiments performed over a range of slow and moderate strain rates in the range of 0.0001 sec^{-1} – 200 sec^{-1}. An MTS servohydraulic system was used for the slower tests and an Instron/Dynatup instrumented drop weight impact machine was used for the faster experiments. Experiments were conducted at room temperature, 175 ^{O}F, and 350 ^{O}F. Results show that the yield strength, ultimate strength, failure strain, and percentage of area reduction depend on strain rate and temperature to varying degrees for all three candidate materials.

INPUT

This report was created based on quality assured technical data. The qualification status of the data can be verified by using the Data Tracking Numbers in the Technical Data Management System.

- Results Of Tensile Testing Of Alloy C22 And Steel316L Under Various Strain Rates In MTS Environmental Chamber With Data Tracking Number: MO0307UCC024BO.002.
- Tensile Testing Data For Titanium Grade 7, Stainless Steel 316L And Alloy 22 Under Impact Loading In Instron Environmental Chamber At Room And Elevated Temperatures With Data Tracking Number: Data Not Yet Incorporated Into YMP TDMS

Stainless Steel 316L

- Results Of Tensile Testing Of Stainless Steel 316l Under Various Strain Rates With Data Tracking Number: Mo0205ucc024kz.020.
- Mts Tensile Test Results For Stainless Steel 316l Specimens Under Tensile Loading In The Mts Environmental Chamber At Elevated Temperature (175 °F And 350 °F) With Data Tracking Number: Mo0306ucc024hw.002.
- Mts Test Results For Steel 316l Under Low Strain Rate Tensile Testing (Batch #1) With Data Tracking Number: Un0110spa024mt.006.
- Mts Tensile Test Results For Steel 316l Under High Strain Rate Loading (Batch #2) With Data Tracking Number: Un0110spa024mt.007.
- Mts Tensile Test Results Of Steel 316l Under High Strain Rate Loading (Batch #3) With Data Tracking Number: Un0110spa024mt.008.
- Instron Tensile Test Results For Stainless Steel 316l Under Moderate Strain Rate, Specimen 10s With Data Tracking Number: Un0201spa024mt.014.
- Instron Tensile Test Results For Stainless Steel 316l Under Moderate Strain Rate, Specimen 12s With Data Tracking Number: Un0201spa024mt.015.
- Instron Tensile Test Results For Stainless Steel 316l Under Moderate Strain Rate, Specimen 15s With Data Tracking Number: Un0201spa024mt.016.
- Instron Tensile Test Results For Stainless Steel 316l Under Moderate Strain Rate, Specimen 20s With Data Tracking Number: Un0201spa024mt.017.
- Instron Dynatup Tensile Test Results For Stainless Steel 316l Specimens Under Impact Loading In The Machine Environmental Chamber Under Room And Elevated Temperatures (175 °F And 350 °F) With Data Tracking Number: Mo0306ucc024sd.003.

Alloy C22

- Results Of Tensile Testing Of Alloy C22 Under Various Strain Rates With Data Tracking Number: Mo0205ucc024kz.019.
- Mts Tensile Test Results For C22 Alloy Specimens Under Tensile Loading In The Mts Environmental Chamber At Room Temperature And Elevated Temperature (175 °F) With Data Tracking Number: Mo0306ucc024hw.001.
- Mts Tensile Test Results Of Alloy C22 Under Low Strain Rate Loading (Batch #1) With Data Tracking Number: Un0110spa024mt.009.

- Mts Tensile Test Results Of Alloy C22 Under High Strain Rate Loading (Batch #2) With Data Tracking Number: Un0110spa024mt.010.
- Mts Tensile Test Results Of Alloy C22 Under High Strain Rate Loading (Batch #3) With Data Tracking Number: Un0110spa024mt.011.
- Instron Tensile Test Results For Alloy C22 Under Moderate Strain Rate (Batch #4) With Data Tracking Number: Un0201spa024mt.012.
- Instron Tensile Test Results For Alloy C22 Under Moderate Strain Rate (Batch #5) With Data Tracking Number: Un0201spa024mt.013.
- Mts Tensile Test Results For Alloy C22 Under Low Strain Rate (Batch #6) With Data Tracking Number: Un0201spa024mt.018.
- Instron Dynatup Tensile Test Results For Alloy C22 Specimens Under Impact Loading In The Machine Environmental Chamber Under Room And Elevated Temperatures (175 F And 350 F) With Data Tracking Number: Mo0306ucc024sd.002.

Titanium Alloy Grade 7

- Results Of Tensile Testing Of Titanium Alloy Grade 7 Under Various Strain Rates With Data Tracking Number: Mo0205ucc024kz.021.
- Batch #1 Mts Test Results For Titanium Grade 7 Under Low Strain Rate Tensile Testing With Data Tracking Number: Un0109spa024mt.001.
- Batch #2 Mts Test Results For Titanium Grade 7 Under Low Strain Rate Tensile Testing With Data Tracking Number: Un0109spa024mt.002.
- Batch #3 Mts Test Results For Titanium Grade 7 Under Low Strain Rate Tensile Testing With Data Tracking Number: Un0109spa024mt.003.
- Batch #4 Instron Dynatup Tensile Test Results For Titanium Grade 7 Under Impact Loading With Data Tracking Number: Un0109spa024mt.004.
- Batch #5 Instron Dynatup Tensile Test Results For Titanium Grade 7 Under Impact Loading With Data Tracking Number: Un0109spa024mt.005.
- Instron Dynatup Test Results For Titanium Grade 7 Under Impact Loading In The Machine Environmental Chamber Under Room And Elevated Temperature With Data Tracking Number: Mo0302ucc024sd.001.

CHAPTER 1

INTRODUCTION

The nuclear waste package is designed to transport and store different types of nuclear waste. According to the Reference Design Description for a Geologic Repository [1], the nuclear waste package should be designed to contain uncanistered spent nuclear fuel, canistered spent nuclear fuel, and high-level radioactive waste. It is obvious that reduction of integrity of the package at any stage of transportation or storage can be very harmful to anyone in the vicinity of the package as well as for the environment. Therefore, the waste container should be able to withstand loads caused by impact in accidents. The objective of the project is to improve understanding of this phenomenon by experimentally studying the tensile mechanical properties of candidate materials of the nuclear waste package under impact loading.

1.1 Background

Materials loaded at high strain rates can exhibit mechanical characteristics that are different from those obtained under quasi-static loading. Material scientists observed this fact in the early 19^{th} century [2]. Effects of this type of loading on a number of material properties were investigated and documented throughout a number of years of research. The remainder of this paragraph is based on the historical introduction of Harding et al. [3]. Hopkinson in 1905 and Mason in 1934 performed some of the earliest work in this field. Both researchers applied tensile pulses to wires using a falling tup. Ginns carried one of the first research works that attempted to record a dynamic stress-strain curve out in 1937. The setup of his experiment included a spring mechanism that applied an instant load and a resistance-pressure gauge that measured the stress. Later, Brown and Vincent in 1941 obtained load-elongation curves using a pendulum-type impact machine and piezoelectric crystals to measure stress. At that stage, one of the following two methods was used to measure stress. First, the computed stress was based on the principles of the elastic wave propagation theory and thus was limited to the elastic region of material behavior. Second, the stress was measured using a type of semi-mechanical stress measuring mechanism. This approach often led to obtaining data with large stress oscillations. In 1940, however, Fanning and Bassett developed impact strain gauges. Brown and Edmonds applied this method to the pendulum-type impact machine of Brown and Vincent in 1948. They were able to record tensile stress-time pulses, which did not have any distortion from stress oscillations produced in the stress measuring head. While Brown and Edmonds were only interested in comparing yield strengths of materials under static and dynamic loading, Warnock and Taylor in 1949 developed a technique to produce dynamic stress-strain curves using a repeated impact method. At the same time Kolsky introduced the Split Hopkinson Pressure bar (SHPB) apparatus, which made it possible to reach strain rates between 100 and 1000 sec^{-1}. In Kolsky's original setup, a detonator was used to launch compressive waves. Apart form the early works of Hopkinson and Mason, most investigators had ignored the effect of stress wave propagation in the specimen, assuming that the stress measured at the end of the specimen was equivalent to the stress throughout the specimen. Guest, in 1930, stated that stress waves within the test apparatus were responsible for significant errors in the results. This was proven in 1948, when Clark and Duwez applied the theory of plastic wave propagation to the results of earlier tensile tests. In 1949, Clark and Wood offered a design of new testing equipment that used a pneumatic load drive. This new approach allowed reaching maximum loads in a matter of 5 milliseconds and

obtained results that were almost free from the effects of wave propagation within the apparatus.

These early steps of the problem development established the basis of understanding of material properties under high strain rates. However, they did not offer a systematic approach of testing for the whole range of strain rates. Lack of this information significantly limited use of material characteristics under dynamic loading by mechanical designers. In 1980, the National Materials Advisory Board recommended an iterative procedure for design of weapons that incorporated dynamic testing of material properties and computer modeling [2]. The procedure relied on test firings of weapons followed by a refined design. The process continued till the design objectives were obtained. The following reasons necessitated the expensive approach:

1. Dynamic material failure was inadequately understood;
2. There was a lack of accurate dynamic material response properties;
3. It was unclear whether existing dynamic testing techniques were appropriate.

The inability of failure analysis techniques to differentiate between improper design, misuse, and manufacturing defects has resulted in a growing need for the use of appropriate dynamic testing techniques to determine product liability. All the different available techniques of impact testing were later summarized along with conditions of their appropriate applications [2]. This work recommended several experimental methods for different strain rates, which can be defined as the rate of strain, $\dot{\varepsilon}$, with respect to time, t:

$$\dot{\varepsilon} = \frac{d\varepsilon}{dt} \tag{1-1}$$

where, ε can represent either engineering or true strain. The strain rate is measured in units of 1/sec. It was suggested that standard mechanical testing procedures are well suited for low strain rate testing:

$$\dot{\varepsilon} < 0.1 \text{ sec}^{-1}$$

For such low strain rates, effects of wave propagation are not significant. The next range of tensile testing is characterized by the medium strain rates,

$$0.1 \text{sec}^{-1} \leq \dot{\varepsilon} \leq 200 \text{ sec}^{-1}.$$

Servo-hydraulic frames with high-capacity valves, cam plastometer, or drop test machines can be used to conduct testing within this range. Wave propagation has some affect on the load measurements. A Split Hopkinson pressure bar is required for strain rates of,

$$200 \text{ sec}^{-1} \leq \dot{\varepsilon} \leq 10^5 \text{ sec}^{-1}$$

Propagation of stress waves at strain rates of this magnitude can have significant effect on the measurement of loads. More sophisticated equipment, such as the flyer plate impact technique, is needed for higher strain rates of:

$$\dot{\varepsilon} \geq 10^5 \text{ sec}^{-1}$$

1.2 Methods Of Material Testing Under Dynamic Loading

A number of different testing systems are currently used for dynamic materials testing. As stated in the previous section, standard tensile testing machines have been successfully used for material testing under low strain rates. A typical tensile testing machine, presented in Figure 1-1, consists of two heads (3) that are equipped with clamping mechanisms, which are used to grip a

specimen (5). The driving mechanism could be mechanical (power screw) or hydraulic. Usually, the lower clamping head is attached to the base (4) while the upper head is attached to a sliding bar (2), which leads it along the guides (1).

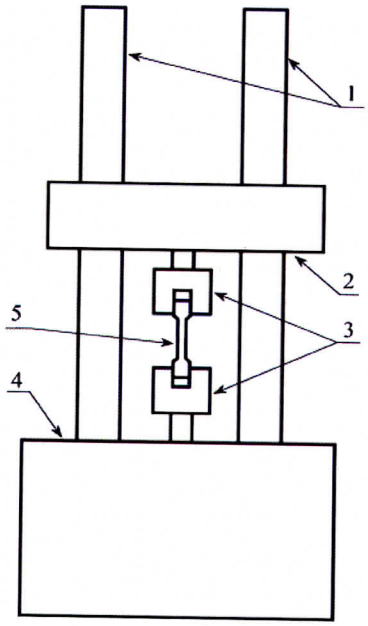

Figure 1-1 General Tensile Testing Machine Setup

Medium strain rates can be obtained using drop weight or pendulum testing machines. Drop-weight tower impact testing machines have been successfully used in the automobile industry. This testing machine is usually used for puncture tests of plate specimens. A typical drop weight tower-testing machine shown in Figure 1-2 consists of two major parts:

a. Fixture for holding the specimen (4) that is attached to a base (5),
b. Tup (1) that slides along guides (3), which is used for the impact loading of the specimens.

The tup mass can be varied to meet different conditions of impact loading. The tup and an attached striker (2) are raised to the desirable height and then released to impact the specimen. Load cells could be positioned either in the stationary part or on the tup. This type of testing equipment is used to measure several variables including maximum fracture load, amount of absorbed energy, displacement in the fracture zone and velocities of the striker.

Testing at strain rates higher than 200 sec^{-1} requires the use of SHPB. The most typical setup of the equipment for tensile testing as shown in Figure 1-3 includes a threaded specimen (4) and a split shoulder or collar (5) to protect the specimen from initial pre-compression. After the specimen has been screwed into the bars (2, 3), the collar (5) is placed over the specimen, and the specimen is screwed in until the pressure bars fit tightly against the shoulder. The shoulder is made of the same material as the pressure bars. It has the same outer diameter as the bars, and it has an inner diameter that just clears the specimen. When the input bar (2) is struck by a striker (1) the input compressive wave is transmitted almost entirely through the collar to bar (3). When this compressive pulse reaches the free and of the transmitter bar, it is reflected as a tensile pulse.

This tensile pulse is used to load the specimen, since the collar is unable to sustain any tensile load. Each of the testing techniques described above have their advantages and limitations as can be seen in the next section, which reviews relevant previous research.

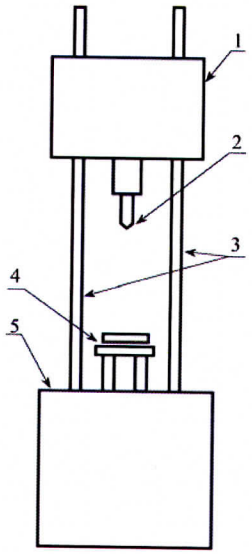

Figure 1-2 General Drop Weight Tower Impact Machine Setup

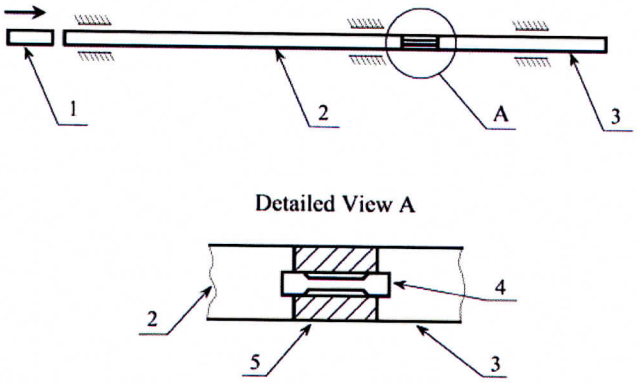

Figure 1-3 General SHPB Impact Tensile System Setup

1.3 Disadvantages Of The Current Methods

The results of tensile tests conducted on traditional tensile testing machines could be affected by a number of different parameters that influence the actuator speed. First, the speed of an unloaded actuator can be much higher than that of a loaded one. Second, machines with a long working range achieve the desired velocity after a considerably longer distance of travel, which may lead to situations when the maximum strain is reached before the actuator attains the desired velocity. This means that material is tested at a significantly lower strain rate. Third, since the ability to control speed is a function of the response capability of a servo-controlled machine working in a closed-loop mode, open-loop machines provide speeds that may be affected by strength of a specimen and cannot easily reproduce predetermined velocities or strain rates on

materials with different yield strengths or strain-hardening behaviors [2]. Although it is believed that at strain rates up to 100 sec^{-1}, the elastic wave propagation does not have a considerable effect on the load-displacement reading, there are indications that the data may display large oscillations [4]. This problem was addressed by stating that only mean values of load waves were considered.

Drop weight impact testing has been successfully used for impact testing of materials. Although the technique is considerably different from the one discussed above, it proved to be a quick and inexpensive alternative of conducting dynamic impact tests of relatively small test specimens [5, 6]. Despite its wide application for plate testing and compression testing of materials, it has rarely been used for tensile testing. To carry out a tensile test under high strain rate, the machine should incorporate a special holding fixture. Thus for example in [7], an experiment of tensile bolt testing is carried out using a drop weight impact test machine which incorporates a fixture with four bolts loaded simultaneously in tension. Presented results reviewed strain rate change and elongation of the specimens sighting increase in elongation of bolt shanks with increase of the energy of the impact. It was also pointed out that the strain varies over time and this variation decreases for experiments with higher energy input. Besides a need for an additional specimen support fixture, another big problem is that a drop weight tower testing machine does not necessarily take into account wave propagation that influences the results at high strain rates.

The Split Hopkinson Pressure Bar (SHPB) apparatus proved to be a fairly reliable and accurate technique of impact material testing in tension and compression. Despite SHPB method's wide acceptance, this approach is not free from various disadvantages. It was pointed out early on that there was no equilibrium condition in the tested sample during the first few microseconds. The data corresponding to that region should be considered unreliable [8]. Another research work stated that for small strains, the relation between specimen strain and displacement is nonlinear [9]. Using this method, it is virtually impossible to determine Young's modulus of elasticity. According to the same source, Split Hopkinson bar results can only be used to obtain flow stress data outside of the elastic region. This goes in agreement with another publication where the author noticed that the slope of the stress-strain curve in the elastic region was anomalously low [10]. Data in this region may be invalid because stress equilibrium has not yet been achieved in the specimen.

Other research has suggested a number of additional limitations of the technique. SHPB is based on the one-dimensional theory of wave propagation [11]. The average stress and strain in the specimen are obtained from incident, reflected and transmitted stress pulses, and it is assumed that the stresses and strains are the same throughout the specimen. This assumption neglects the effect of axial inertia on the specimen. This conclusion agrees with earlier research work stating that a small specimen will approach a uniform strain distribution mode in a short time [8]. Using the same assumption of uniform strain distribution throughout the gage length, the true stress and strain can be calculated. However, if localized deformation (necking) takes place, the local stress and strain can be obtained only be measuring the change of length of the small region and assuming a state of uniform strain [8]. The author also stated that if the rate of loading is increased greatly, at any instant of time the load reading at the load cell might be different from the load carried by the specimen. Validity of the uniform strain distribution assumption is in question since strain distribution can also vary within the gage length because of finite rate of stress and strain propagation [8]. A detailed analysis of the wave reflections and interaction in the plastically deformed specimen is difficult and complex. Modification of the

SHPB apparatus along with incorporating fast speed photographic equipment was addressed in a different work. The tests using synchronized camera yield satisfactory results but the data handling became very complicated [12]. On the other hand, a different technical paper [13], stated that although it is possible to get the true strain rate of some materials, providing the total elongation of the specimen is sufficient to permit the measurement of diametral changes during the "necking down" phase. This is impossible if the "necking down" phase is absent.

Another research work [14] offered an explanation of the mechanism of the wave propagation through the specimen by using finite element analysis. The author showed that the strain rate increases suddenly at one end of the specimen upon the arrival of the impact wave to it. As time increases, the peak of local strain wave continues to propagate along the axis of the specimen. Once the wave reaches the other end of the specimen it is partially reflected, which in turn affects the strain distribution throughout the specimen. Strain distribution may be made more uniform if the mass of the hammer is increased

Tensile testing of the materials at high impact rates has other factors that can affect the quality of the results of the experiment. In 1960, Harding identified eccentricity of loading and indeterminate gauge length as some of them [3]. Finally, the operation of the tester and the interpretation of the records require a thorough understanding of the mechanical and electrical systems involved. This, unfortunately, prevents the SHPB from becoming a simple routing test.

1.4 Material Behavior Under High Strain Rates

A number of publications offer numerous results on the identification of mechanical properties of materials under high strain rates. Using prestressed loading, a number of stress-strain curves were generated at strain rates ranging from 10^{-2} to 808 sec^{-1} for such stainless steels as AISI 304 (plate), 304L (cold worked) and 347 (bars), [15]. For these three materials an increase of flow stress and the ultimate stress with increase of strain rate was reported. On the other hand, the total elongation decreased with an increase in strain rate. In [9], several stainless steels were tested: AISI 304 (rod), 321 (bar), and 410 (annealed rod). The results generally agreed with those of [15] with respect to relation between flow stress and strain rate for rates of approximately 10 to 10^2 sec^{-1}. However, total elongation did not show considerable strain rate sensitivity for the tested materials [9].

Results reported in [9] regarding mechanical properties of steel at different strain rates offered a range of materials involved. Such steels as AISI 1020 (unknown), AISI 4340 (annealed rod), AF 1410 (plate), 300M (aged), and 10B22 (water quenched and tempered) showed consistent increase of ultimate and yield strengths. Total elongation of the specimen varied considerably. In the case of Maraging steel 300M and AF 1410 modified steel, total elongation decreased with increase of strain rate from $4x10^{-4}$ to 500 sec^{-1}. The total elongation of Steel AISI 4340, 10B22 and AISI 1020 showed slight dependence on strain rate within the same strain rate range [9]. In [13] Steel 1018 (cold-rolled) showed small change of yield and tensile stresses with increase of strain rate from $2.8x10^{-5}$ to 54 sec^{-1}, whereas the total elongation more than doubled within the same range of strain rate. Another work [9] showed dependency of mechanical properties of 1044, Mar–M 200 and Mar-M 300 steels on strain rate. Experiments included tensile testing at strain rates of 10^{-4} to 1200 sec^{-1}. All of the steels tested showed increase in yield and ultimate strengths as strain rate was increasing. Total elongation did not show a consistent trend with increasing strain rate. For steel Mar-M 200, total elongation was increasing from strain rates of 10^{-4} to 1 sec^{-1} but decreased slightly at a strain rate of 240 sec^{-1}.

Titanium alloys showed slightly different behavior of their properties with increasing strain rate. Research [13] included such titanium alloys as RS-55, RS-70, RS-110B, RS-120A and RS-120AV. All test results indicated an increase in yield and ultimate strengths for the strain rates of 10^{-2} to 10 sec^{-1}. Furthermore, these alloys evidenced some loss in ductility with an increase in strain rate. Elongation at fracture was decreasing with increase of strain rate for all the materials tested [13]. In [9], research studied the performance of such titanium-based alloys as Ti-6Al-4V (forged bar), Ti-6Al-6V-2Sn (forged bar), Ti-7Al-4Mo (forged bar), and Ti-8Al-1Mo-1V (forged bar). They observed an increase in flow stress with strain rate as strain rate increased. This behavior is more apparent at higher strain rates. Research also showed a slight decrease in total elongation for Ti-6Al-4V, Ti-7Al-4Mo and Ti-8Al-1Mo-1V. The total strain of Ti-6Al-6V-2Sn material showed slight increase as strain rate went up. Another research study [16] compared the values of maximum stress, total elongation and absorbed energy at strain rates in the range of 10^{-3} to 10^{3} sec^{-1} for Ti-15-3 (annealed). According to this report, these three variables showed noticeable increase as strain rate increased.

Comparing the results of the above-mentioned work, it was observed that for all of the materials tested in the strain rate of 10^{-4} to 10^{3} sec^{-1}, the increase of yield and ultimate strengths of the materials was under 100%. For all the reviewed test results, it was reported that the values of modulus of elasticity did not show any dependency on strain rate. Total elongation of various materials showed varying results, depending on the material and strain rate of tensile testing. Thus, for example, the maximum fracture strain did not exceed 30% at the strain rate of 10^{-4} to 10^{3} sec^{-1} for the titanium alloys reviewed above. Fracture strain decreases with the increase of strain rate for some titanium alloys while increasing for others. Various types of stainless steel also showed some variation in strain at fracture in the same range of strain rates. Reviewed test results showed maximum change in total strain of about 18%. Similar to the case with titanium alloys, the total strain exhibited both increasing and decreasing values with increasing strain rate for different types of stainless steels. Other steels showed very similar behavior to that of stainless steels showing a maximum fracture strain change of 15%.

It is also worth pointing out that although a number of different steels exhibited some drop of strength after reaching the upper yield point, available data showed absence of this phenomenon in stainless steels. During the process of literature review, there was not any information regarding the relation between mechanical properties of many materials, such as chromium alloys, and strain rates.

1.5 Elevated Temperature Testing

Testing at elevated temperature can be carried out in any usual tension testing machine if it has a provision for heating the specimen, provided that: a) the fixture and other parts on the test machine should be temperature and corrosion resistant, and b) the actual temperature should be controlled within a few degrees of the desired temperature, where the temperature is steady and uniform along the gage length. This is an important consideration as the plastic flow of the specimen depends on temperature. For example, if the specimen experiences local hot spots due to thermal gradients along the gage length, it can result in premature failure of the specimen, thus leading to inaccurate data.

Minimization of the temperature gradients and steady temperature along the gage length of the specimen are greatly dependent on the heating method. Three methods are generally used to heat specimens:

- The multiple-zone resistance wound tube furnaces are typically used at temperatures greater than or equal to 300 °C (570 °F). For uniform temperature regions, appropriate adjustment of power to each zone has to be done. If oil bath or air ovens are used to operate between room temperature and 300 °C (570 °F), improved flow of the heated medium and/or improved mixing may be required for uniformity.
- Induction heating with and without susceptors is also commonly used. This may require changes in the coil or susceptor design, while single-piece or wire mesh heaters typically used in vacuum testing may require material to be cut from the heating element to lessen the temperature differences.
- Self-resistance heating of the specimen can also be used.

The way tensile testing at elevated temperatures is approached depends on the testing equipment. This is important as the stress waves produced due to additional testing of the fixture and other parts near to the specimen may interfere with the stress waves of the specimen, leading to misleading results. Some of the approaches are listed below:

- According to M.M. Al-Mousawi, S.R. Reid and W.F. Deans [11], the long pressure bars in SHPB make the heating of the entire assembly impractical. In order to prevent unwanted wave reflections from positions other than the specimen, the mechanical impedance of the bars must be kept constant for the entire bar. Sections of the bars near the specimen are enclosed in the furnace; so thermal gradients are developed in the incident and transmitted bars. Heating the sample and a short section of the pressure bars requires estimating or measuring the temperature gradient in the pressure bars.
- Lankford [17] used short intermediate ceramic bars that are kept in direct contact with the specimen inside the furnace. The Split Hopkinson steel bars are placed in contact with the cold end of the aluminum oxide bars. Since the acoustic impedance of the aluminum oxide is approximately the same as that of the steel, stress waves pass through their interfaces without perturbation.
- Chiddister and Malvern [18] corrected the effect of the temperature gradient by calculating repeated partial reflections in the heat-affected zone of the bars.
- Eleiche and Duffy [19] obtained a different solution by tapering the torsion bars to counteract the thermal gradient. This method, however, requires a initial temperature survey and also, the tapered bars cannot be used for room temperature tests.
- Gillat and Wu [20] used the pre-stored torque to load short thin walled tubes, which are attached to the bars by special adapters. A very fast heating technique was applied using eight miniature torches equally spaced around the specimen, which took about forty seconds to heat the specimen to 1000°C.
- Elwood and Hillery [21] used two impact hammers mounted on each side of the flywheel for high speed tensile testing at elevated temperatures with strain rates ranging from 50 s^{-1} to 1000 s^{-1} and at temperatures from room to 700°C. The hammers are placed on the periphery of the flywheel so that they can impact the specimen once the desired rotational speed of the flywheel is attained. The moment of inertia of the flywheel is chosen with caution since a larger moment of inertia will take longer time to speed up and a smaller moment of inertia will lead to fluctuations in the speed. A specimen with a circular cross section was mounted between a fixed clamp and a crosshead by two connection bars. The specimen is heated using an induction heater with water-cooled copper coils. Since the thermal conductivity of the material (specimen) is less than the connection bars, the flow of heat from the specimen is restricted.

1.6 General Effects of Strain Rate and Temperature

Strain rate, or the rate at which the specimen deforms, is an important parameter in determining the strength of the material. According to [2], for most materials, strength properties such as yield strength of the material increases at higher rates of deformation. At lower deformation rates, relatively large rate changes are required to notice considerable increase in the yield strength. But, after some critical value, strength becomes more sensitive to rate. The sensitivity of strain rate to elongation of the material is very slight.

Temperature is another important consideration for strength of materials. The elevated/low temperature tests are conducted in the same way as the room temperature test, except that the specimen is heated/cooled to the desired temperature. According to [2], stress-strain curves at elevated/low temperatures have the same appearance as in room temperature. Materials usually become stronger, less ductile at low temperatures and weaker at elevated temperatures. Although some stable alloys exhibit increased ductility at elevated temperatures, the general behavior of most materials greatly varies. The primary cause for the behavior is the effect of temperature on the slip. The behavior of materials with respect to homologous temperature is also studied in [2]. (Homologous temperature is defined as the ratio of the test temperature to the melting point of the material with both temperatures expressed in degrees Kelvin). At low temperatures (0.3 times the homologous temperature), the strain hardening mechanisms such as dislocation interactions and pileups, increase the load required for continuing deformation. But the specimen fractures once the local stress concentration at these dislocations or pileups exceed the fracture stress. At higher temperatures (0.3 to 0.5 times the homologous temperature), thermally activated processes such as multiple slip tend to relax the local stresses and thus decreasing the strength of the material.

Researchers [22] showed the behavior of mild steel under the influence of strain rate and temperature. The authors did tensile tests for room temperature, 200, 400 and 600 °C, at rates of strain, which vary from 10^{-6} to 10^{3} per sec. Yield strength, ultimate strength and the elongation are dependent on rate of straining for entire range of strain rates. The ratio of yield to ultimate strength varied from 50% at lowest rate to 95% at highest rate. The author also plotted yield stress and ultimate stress values as a function of temperature (0-400°C) with strain rates 8.5e-4, 0.5, and 300 per sec. The peaks of the ultimate strength shifted towards higher temperature at high strain rates. Yield Strength shifted very little with temperature and increasing strain rates. At very high speeds, peaks of yield and ultimate strength occur at practically the same temperature.

Manson and Muralidharan [23] demonstrated that the creep rate of 316 SS is lower by a factor of 2 to10 in compression than in tension, if microstructure of the specimens tested is the same and tests are conducted at identical temperatures and equal and opposite stresses. The results show that constitutive relations cannot be developed at 705 ^{O}C (1300 ^{O}F) based on the assumption that tensile and compressive creep rates are equal at the same stresses and temperature. To maintain the same creep rate at compression and tension, it is necessary to increase the compressive stress by only a small amount. They also performed two types of thermo-mechanical loading. In the first type, the strain and temperature are cycled in phase so that high temperature and tensile stress are obtained simultaneously. In the second type of loading, the strain and temperature are out of phase, producing compressive stresses. These tests were conducted to see the response of stresses as a function of temperature during the in-phase and out of phase loading. The fact that compressive stresses reached are larger than the tensile values, verifies that creep rates are lower in compression than in tension. It was concluded that it

is impossible to compare specimens in compression to tension, though they are subjected to same temperatures.

Researchers [24] studied the true stress-true strain properties of commercially pure titanium from +800°F to –319°F at strain rates 0.001- 0.1 per min. At room temperature, tensile strength increases from 61,000 psi at 0.001 per min to 109,000 psi at 3e03 per min. Over the same range of strain rates, true stress at maximum load increases from 76,000 psi to 127,000 psi. Ductility, as measured by elongation, decreases with increasing strain rate from 35% to 26%. However, over the same range of strain rates, there was no appreciable change in the percent reduction in area. The effect of temperature on tensile strength, true stress at maximum load, and ductility at 0.001 per min is: Tensile strength decreased from 60,000 psi at 100 °F to 30,000 psi at 800 °F. True stress at maximum load decreased from 80,000 psi at 100 °F to 40,000 psi at 800 °F. The ductility decreased from 30% at 100 °F to 20% at 800 °F. Reduction in area increases. True strain at maximum load at 0.001 per min as a function of temperature from 0 °F to 550 °F, at first increases and then decreases.(the values are approximate and derived from the graph).

Another researcher [25], showed the effect of material properties of TiAl(FL) at a range of strain rates (100 - 800 per sec) under impact loading. All specimens fractured before they were plastically strained to 0.2%. It is concluded that TiAl(FL) is strain rate sensitive and exhibits high velocity ductility under tensile impact. This means that the higher the strain rate, the larger is the critical strain in maximum stress of TiAl(FL). Also, ultimate tensile strength and failure strain are perfectly linear with strain rate. Elevated temperature tensile behavior of Ti-25Al-10Nb-3v-1Mo was carried by [26]. Tensile testing of both round and flat specimens in vacuum was done from 25°C to 650°C, for three different microstructures (10/F,0/F,0/C).Yield strengths dropped by approx 30% from room temperature to 450°C, where they remained constant to 650°C; after 650°C, they began to fall again. Ultimate tensile strengths fell continuously with temperature. Plastic elongation to failure for microstructures 10/F remained approximately constant at values around 30% in temperature range 450°C to 750°C. In this same temperature range, the reduction of area increased from 45% to 75%(approx). A similar trend was observed in microstructure 0/F, where the plastic elongations also remained near 30%. However, the reduction of area values ranged from 35- 85% (approx). Microstructure 0/C demonstrated increasing elongation >30% at 600° C, after which the elongation fell discontinuously to a value of 20%(approx) at 650° C. Reductions of area for microstructure 0/C paralleled the trend in elongation and were significantly lower than those observed in microstructures 10/F and 0/F. The true fracture stress and strain for microstructures 10/F and 0/F as a function of temperature are evaluated. Each microstructure exhibited approximately 50% higher true fracture stress at 450°C than at room temperature. These values remain nearly constant to 600°C and then drop precipitously above this temperature. Additionally, there appears to be a dependence of the true fracture stress on strain rate above 600°C in microstructure 10/F. The fracture stress at slower strain rate, 10-4 per sec, was approx. 600 MPa lower than at 10-2 per sec in this temperature range. The true fracture strain increased with the temperature for microstructures 10/F and 0/F. This increase was nearly linear for microstructures 10/F, but it appeared parabolic for microstructure 0/F. The true fracture strain increased for microstructure 0/C to 600°C, after which it dropped by nearly 40% at 650°C. [25] also analyzed the variation of strain hardening exponent in two strain regions ($0.01<\varepsilon<0.1$ and $\varepsilon>\varepsilon_u$ where ε_u is the uniform elongation). For this, the engineering stress- strain curves were converted to true stress-strain curves. Strain hardening exponents were determined from these curves by fitting the data to a Holloman equation describing power law hardening, where $\varepsilon=\varepsilon(e)+\varepsilon(p)$ and $\sigma = K^* \varepsilon^n$.

Within each microstructure, there did not appear to be a large variation in n with strain rate below 650° C. In general, the n value for the higher crosshead speed was slightly higher than, or equal to. The n value measured above 600°C for microstructure 10/F were greater at the higher strain rate than at the lower strain rate.

1.7 Objective Of The Research

While high strain rate testing has been conducted for a number of years, there is no documented dynamic mechanical property data for candidate materials of the various nuclear waste package container designs. Specifically, no high strain rate tensile data could be found for candidate materials such as Stainless Steel 316L, Titanium Alloy Grade 7, and Alloy C22. This project aims to create an alternative technique for determination of tensile properties under moderate strain rates and at elevated temperatures up to $350^{O}F$. The scope of the research is focused on determination of the following tensile properties of the three above listed materials at room temperature, $175^{O}F$, and $350^{O}F$:

1. Yield Strength
2. Ultimate Strength
3. Strain at Yield stress
4. Strain at Ultimate stress
5. Total elongation

CHAPTER 2

MATERIALS AND EQUIPMENT

In this chapter, chemical and mechanical properties of three candidate materials for the nuclear waste package are identified. Specimen geometry is defined, and two testing machines were selected for the project using values of maximum load and maximum energy needed to break the specimens.

2.1. Nuclear Waste Package Candidate Materials

This project studies several materials that have been identified by the Department of Energy as candidate materials for the design of a nuclear waste package [1]. The list includes Stainless Steel 316L, Titanium alloy Grade 7 and Alloy C22. Typical chemical composition of the materials and some of their properties are provided in Tables 2-1 through 2-3.

Steel 316L is a molybdenum-bearing austenitic stainless steel. This material is more resistant to general corrosion and pitting than many conventional chromium-nickel austenitic stainless steels such as type 304 [27]. This alloy also has a higher creep, stress-to-rupture and tensile strength at elevated temperatures. In addition to high corrosion resistance and strength properties Steel 316L has excellent formability. Table 2-1 provides the chemical composition for Stainless Steel 316L [27].

Table 2-1 Chemical Composition of Stainless Steel 316L (non-Q, for information only)

Element	%
Carbon	0.030
Sulfur	0.030
Phosphorus	0.045
Nitrogen	0.10
Silicon	0.75
Manganese	2.00
Molybdenum	2.00/3.00
Chromium	16.00/18.00
Nickel	10.00/14.00
Iron	Balance

Titanium Alloy Grade 7 has low density and a high strength-to-weight ratio. It is considered one of the best materials for many corrosive chemical environments, including oxidizing chloride solutions, seawater, and chlorine-based bleaches [28]. Grade 7 is palladium alloyed CP titanium, which has very good resistance to crevice corrosion. Besides its excellent mechanical properties, it also has good formability. Table 2-2 provides the chemical composition for titanium alloy grade 7 [28].

Alloy C22 is a Ni -Cr-Mo alloy that provides good resistance to pitting, crevice corrosion and stress corrosion cracking [29]. The combination of Cr, Ni, Mo, and W provides very good resistance to oxidizing and reducing environments. This alloy possesses high strength and good ductility as well as excellent welding and forming characteristics. Table 2-3 provides chemical compositions for the Alloy C22 [29].

Table 2-2 Chemical Composition of Titanium Grade 7 (non-Q, for information only)

Element	%
Aluminum	-
Vanadium	-
Molybdenum	-
Nickel	-
Hydrogen	0.015 (max)
Nitrogen	0.03 (max)
Carbon	0.08 (max)
Palladium	0.2
Oxygen max	0.25
Iron	0.3
Titanium	Balance

Table 2-3 Chemical Composition of Alloy C22 (non-Q, for information only)

Element	%
Carbon	0.015 (max)
Sulfur	0.02 (max)
Silicon	0.08 (max)
Vanadium	0.35 (max)
Cobalt	2.5 (max)
Tungsten	2.5/3.50
Iron	2.00/6.00
Molybdenum	12.5/14.5
Chromium	20.0/22.5
Nickel	Balance

Mechanical properties of these materials are provided in Table 2-4. According to the references for Stainless Steel 316L [27, 43], Titanium alloy Grade7 [28, 44] and Alloy C22 [29, 45], the materials tested were of typical chemical composition provided in the plate type stock with annealing specified as a heat treatment.

Table 2-4 Mechanical Properties of Selected Materials [27-29, 43-45] (non-Q, information only)

Material/Properties	Stainless Steel 316L	Titanium alloy Grade7	Alloy C22
Yield Strength (ksi)	86.3	50.11	47
Ultimate Strength (ksi)	101.4	67.85	108
Strain at Fracture (%)	42	27.1	66
Young's Modulus (Msi)	29	15	30

2.2 Selection of the Specimens

Selecting appropriate specimen geometry and equipment was one of the first steps of the project. It was necessary to choose a standard specimen that would best fit both types of testing: at low strain rates (10^{-4} – 1 sec^{-1}) and at medium strain rates (1 - 200 sec^{-1}).

The selection of specimen geometry was based on recommendations found in the ASTM standard for tensile testing of metallic materials [30]. The final selection of specimen geometry was also influenced by specimen used in similar research studies to make it easier to compare results. The literature review yielded a number of different dimension types of flat and cylindrical tensile specimens. The specimen geometry chosen for this study is the same as samples used for tension SPHB experiments and is shown in Figure 2-1 and Table 2-5.

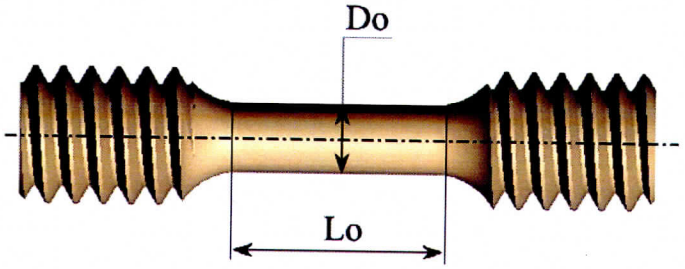

Figure 2-1 Threaded Tension Hopkinson Bar Specimen [9]

Table 2-5 Round Tension Test Specimens [9]

Dimensions	Threaded Tension Specimen Specimen # 2
D_o (in)	0.125
L_o (in)	0.350

2.3 Selection of the Testing Machines

The emphasis of the project is determining material properties, so the design and fabrication of custom testing machines was avoided. The lower strain rate experiments are well suited for a standard screw-driven or servo-hydraulic universal testing machine. The speeds required for the medium strain rate experiments can be obtained with existing commercial instrumented drop weight tower impact testing machines. Maximum forces, total energy at failure, and maximum speeds needed to fracture the specimens were estimated and used to select the appropriate testing machines.

2.3.1 Selection of the quasi-static tensile testing machine

To select a material testing system for the low strain rate experiments, the maximum required load to break the specimen was estimated using

$$P = nS_u A_s \tag{2-1}$$

where S_u is the ultimate strength, A_s is the cross-sectional area of the specimen in the gage region and n is the approximate relation between the static and dynamic values of the ultimate strength. As it was pointed out in Chapter 1, the values of yield and ultimate strengths in all reviewed cases differed by less than 100 present. That is why to determine a maximum load in the conservative way the coefficient is taken to be equal two. Using this equation for all types of the specimen along with all three materials, a number of maximum load values were obtained. The loads calculated using equation (2-1) are presented in Table 2-6 [37].

Table 2-6 Load Required to Break Tensile Specimens (non-Q, for information only)

Material/Specimen No.	Stainless Steel 316L	Titanium alloy Grade7	Alloy C22
Specimen #1 (lbf)	8,128	5,806	12,192
Specimen #2 (lbf)	1,718	1,227	2,577
Specimen #3 (lbf)	2,710	1,936	4,065
Specimen #4 (lbf)	1,056	0,754	1,584

According to the results reported in Table 2-6, the maximum load required to fracture a specimen is equal to

$$P_{\max} = 12{,}192\ lbf \tag{2-2}$$

Therefore, an existing MTS Axial/Torsion material testing system was adopted for low strain rate material testing since it has a maximum load of 55,000 lbf.

2.3.1 Selection of impact tensile testing machine

Two different cases were considered in choosing a material testing system for tensile impact experiments. The first case is when the energy applied by the striker is only sufficient to yield the material of the specimen. In this case the full energy consists of two parts: the energy to yield the material and the energy of the striker rebound. Any other energy loss mechanisms are assumed to be negligible [5, 6, and 31]. The second case is when the specimen is completely broken after the impact.

To determine energy required for the first case, two values of the energy were determined:

1. Energy that is required to yield the specimen, [31]:

$$U_y = \frac{nS_y^{\,2}V}{2E} \tag{2-3}$$

where, V is the volume of the gage region of the specimen including filleted part of the sample, E is Young's modulus of elasticity and S_y is the yield strength. Results of the calculation found using equation (2-3) are presented in the Table 2-7 [37].

Table 2-7 Energy Required to Yield the Specimens (U_y) (non-Q, for information only)

Material/Specimen No.	Stainless Steel 316L	Titanium alloy Grade7	Alloy C22
Specimen #1 (lbf-in)	1.773	8.775	6.855
Specimen #2 (lbf-in)	0.177	0.877	0.685
Specimen #3 (lbf-in)	0.394	1.951	1.525
Specimen #4 (lbf-in)	0.141	0.697	0.544

2. Rebound energy of the striker, [31]:

$$U_r = \frac{M(v_2)^2}{2} \tag{2-4}$$

where, M stands for the mass that can be defined as, [21]:

$$\frac{1}{M} = \frac{1}{M_1} + \frac{1}{M_2} \tag{2-5}$$

where, M_1 and M_2 are the masses of the striker and the tested part. In the presented case the total mass is equal to 100 lbm. v_2 stands for the velocity of the striker after the impact. This velocity can be computed using the following equation, [31]:

$$v_2{}^2 = v_1{}^2 e^2 \tag{2-6}$$

Where, v_1 is initial velocity of the striker and e is the coefficient of restitution. Coefficient of restitution is determined using this equation, [31]:

$$e = 3.8\left(\frac{nS_y}{E_t}\right)^{\frac{1}{2}}\left[\frac{1}{2}M\frac{(v_1)^2}{nS_yR^3}\right]^{\frac{1}{8}} \tag{2-7}$$

where, R is equal to

$$\frac{1}{R} = \frac{1}{R_1} + \frac{1}{R_2} \tag{2-8}$$

R_1 and R_2 are the radiuses of the striker and impacted surface. In the presented case it is assumed that the radius of the impacted surface is equal to a very big number thus:

$$\frac{1}{R_2} \to 0 \tag{2-9}$$

E_t is defined as

$$E_t = \frac{E_sE_m}{E_s + E_m} \tag{2-10}$$

where, E_s stands for the Young's modulus of the material of the striker; E_m stands for the Young's modulus of the tested material. Incorporating the above listed equations into equation (2-7), it can be rewritten as

$$e = 3.8\left[\frac{nS_y}{\left(\frac{E_sE_m}{E_s + E_m}\right)}\right]^{\frac{1}{2}}\left[\frac{1}{2}M\frac{(v_1)^2}{nS_yR^3}\right]^{\frac{1}{8}} \tag{2-11}$$

The equation for the energy of the rebound motion can be rewritten as,

$$U_r = \frac{M}{2}(v_1)^2\left[3.8\left[\frac{nS_y}{\left(\frac{E_s E_m}{E_s + E_m}\right)}\right]^{\frac{1}{2}}\left[\frac{1}{2}M\frac{(v_1)^2}{nS_y R^3}\right]^{-\frac{1}{8}}\right]^2 \quad (2\text{-}12)$$

Assuming that the material of the striker has a Young's modulus equal to 29.01×10^6 psi, the radius of the indenter is equal to 0.36 inches, and the mass of the striker equals 100 lb; the estimated total impact energies were calculated for all types of specimens and materials chosen for evaluation and are presented in Table 2-8 [37].

Table 2-8 Energy for Striker Rebound and Material Yield. (U_r+U_y)
(non-Q, for information only)

Material/Specimen No.	Stainless Steel 316L	Titanium alloy Grade7	Alloy C22
Specimen #1 (lbf-in)	1,432	3,785	3,353
Specimen #2 (lbf-in)	1,431	3,777	3,347
Specimen #3 (lbf-in)	1,431	3,778	3,348
Specimen #4 (lbf-in)	1,431	3,777	3,347

In addition to the above calculations the total energies required to break the specimens were calculated. Values of energy needed to fracture the specimen at moderate strain rates are equal to the area under stress-strain curve obtained at low strain rate and adjusted by increasing the value according to the adopted earlier coefficient *n*. Assuming that the area of that segment can be presented as an area of a triangle and a trapezoid the equation of the energy could be written as

$$U_f = nV\left[\frac{S_y^{\,2}}{2E} + \frac{(S_y + S_u)}{2}\left(\varepsilon_f - \frac{S_y}{E}\right)\right] \quad (2\text{-}13)$$

The area of the triangle represents the elastic region of material behavior and the trapezoidal area represents the plastic region of material behavior. In the above equation '*y*', '*u*', and '*f* ' represent yield, ultimate and fracture points on the stress-strain curve respectively. The results obtained using equation (2-13) are presented in the Table 2-9 [37].

Table 2-9 Breakage Energy of the Specimens (non-Q, for information only)

Material/Specimen No.	Stainless Steel 316L	Titanium alloy Grade7	Alloy C22
Specimen #1 (lbf-in)	3,121.12	1,470.81	8,529.87
Specimen #2 (lbf-in)	311.95	146.90	852.43
Specimen #3 (lbf-in)	694.09	326.83	1,897.69
Specimen #4 (lbf-in)	257.83	116.71	677.23

The existing Instron Dynatup Model 8250 Drop Weight Impact Tower at UNLV has a maximum available impact energy of 7,400 in-lbf. It can be used for impacting all of the potential specimen configurations except Specimen #1. Specimen #2 was ultimately chosen because it could be used with available testing equipment and it most closely matches specimen

used in similar research studies [3 and 9]. According to the results reported in Table 2-9, energy requirements to fracture this specimen are equal to

$$U_f = 852.43 lbf \cdot in \tag{2-14}$$

which is well within the limits of the Instron Dynatup machine.

2.4 Description Of The Equipment

2.4.1 Description of the MTS tensile testing machine

The MTS Axial Torsional Test System at UNLV is used for carrying out the low strain rate tensile tests for this study. The MTS testing system is composed of a number of integrated systems [32]. It includes a load frame (1), computer (2), load unit control panel (POD) (3), grip supply (4), strain gage conditioner (5), temperature controller (6), control box (7), hydraulic service manifold (8), and a hydraulic pump (9) as shown in Figure 2-2. Load Frame Specifications of the MTS Tensile/Torsion material testing system are presented in the Table 2-10 and a photograph of the system is shown in Figure 2-3.

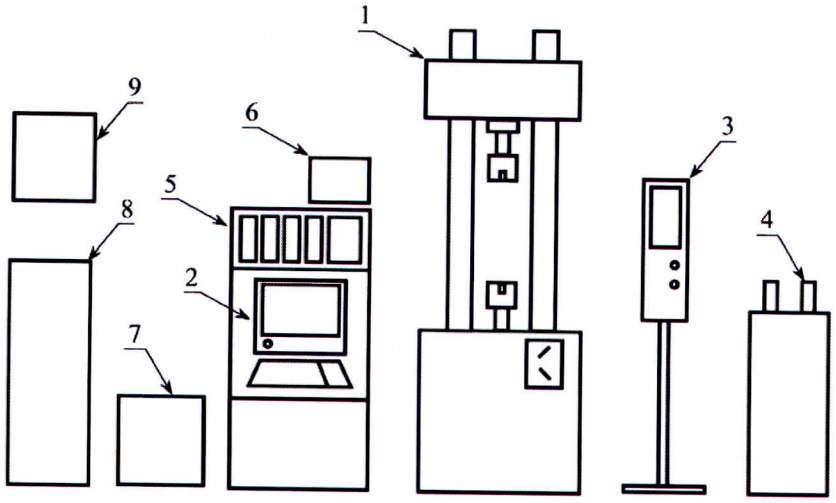

Figure 2-2 MTS Tensile System Components

Table 2-10 MTS Load Frame Specifications

MTS tensile system parameters	Values
Working Dimensions	25 inches wide by 57.6 inches high
Axial Load Transducer	55,000 lbf
Torsional Load Transducer	20,000 in-lbf
Linear Actuator	±3 in, measured with an LVDT
Rotary Actuator	100° static rotation (± 50°), 90° dynamic rotation (± 45°)
Frequency Rating	Axial and rotary actuators are controlled by separate servovalves. Maximum frequency will vary with specimen stiffness.

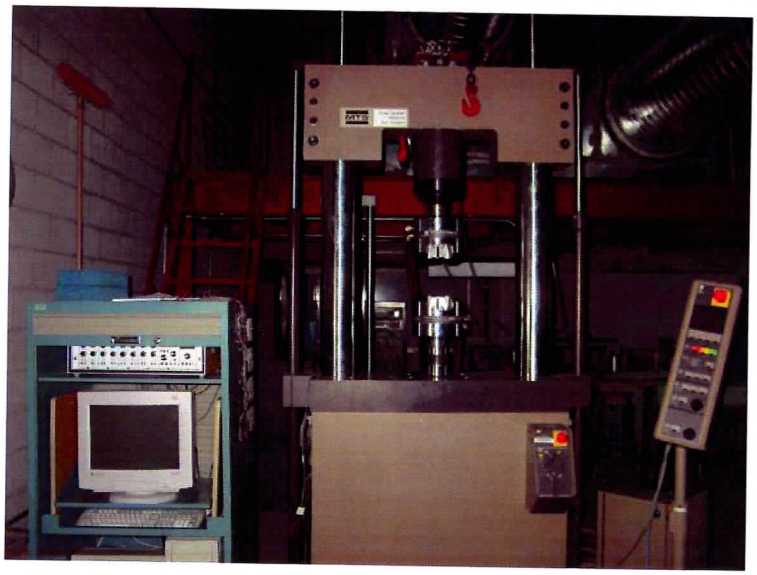

Figure 2-3 MTS Tensile System.

The MTS system has a high temperature environmental chamber, shown in Figure 2-4, with Model No. 652.02 designed for low-cycle fatigue, fatigue rack growth, and fracture toughness testing at temperatures from 200 °C up to 1000 °C. The furnace is configured with two independent heating zones to improve the temperature gradient across the test specimen. A viewing window is available to monitor the specimen during the test. Specifications of this chamber are listed in Table 2-11.

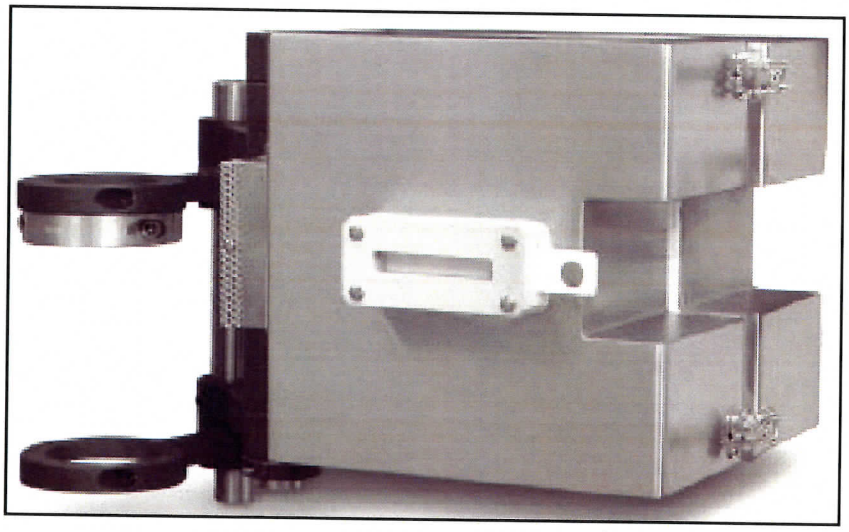

Figure 2-4 MTS Environmental Chamber

Table 2-11 Specifications of MTS Environmental Chamber (Model No. 652.02)

Specification	Value
Maximum Temperature	1000°C
Minimum Temperature	200°C
Control point stability	+/- 1°C
Overall Height	260mm (10.25 in)
Hot zone height	210mm (8.25 inches)
Hot zone width	125mm (5 inches)
Hot zone depth	125mm (5 inches)
Number of zones	2

This material testing system uses the TestStar and TestWareSX control and data acquisition software that collects the readings of the load cell and the displacement reading of the actuator with user specified frequency. TestWareSX software allows setting up a step-by-step testing procedure for the experiment.

2.4.2 Description of the Instron Dynatup Impact test machine

For the purpose of dynamic tensile testing, an impact testing machine was selected using the maximum energy selection criterion described earlier. A number of different conventional impact systems were evaluated. The Instron Dynatup 8250 testing machine was accepted for the impact testing with moderate strain rates. It satisfied the required energy demands of the tensile testing.

The Instron Dynatup testing equipment is an instrumented drop weight tower consisting of a number of elements as shown in Figure 2-5. The primary components of the Instron Dynatup 8250 impact testing machine [33] include a tup (1), load cell (2), striker (3), tup guides (4), brakes (5), base that holds all the equipment of the machine (6), control panel (7), computer with data acquisition system (8), specimen fixture (9), "flag" that is used to start the data collecting process (10), and a stationary trigger mechanism (11) that sends a signal to the data acquisition board once the "flag" passes through it.

Different set-up options for the equipment allow running impact tests in gravity driven mode or with pneumatic assist. The tup mass can be changed from 5.5 lbs to 10, 25, 50, 75 and 100 lbs using a number of additional mounting plates. The ability to change both the mass and velocity of impact provides considerably flexible access to different levels of energy and velocity output of the equipment. Maximum and minimum values of velocities and energies for each of the main working modes of the Instron Dynatup 8250 impact test machine are presented in the Table 2-12.

This machine uses a load cell calibrated to 5000 lbf. The data measured by the load cell is collected by the data acquisition system. The Instron Dynatup drop weight testing system incorporates I-940 data acquisition software. This software allows creation of custom test setup, test reports and can export data files. The software records 4096 data points within the given time frame of the experiment. Curves of load, time, velocity, or deflections can quickly be plotted right after the test. Using the set-up procedure, a number of different tests can be arranged. The tests can be conducted in gravity mode and using pneumatic-assist. The latter allows increasing velocity of the tup to 528 in/sec.

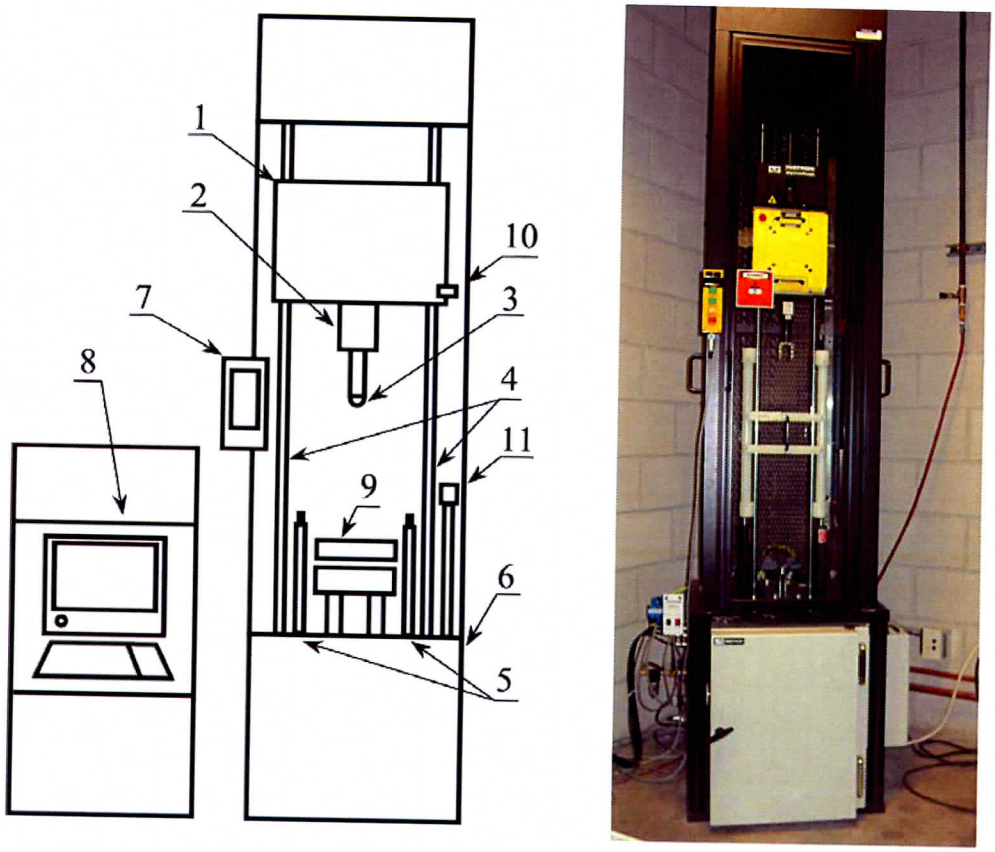

Figure 2-5 Instron Dynatup 8250 Impact Test Machine Components.

Table 2-12 Characteristics of Instron Dynatup Testing Machine

Working Parameters	Gravity-Driven		Pneumatically-Assisted	
	Min	Max	Min	Max
Impact Energy (lbf in)	6.00	2,688.00	6.00	7,440.00
Impact Velocity (in/sec)	24.00	144.00	24.00	528.00

There are a few options for triggering the mechanism of data collection. One of the most convenient options is the 'Flag trigger mode'. This type of data collection triggering initiates a data collection process when the second leading edge of the double- edged 'flag', shown in the Figure 2-6, passes through the 'Velocity Detector', shown in Figure 2-7. This option of data collection initiation allows for starting the data acquisition system right before the collision of striker and the specimen and also allows obtaining velocity of the tup prior to the impact, which in turn is used to calculate the displacement and energy. A built-in security system prevents running the equipment with an open access door. Safety "H" bar is used when installing and uninstalling the specimens.

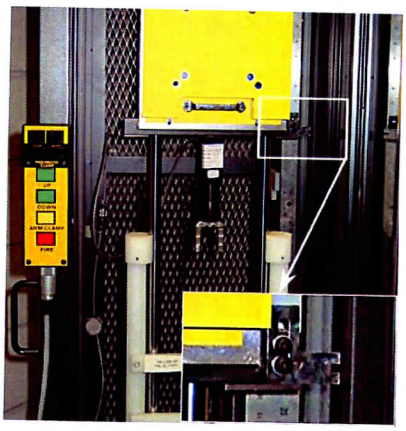

Figure 2-6 Instron Dynatup 8250: Close Up View of the 'flag'

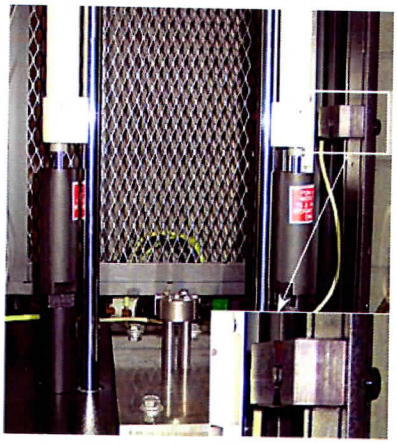

Figure 2-7 Instron Dynatup 8250: Close Up View of the 'Velocity Detector'

The Instron Dynatup environmental chamber allows for the physical testing of materials in either a high or low temperature environment. The unit features a removable side panel that houses the blower, heating, and cooling systems as well as all electrical connections that run to the remote control unit. The temperature within the chamber is controlled by a microprocessor based controller [34]. It has two output controls for both types of heating. Heating of the chamber is accomplished by means of a 1.3 kW open coil heater since it provided a quick response to controller demands. It is installed in such a way as to avoid direct radiation to the specimens. The chamber is also provided with an expendable gas cooling system, which utilizes either liquid nitrogen or liquid carbon dioxide. The temperature range of the chamber is:

-60°F (-50°C) to +350°F(175°C).

Despite the availability of many convenient features, this impact machine could not be used for the tensile impact testing of cylindrical specimen without certain modifications. The original design of the machine and the clamping fixture that was provided by the manufacturer was designed for puncture tests of plate type specimens. This fixture could not be used for tensile testing. In order to fulfill the goals of the project; a unique fixture was designed to meet all the requirements of the proposed testing.

CHAPTER 3

FIXTURE DESIGN

Design of fixtures that serves the purpose of the research and requires minimum machining and assembly time is the main objective of this stage of the project. Several alternative fixture designs are considered. The availability of potential material stock is checked and all technical drawings are prepared using a number of different CAD packages such as AutoCAD, SolidWorks and Pro/Engineer. This diverse range of software allows the preparation of technical documentation in a short period of time. It also allows for checking the interaction between all parts of the assembly including parts of the testing machines used to attach or hold fixture components. Steel 1045 Annealed material is chosen for the MTS fixture and Steel 4130 material is used for Instron fixture design. Mechanical properties of the materials [35] are presented in Table 3-1.

Table 3-1 Fixture Material Characteristics (non-Q, for information only)

Fixture Material	Stress values in ksi		
	Ultimate Stress (Su)	Yield Stress (Sy)	Young's Modulus (E)
Steel 1045 Annealed	108.9	74.8	27 msi
Steel 4130 Annealed	81.2	52.2	29 msi

3.1 Evaluation Of The Specimen

The fixture design process was started by evaluation of the selected tensile specimen. The process included analysis of the threaded connections of the specimens made of different materials subjected to maximum loads as determined in Chapter 2. The geometry of the selected specimen is presented in Figure 3-1. All parameters of the part are presented in Table 3-2.

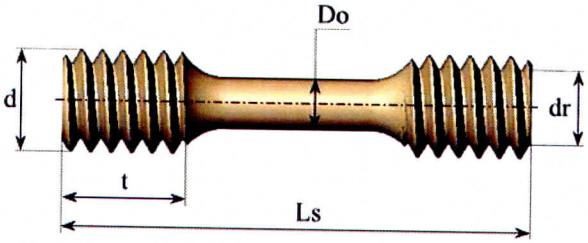

Figure 3-1 Selected Specimen

Table 3-2 Parameters of the Selected Specimen [37] (non-Q, for information only)

Characteristic dimensions of the specimen	Values
Cross sectional area within the gage length	$A_s = 0.012$ in2
Cross sectional area of the threaded part of the specimen	$A_t = 0.049$ in^2
Major diameter of the threaded part of the specimen	$d = 0.25$ in
Minor diameter of the threaded part of the specimen	$d_r = 0.189$ in
Length of the threaded part	$t = 0.292$ in
Length of the specimen	$L_s = 1.15$ in
Pitch of the threads	$p = 0.05$ in

Mechanical properties of the specimen materials are given in Table 2-4. Based on the previous calculations from Section 2.1 and Table 2-6, the maximum tensile force needed to break the specimen is estimated to be

$$P_{\max} = 2{,}577 lbf \tag{3-1}$$

a. Thread Shear ("Stripping") Stress.
The shear stress in the threads is determined from the following expression:

$$\tau = \frac{P_{\max}}{\pi d(0.75t)} \tag{3-2}$$

The safety factor for shear stress is equal to

$$sf = \frac{0.58 S_{fy}}{\tau_{ss}} \tag{3-3}$$

The shear stress safety factors in the fixture threads for tests conducted on all three different specimen materials are shown in Table 3-3. The fixture material will behave in a similar manner to that of the specimen material, but the strength increase of the threaded connections will be absolutely different. According to the findings of [7], the increase of strength varies from 29-52 percent at strain rates of 2.5×10^{-5} sec^{-1} to just 8-15 percent at strain rates of 102 sec^{-1}. The design of all fixture components was carried out using the assumption that although the strength of the tested material will be increasing with accordance to the ratio n, as shown in Section 2.3.1, mechanical properties of the fixture material will exhibit no increase of its mechanical properties.

Table 3-3 Safety Factor for the Shear Stress of the Threads [37] (non-Q, for information only)

Material	Safety Factor
Stainless Steel 316L	0.967
Titanium Grade 7	1.547
Alloy C22	1.934

b. Analysis of the threaded bearing (compressive) stress.

$$\sigma = \frac{4P_{\max}}{\pi\left(d^2 - d_r^2\right)\frac{t}{p}} \tag{3-4}$$

The safety factor for bearing stress is chosen based on the softer of the two materials in contact (fixture or specimen), [36]. The safety factors for the 3 different specimen materials are shown in Table 3-4.

$$sf = \frac{S_y}{\sigma} \tag{3-5}$$

Table 3-4 Thread Safety Factor for the Bearing Stress [37] (non-Q, for information only)

Material	Safety Factor
Stainless Steel 316L	1.195
Titanium Grade 7	1.913
Alloy C22	2.391

3.2 MTS Fixture Designs

A design of the fixture was performed considering the dimensions of the specimen and design constraints of the equipment. An initial fixture, shown in Figure 3-2, was used only for room temperature testing. A second fixture, shown in Figure 3-3, was designed and fabricated for use in the furnace. Detailed stress analyses of all fixture components can be found in Zabotkin and Dusi's thesis reports [37 and 38]. The exploded view of the first MTS tensile fixture, presented in Figure 3-2, is composed of an upper specimen holder (1), a lower specimen holder (5), specimen (2), guides (3), and fixing screws (4).

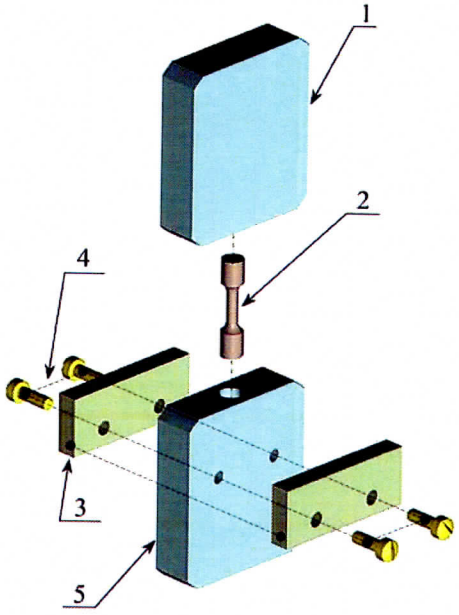

Figure 3-2 Exploded View of the MTS Tensile Fixture

Figure 3-3 shows one half of the fixture used with the high-temperature MTS furnace. The various parts in the figure are: Specimen (A), Adapter (B), Pin (C), and Grips (D). A compete assembly of an installed fixture is shown schematically in Figure 3-4.

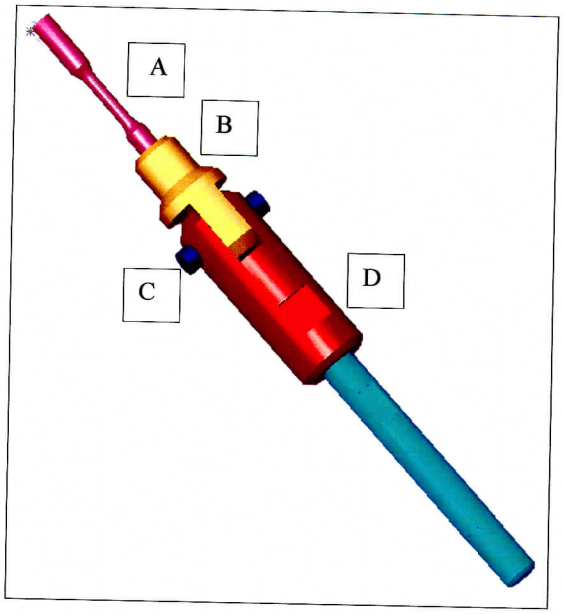

Figure 3-3 One Half Of The MTS High-Temperature Fixture Design

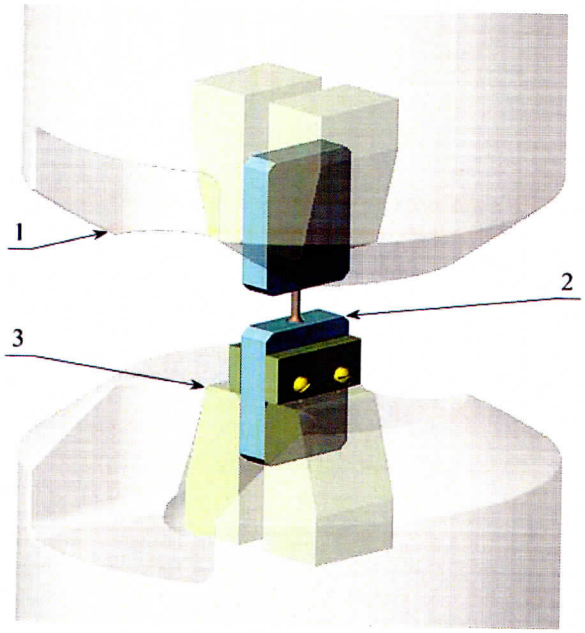

Figure 3-4 MTS Tensile Fixture Setup

3.3 Instron Fixture Designs

Design of the fixture for the Instron Dynatup testing machine was one of the most challenging phases of the project. It has been stated earlier that the available impact testing machines are not designed to conduct tests in the desired fashion. The fixture was supposed to replace the original plate clamping mechanism, satisfy all the design constraints and provide desirable integrity. Collecting information regarding the mating components of the testing machine such as base plate, tup guides and load cell was the first stage of the design. Drawings of the components were collected and evaluated. Based on the obtained data a principal design was offered. The following guidelines were kept in mind:

1. The fixture base should be a massive part providing sufficient support for the specimen holding parts.
2. Specimen holding components should not only provide enough support to the specimen but also allow access to the part that would transmit the impact from the striker to one of the specimen ends.
3. The design should allow an easy way of accessing the specimen for installation and removal. Since the specimen has two threaded ends, it was important to have a design that will allow adjustable positioning of the specimen holders after all the connections are securely tightened.
4. The threaded female part of the load cell was considerably larger than the one required for holding the striker. An additional adapter was introduced to allow the use of a small block for holding the samples that maintains the freedom of the final position of the striker after all the elements are tightly connected.

After a number of modifications of the preliminary drawings, the proposed fixture satisfied all of the design criteria. Detailed stress analysis calculations were carried out [37] to guarantee the safety of the design using the required equations provided in [36].

The exploded view assembly drawing of the room-temperature Instron Dynatup impact testing fixture is presented in Figure 3-5. The components incorporated in the design include a thread adapter (1), striker (2), a set of eight nuts (3), a specimen holder (4), a tensile specimen (5), a transmitter (6), a set of four flat washers (7), a set of eight locking washers (8), a base plate (9), a set of four columns (10), an insert (11), and a flat nut (12) that is used to fix the striker to a thread adapter.

A modified fixture was developed for use in the Instron Dynatup environmental chamber. The various components shown in Figure 3-6 are supporting body (A), plate (B) and specimen holder with four columns (E) from the previous design, specimen (C), upper cylinder (D), transmitter (F), a set of four bolts (G). The significance of the upper cylinder is to provide the appropriate height for the specimen for maximum deflection before the striker reaches the brakes. In other words, it gives the clearance for maximum deflection to the specimen.

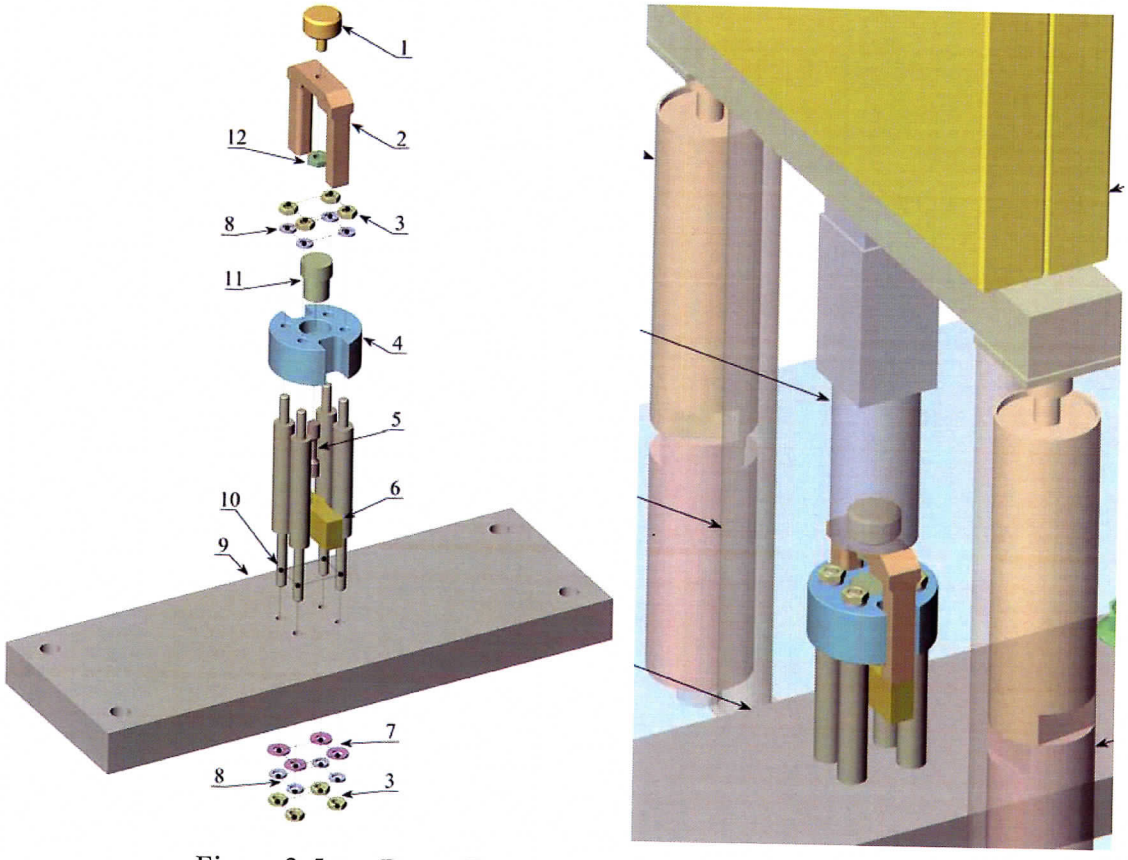

Figure 3-5 Room Temperature Impact Tensile Fixture

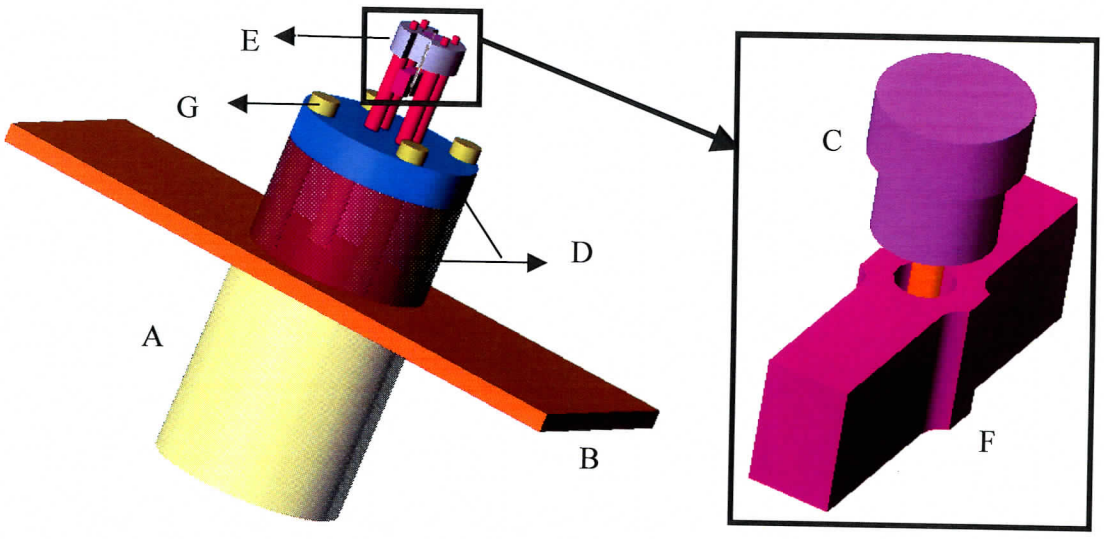

Figure 3-6 Impact Tensile Fixture Setup For The Environmental Chamber

CHAPTER 4

TESTING PROCEDURES

This chapter presents an overview of the testing procedures for the MTS and Instron test machines. This information is based on equipment manuals as well as numerous testing of specimens. Complete details of the procedures are described in:

- IPLV-031 Impact Testing of Tensile Specimens Using Dynatup 8250 with Model 930-I Operating Software [39]
- IPLV-033 Tensile Testing with the MTS Axial/Torsional Material Test System [32]
- IPLV-040 Determination of Mechanical Properties of Materials Under Dynamic Loading [40]
- IPLV-058 Impact Testing of Tensile Specimens in the Environmental Chamber of Dynatup 8250 with Model 930-I Operating Software [41]
- IPLV-061 Elevated Temperature Tensile Testing with the MTS Axial/Torsional Material Test System [42]

4.1 Low Strain Rate Testing Procedures

An MTS servohydraulic axial/torsional test system was used for the low strain rate experiments. The test specimens were threaded into steel blocks with alignment guides that are mounted in a set of hydraulic wedge grips as shown in Figures 3-2 thru 3-4. All experiments were run at a constant velocity while recording time, force, and displacement at predetermined intervals. The average strain rate for the experiment was determined from the displacement versus time data. The maximum strain rate obtainable on this machine was approximately 1 sec^{-1}. Samples tested at elevated temperatures were placed in the gripping fixtures and mounted inside the furnace. The furnace set-point temperatures were set to predetermined values for a minimum time so that the samples were uniformly heated to the desired test temperature. Table 4-1 shows the recommended set-point values and minimum heat up times for the three materials under consideration. The values in the table were determined by drilling a small hole down the center axis of a sample, placing a thermocouple inside the hole, and monitoring the sample centerline temperature while heating.

Table 4-1 Specimen Heat Up Times for MTS Furnace (± 2%)

Material	Target Temperature (^{O}F)	Minimum Time to Reach Target Temperature (Minutes)	Furnace Set-Point Temperature (^{O}F)
C22	175	130	255
C22	350	175	523
Ti Alloy Grade 7	175	150	250
Ti Alloy Grade 7	350	190	520
316L	175	165	255
316L	350	190	530

A typical raw engineering stress-strain curve is shown in Figure 4-1. Strain gages or extensometers were not used due to the small size of the test samples. Strain was calculated based on the displacement reading of the actuator. The strain values recorded in the linear elastic range of all the materials were too high because the LVDT measurement included all the compliance of the entire load path, which resulted in a significantly lower slope of the linear portion of this curve. Since all information found in the literature suggests that the modulus of elasticity does not depend on strain rate for these three materials, composite stress-strain curves were created using standard modulus of elasticity values, Table 4-2, within the elastic range [27-29].

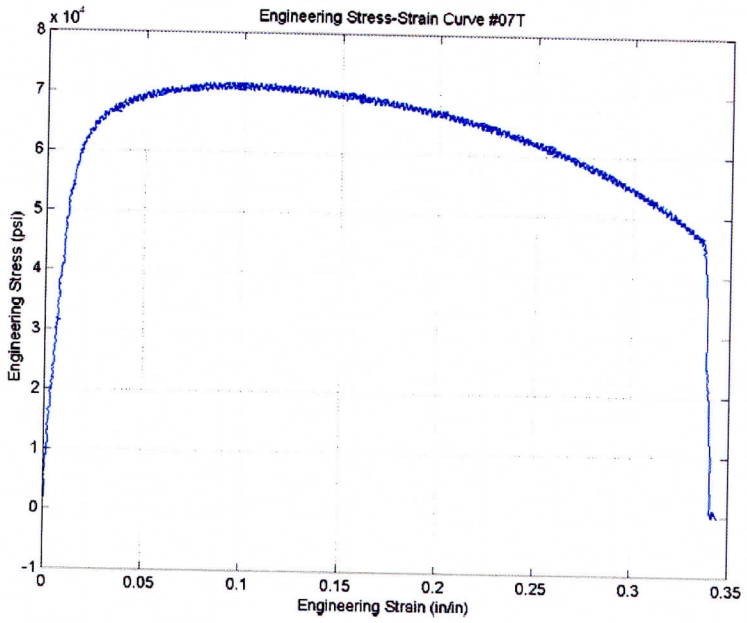

Figure 4-1 MTS Raw Engineering Stress-Strain Curve for Titanium Alloy Grade 7 [47]

Table 4-2 Modulus of Elasticity of Selected Materials [27-29] (non-Q, for information only)

Material	Stainless Steel 316L	Titanium alloy Grade7	Alloy C22
Modulus of Elasticity (Msi)	29	15	30

The determination of the elastic limit of the material was based on fitting a 6^{th} order polynomial curve over the portion of the data that corresponds to the elastic phase and the beginning of the plastic phase of the material behavior. Figure 4-2 shows an example of such a fit for a typical titanium specimen. The second derivative of stress with respect to strain was determined as a function of strain and plotted on a graph as in Figure 4-3. The yield strain was defined as the average of the strain value at the first local minimum and the second local maximum on this second derivative curve. The yield strength was defined as the stress value corresponding to this yield strain as determined from the stress-strain curve.

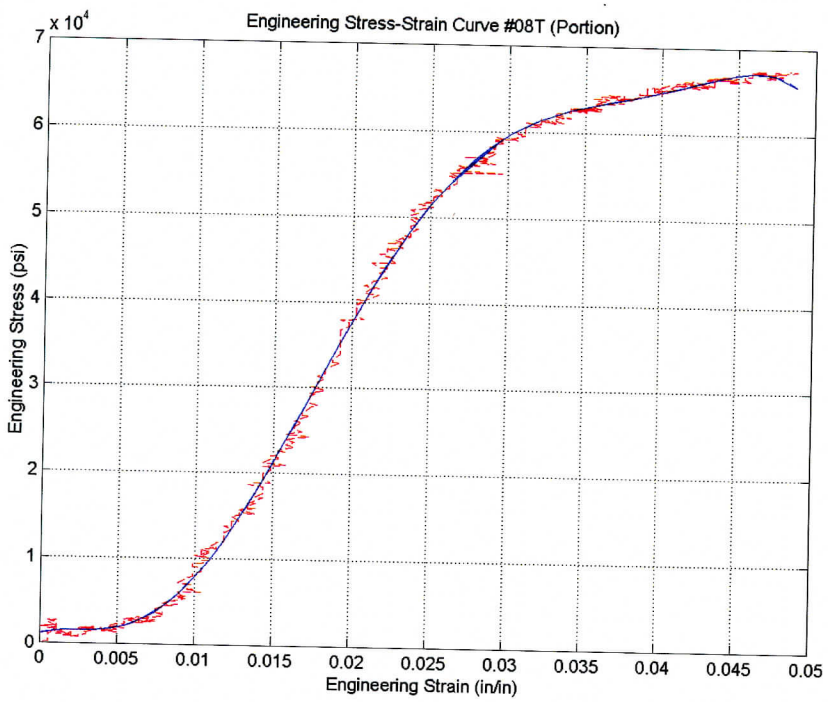

Figure 4-2 Raw Stress-Strain Data with Fitted Curve for Titanium Sample [48]

A modified yield strain was determined based on the yield strength calculated in the procedure described above. The modified yield strain is calculated using the linear stress-strain relationship $\varepsilon_Y = \sigma_Y/E$. The strain at yield established a needed reference point for shifting the rest of the stress-strain curve. A composite engineering stress-strain curve was created after determination of the yield strength and yield strain. This composite curve consists of two segments. Segment one was a straight line that started from (0, 0) and ended at (σ_y/E, σ_y). The second segment was represented by the data points starting from the yield strength and ending at the last relevant data point. Strain values were shifted by a value equal to the difference between strain at yield as determined above and strain at yield of the raw data. An example of a composite curve for titanium is shown in Figure 4-4 along with a picture of the broken sample. A summary of the results obtained from the test are presented in Table 4-2.

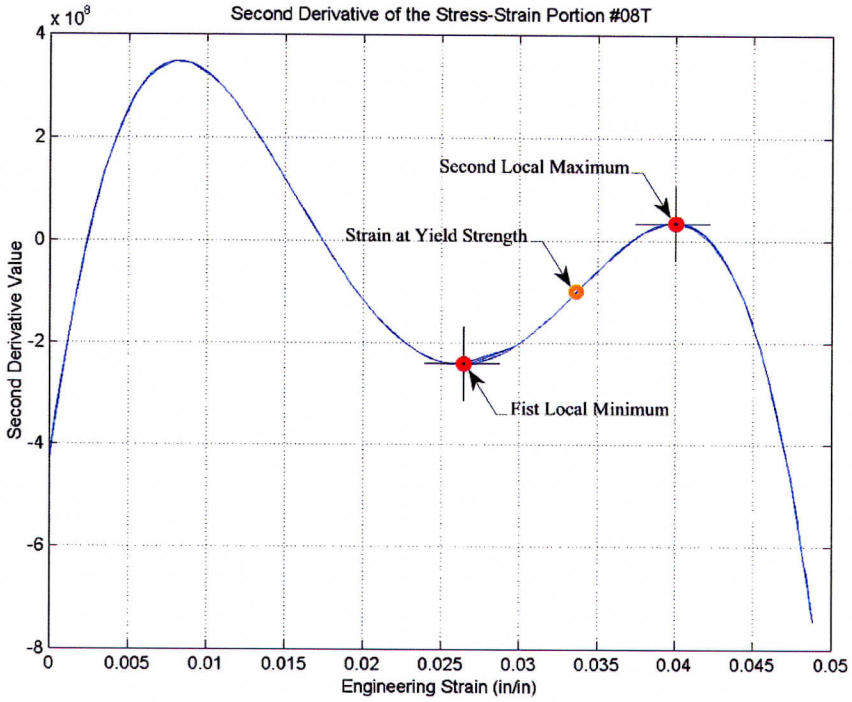

Figure 4-3 Second Derivative of the Stress-Strain Curve Identifying the Yield Point [48]

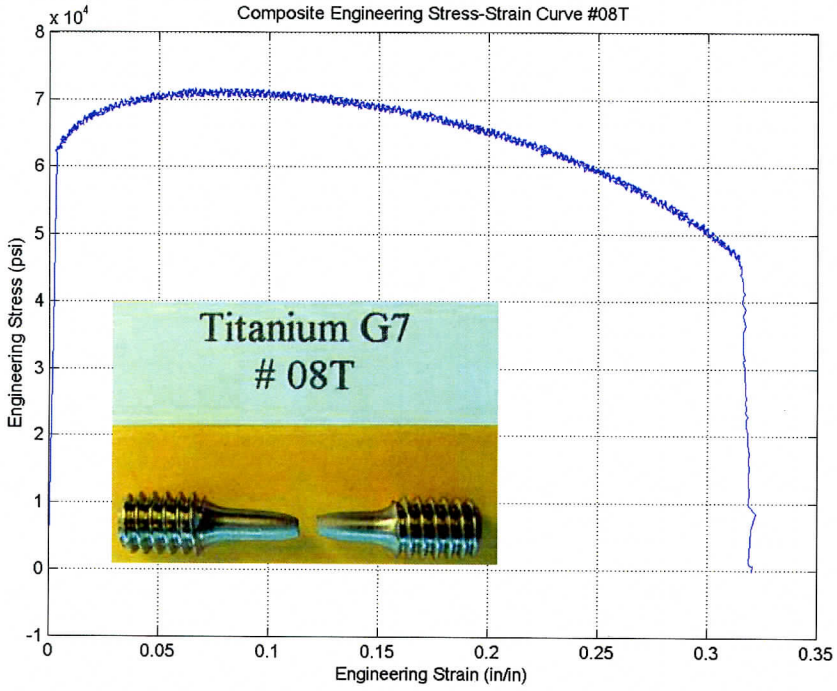

Figure 4-4: Composite Stress-Strain Curve for Titanium [48]

Table 4-3 Test Data And Results For Titanium Sample [48]

Characteristic	Units	Value
Velocity of the Test	in/sec	4.167E-03
Duration of the test	sec	2.446E+00
Average Strain Rate	1/sec	1.392E-01
Area Reduction	%	59.42%
Final Eng. Strain (raw)	%	35.07%
Final Eng. Strain (modified)	%	32.04%
Final Eng. Strain (actual)	%	34.11%
Strain Error	%	7.19%
Yield Strength	psi	62073.00
Ultimate Strength	psi	71772.07
Yield/Ultimate Strength	%	86.49%
Strain at Ultimate Strength	%	6.63%
Strain at Yield Strength	%	0.38%

4.2 Moderate Strain Rate Testing Procedures

The tensile impact tests at moderate strain rates were performed on an Instron/Dynatup 8250 test machine. The procedure for running the tensile impact experiments involves placing a sample in the fixture, Figures 3-5 through 3-6, and positioning the weighted striker at a predetermined height to achieve the desired impact velocity and impact energy. The fixture is placed in the environmental chamber, shown in Figure 2-5, for elevated temperature tests and heated according to the information in Table 4-4 [38]. The striker is allowed to fall due to gravity or it can be pneumatically pushed to achieve higher velocities. A sensor initiates data acquisition a few milliseconds prior to the impact.

Table 4-4 Specimen Heat Up Times for the Instron Environmental Chamber (± 2%) (non-Q, for information only)

Material	Set Point Temperature (°F)	Temperature Attained (°F)	Minimum Time To reach Temperature (Minutes)
Titanium Gr7	175	172	90
Titanium Gr 7	350	344	180
Steel 316L	175	172	80
Steel 316L	350	344	160
Alloy 22	175	172	75
Alloy 22	350	344	150

The only data collected during an experiment are force and time. The data processing software uses these data along with the initial velocity to calculate deflection, energy and velocity as a function of time. The raw deflection and force data are subsequently used to construct an engineering stress-strain curve as shown in Figure 4-5. The raw stress-strain curve is wavy due to the dynamic nature of the experiment. To determine yield and ultimate points, the

portion of the curve that corresponds to the elastic phase and the beginning of the plastic phase of the material behavior is fitted with a 6^{th} order polynomial as described in the previous section. The lower boundary of the yield region is defined at the point of maximum slope in the stress-strain curve. The upper boundary of the yield region is defined by averaging the midpoint values of the first two wave segments as shown in Figure 4-6. Yield strength is defined as the average value between the lower and upper boundaries. The yield strain is determined by assuming a value of the modulus of elasticity, Table 4-2, and using $\varepsilon_Y = \sigma_Y/E$. A three-part composite curve is created using a straight line from the origin to the yield point as part one, using the midpoints of all the wave segments to create part two, and using the actual data when there are no waves at the end as part three. A composite curve for a titanium specimen is shown in Figure 4-7 and a summary of the experimental data and results for that specimen are shown in Table 4-5.

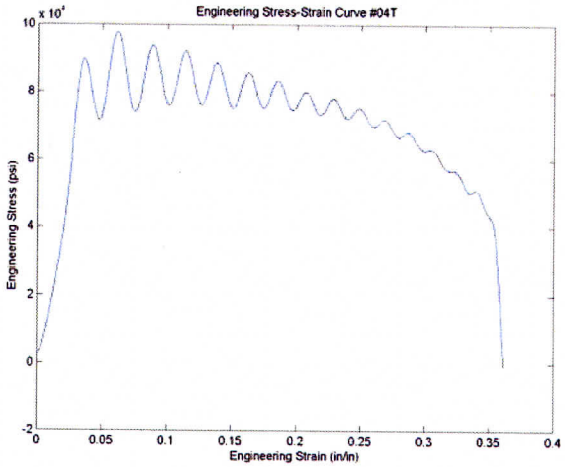

Figure 4-5: Dynamic Stress-Strain Curve From Raw Data For Titanium Sample [49]

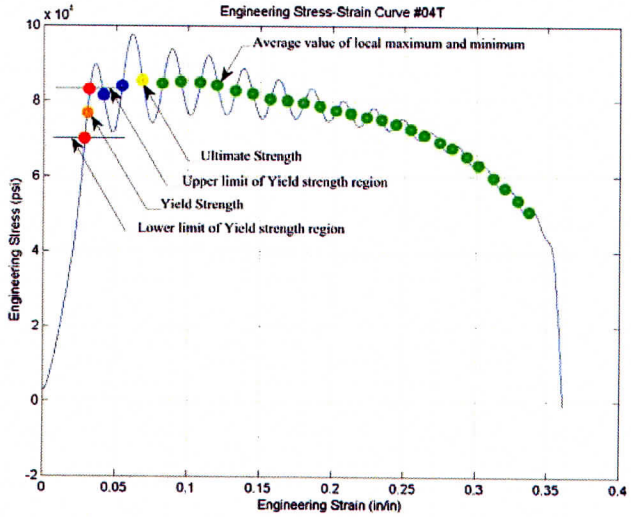

Figure 4-6: Construction of the Dynamic Composite Stress-Strain Curve [49]

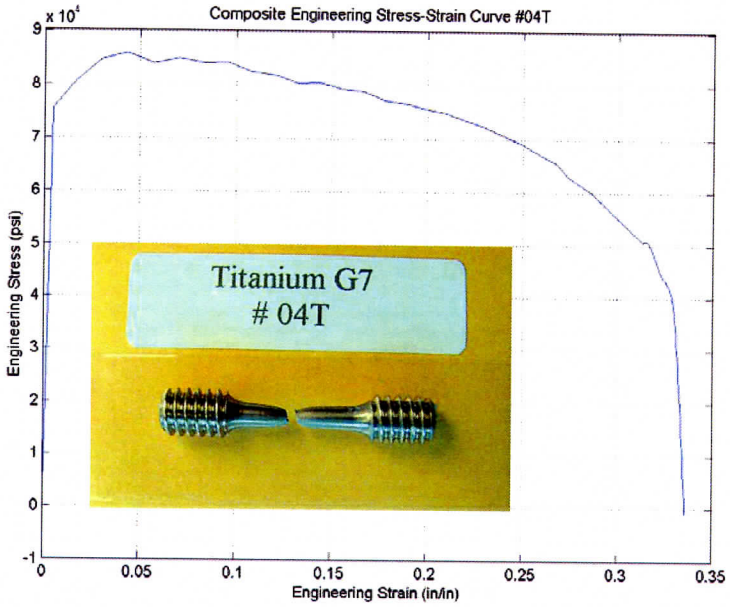

Figure 4-7: Dynamic Composite Stress-Strain Curve for Titanium [49]

Table 4-5 Dynamic Test Data And Results For Titanium Sample [49]

Characteristic	Units	Value
Test Height	in	1.392
Velocity of the Test	in/sec	3.279E+01
Duration of the test	sec	5.105E-03
Average Strain Rate	1/sec	7.285E+01
Area Reduction	%	58.17%
Final Eng. Strain (raw)	%	41.49%
Final Eng. Strain (mod)	%	33.60%
Final Eng. Strain (actual)	%	33.86%
Strain Error	%	2.11%
Yield Strength	psi	75633.87
Ultimate Strength	psi	85897.00
Yield/Ultimate Strength	%	88.05%
Strain at Ultimate Strength	%	4.32%
Strain at Yield Strength	%	0.46%

4.3 Data Handling for all QA Experiments

Data controlled electronically were protected by password protection on host machines, and limiting physical access; data were backed up and verified when transferred from one machine to another.

CHAPTER 5

RESULTS

This chapter presents test results obtained using the MTS axial/torsional and Instron Dynatup impact test machines. All tests and data reduction operations were carried out according to the procedures described in Chapters 4. Three candidate materials described in Chapter 2 were tested at a number of different strain rates ranging from 10^{-4} to 10^{2} sec^{-1}. The materials were tested at three different temperatures: ambient, 175 ^{O}F, and 350 ^{O}F. The testing was performed over a two-year period. Initial experiments were performed at room temperature. A second round of room temperature experiments was conducted because new fixtures were developed and a new material supplier was used when elevated temperature testing began. We wanted to determine if either of these factors would affect results.

5.1 Stainless Steel 316L

5.1.1 Initial Room Temperature Results for Stainless Steel 316L

Eleven tensile Stainless Steel 316L specimens were initially tested at room temperature to acquire mechanical properties at low and moderate strain rates. These samples were procured from the Metal Samples Company of Mumford, AL. Figures 5-1 through 5-7 show the variation of the following mechanical properties with strain rate:

Figure 5-1 Yield Strength vs. Strain Rate
Figure 5-2 Ultimate Strength vs. Strain Rate
Figure 5-3 (Yield Strength)/(Ultimate Strength) vs. Strain Rate
Figure 5-4 Final Cross-Sectional Area Reduction vs. Strain Rate
Figure 5-5 Failure Strain vs. Strain Rate
Figure 5-6 Ultimate Strain vs. Strain Rate
Figure 5-7 Error Between Computed Failure Strain and Measured Failure Strain

Each of these figures shows the average results for the 316L stainless steel as a solid green dot. The dots are fitted with a solid green power-law trendline and the equation is displayed on each figure. In addition, similar data were found in [9] for 304 stainless steel. This data was plotted as red diamonds and also fitted with a red dashed power-law trendline. This legend information is summarized in Table 5-1.

Table 5-1 Legend for Room Temperature Stainless Steel 316L Results Figures

Symbol	Presented Result
	Stainless Steel 304 data points [9]
	Fitted Curve of Stainless Steel 304 data points
	Stainless Steel 316L data points
	Average Values of Stainless Steel 316L data points
	Fitted Curve of Stainless Steel 316L data points

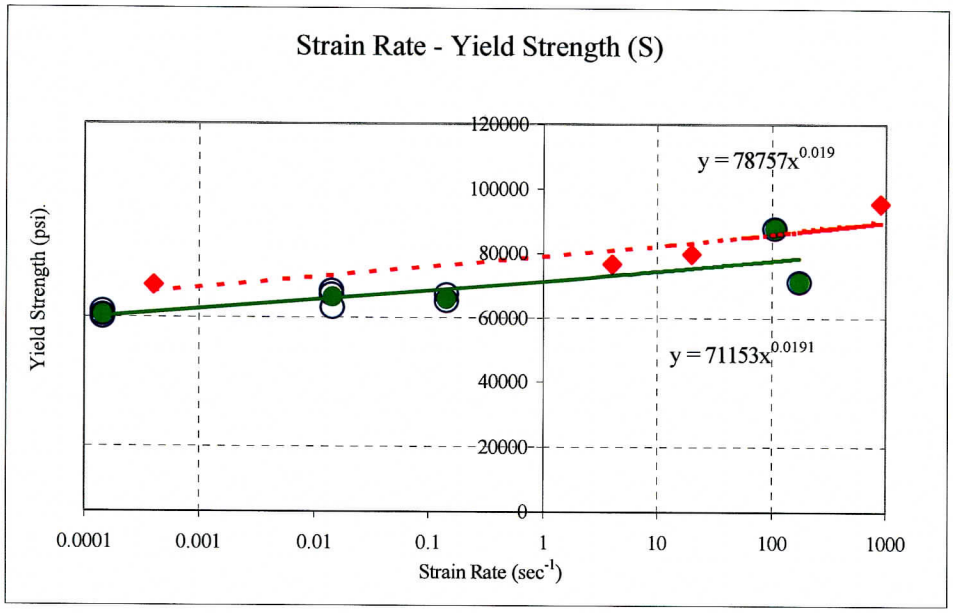

Figure 5-1 Room Temperature 316L Yield Strength vs. Strain Rate [50-56]

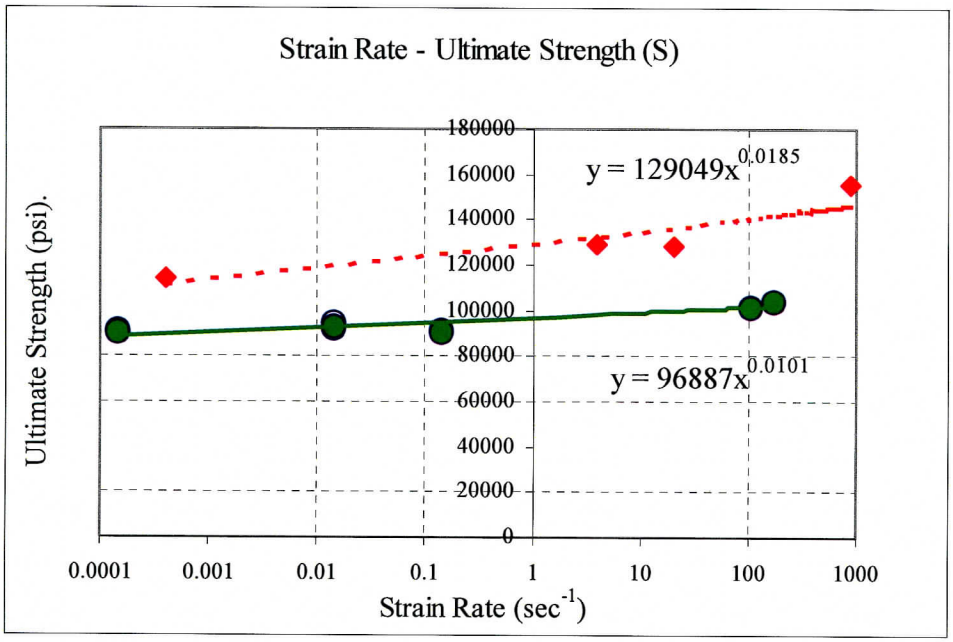

Figure 5-2 Room Temperature 316L Ultimate Strength vs. Strain Rate [50-56]

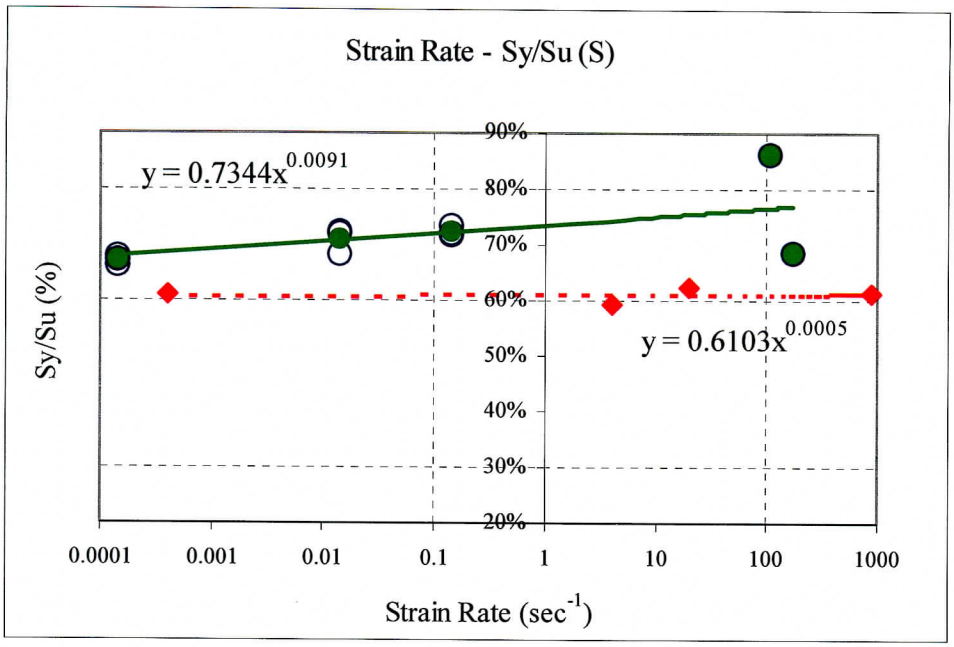

Figure 5-3 Room Temperature 316L σ_y/σ_u Ratio vs. Strain Rate [50-56]

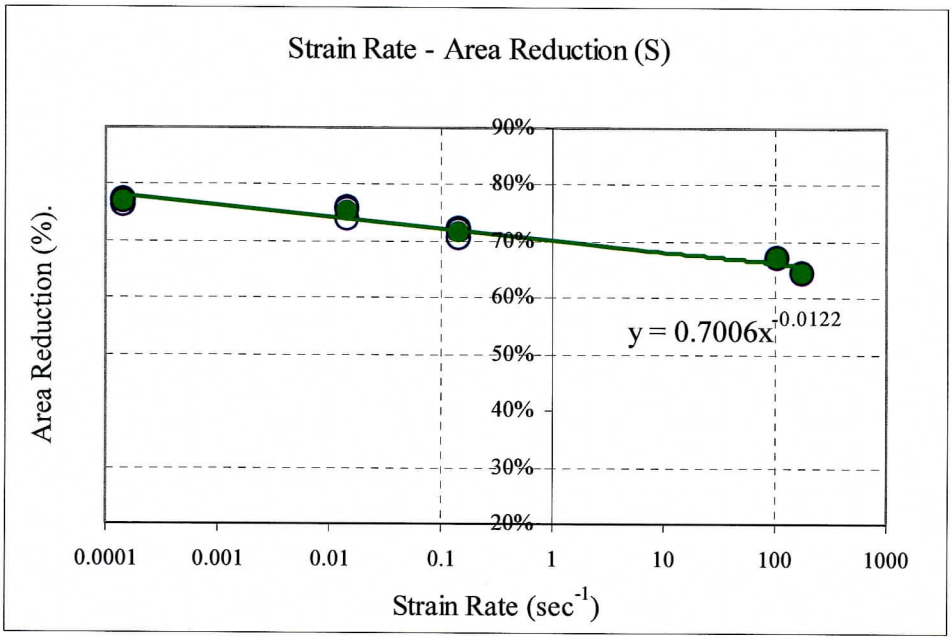

Figure 5-4 Room Temperature 316L
Final Cross-Sectional Area Reduction vs. Strain Rate [50-56]

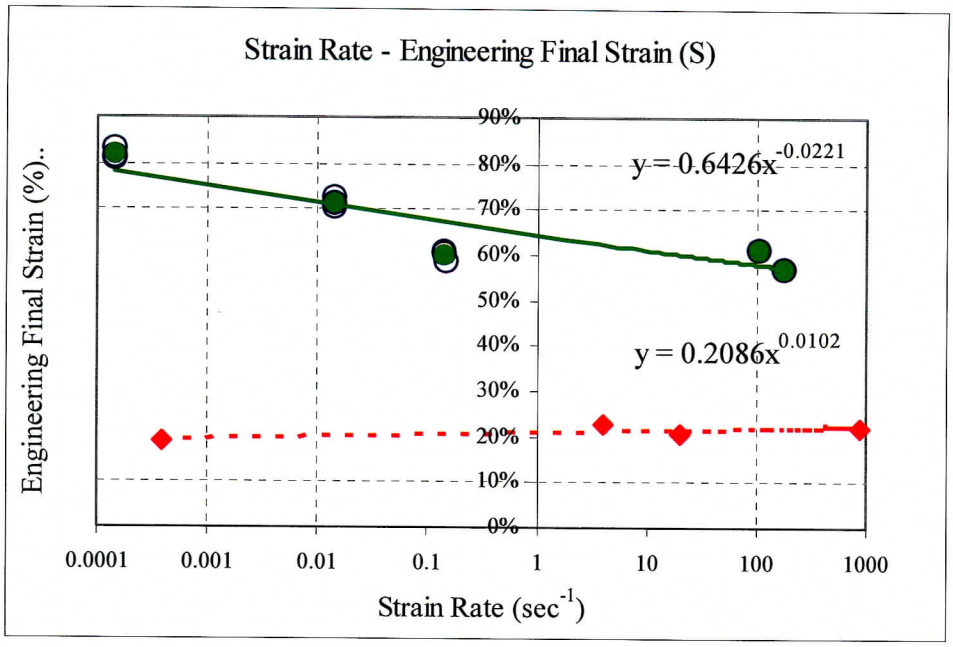

Figure 5-5 Room Temperature 316L Failure Strain vs. Strain Rate [50-56]

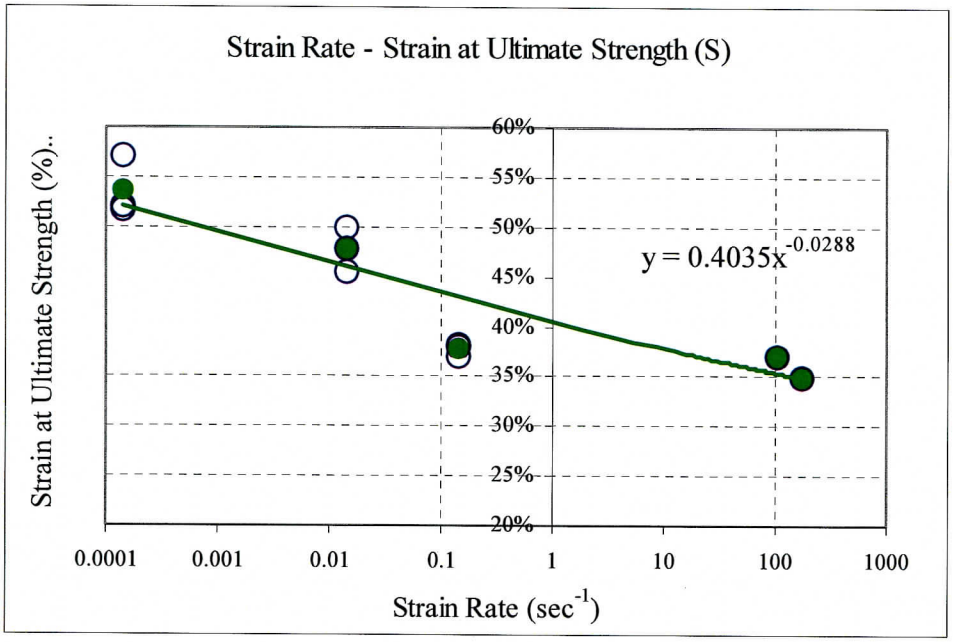

Figure 5-6 Room Temperature 316L Ultimate Strain vs. Strain Rate [50-56]

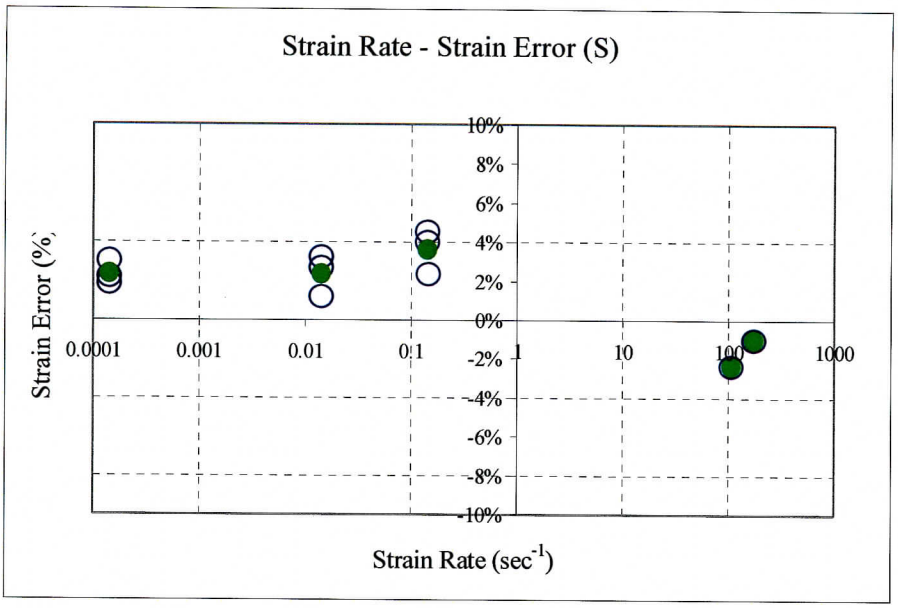

Figure 5-7 Room Temperature 316L Failure Strain Error vs. Strain Rate [50-56]

5.1.2 Elevated Temperature Results for Stainless Steel 316L

Eighteen tensile stainless steel 316L specimens were tested to acquire mechanical properties of this material at various strain rates and temperatures. These samples were procured from Laboratory Testing incorporated of Hatfield, PA. Figures 5-8 through 5-14 show the variation of the following mechanical properties with strain rate and temperature:

Figure 5-8 Yield Strength vs. Strain Rate
Figure 5-9 Ultimate Strength vs. Strain Rate
Figure 5-10 (Yield Strength)/(Ultimate Strength) vs. Strain Rate
Figure 5-11 Final Cross-Sectional Area Reduction vs. Strain Rate
Figure 5-12 Failure Strain vs. Strain Rate
Figure 5-13 Ultimate Strain vs. Strain Rate
Figure 5-14 Error Between Computed Failure Strain and Measured Failure Strain

The legend information for these figures is summarized in Table 5-2.

Table 5-2 Legend for Elevated Temperature Stainless Steel 316L Results Figures

Symbol	Presented Result
■	Average Data Points of the Material at Room Temperature
▲	Average Data Points of the Material at 175 °F Temperature
◆	Average Data Points of the Material at 350 °F Temperature
□	Data Points of the Material at Room Temperature
△	Data Points of the Material at 175 °F Temperature
◇	Data Points of the Material at 350 °F Temperature
—	Fitted Curve of the Material Data Points at Room Temperature
—	Fitted Curve of the Material Data Points at 175 °F Temperature
—	Fitted Curve of the Material Data Points at 350 °F Temperature

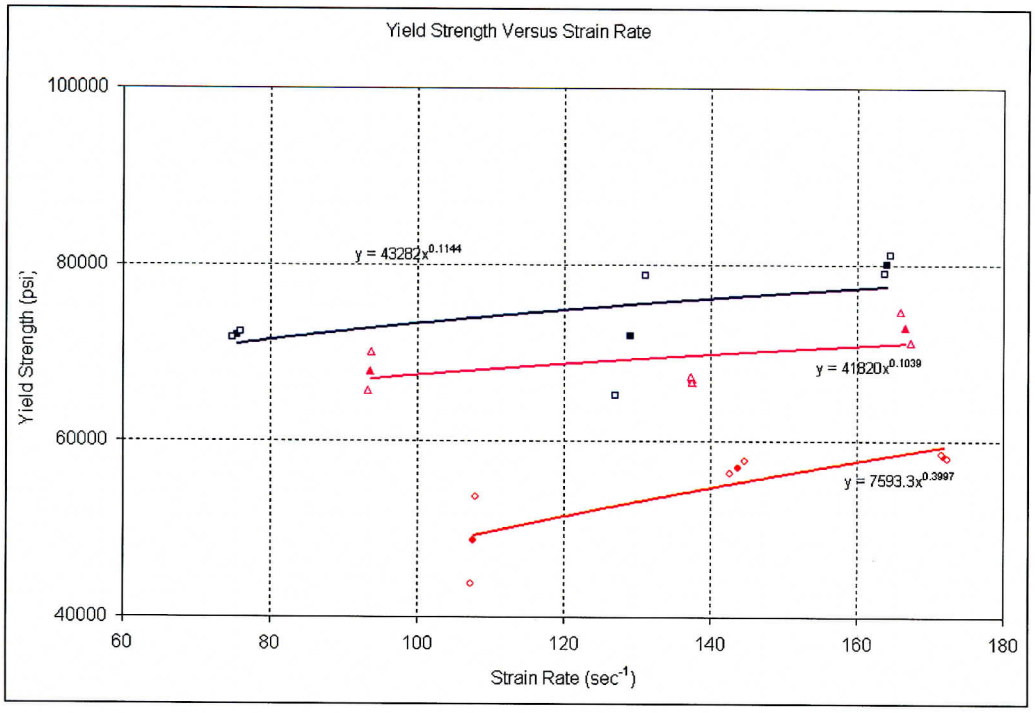

Figure 5-8 Stainless Steel 316L Yield Strength vs. Strain Rate and Temperature [57]

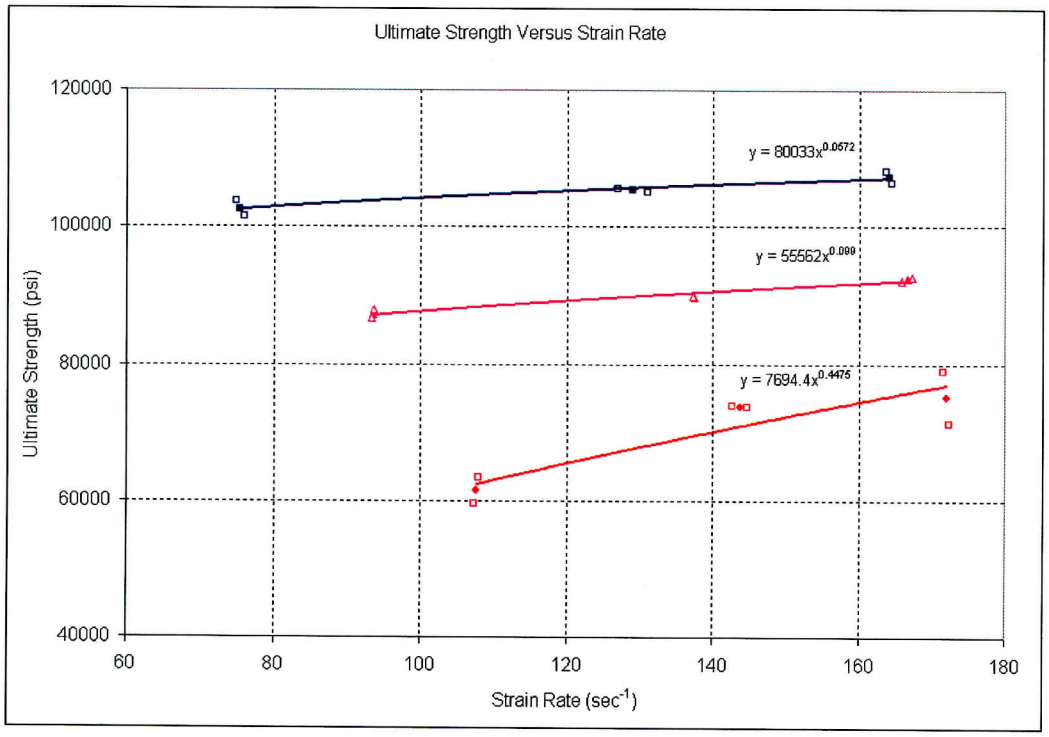

Figure 5-9 Stainless Steel 316L Ultimate Strength vs. Strain Rate and Temperature [57]

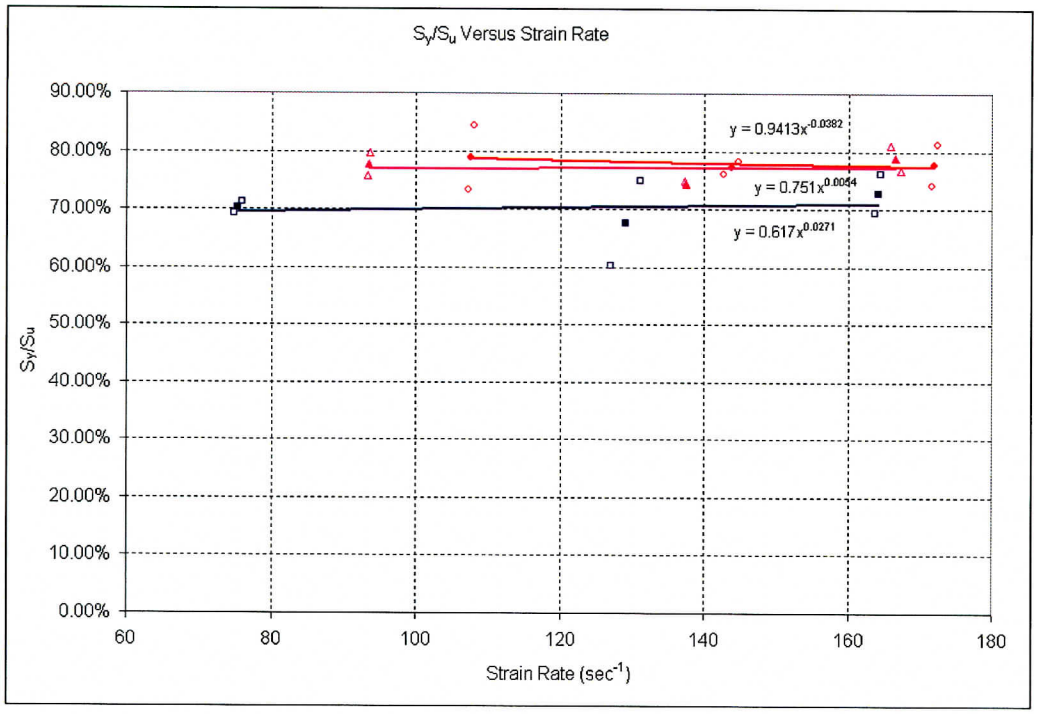

Figure 5-10 Stainless Steel 316L σ_y/σ_u Ratio vs. Strain Rate and Temperature [57]

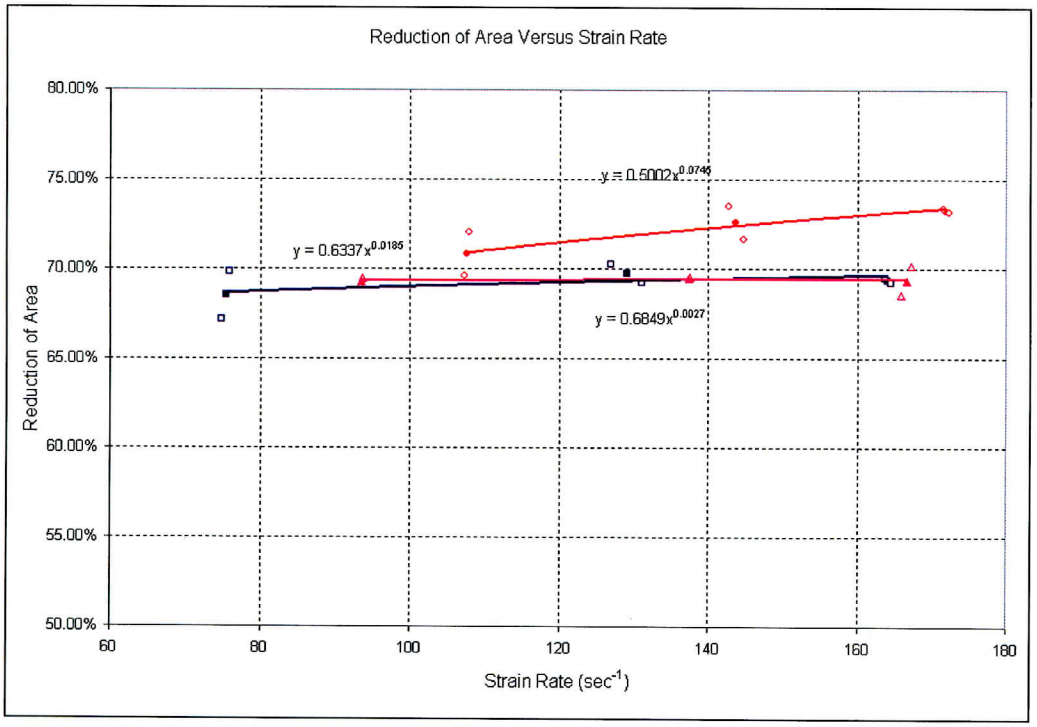

Figure 5-11 Stainless Steel 316L Final Area Reduction vs. Strain Rate and Temperature [57]

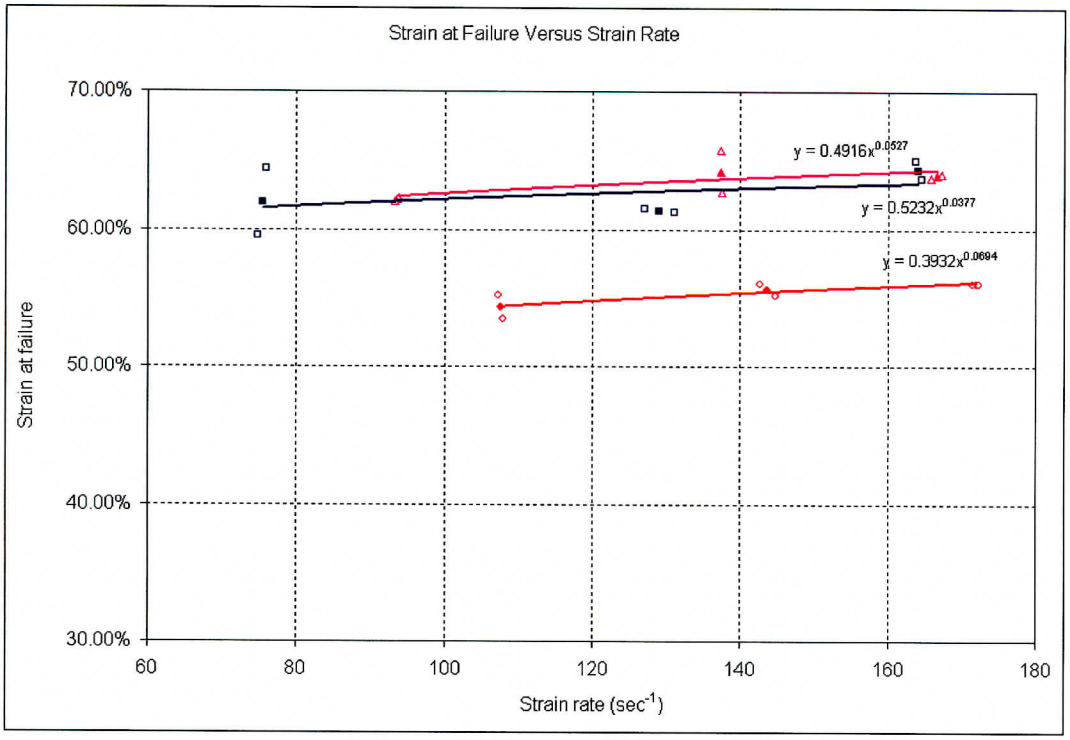

Figure 5-12 Stainless Steel 316L Failure Strain vs. Strain Rate and Temperature [57]

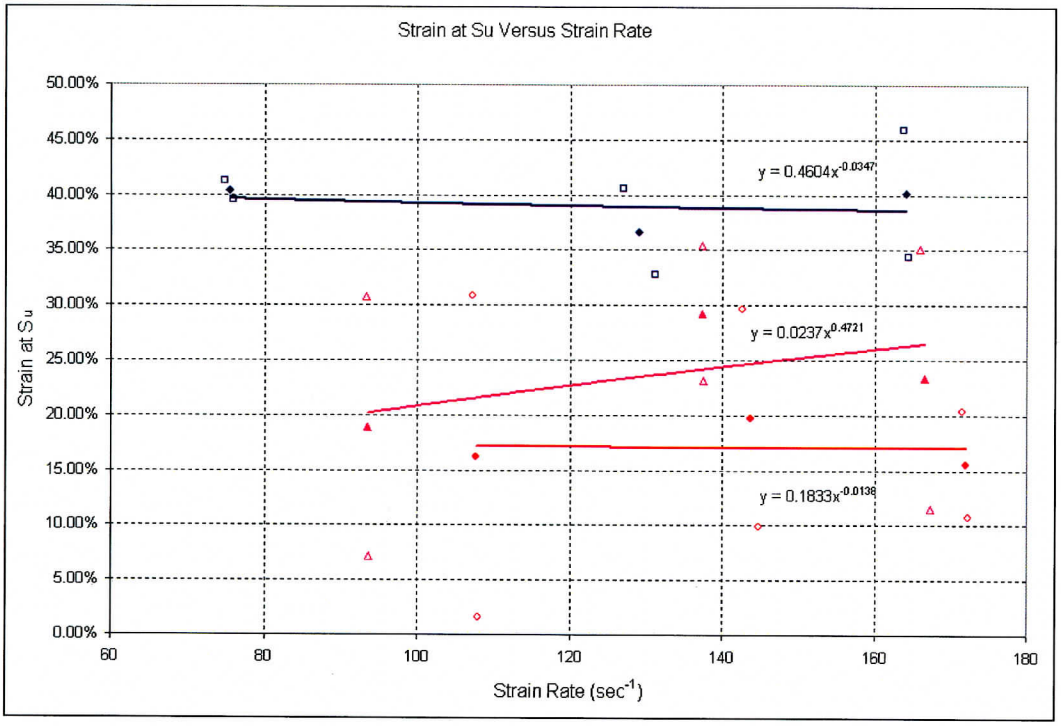

Figure 5-13 Stainless Steel 316L Ultimate Strain vs. Strain Rate and Temperature [57]

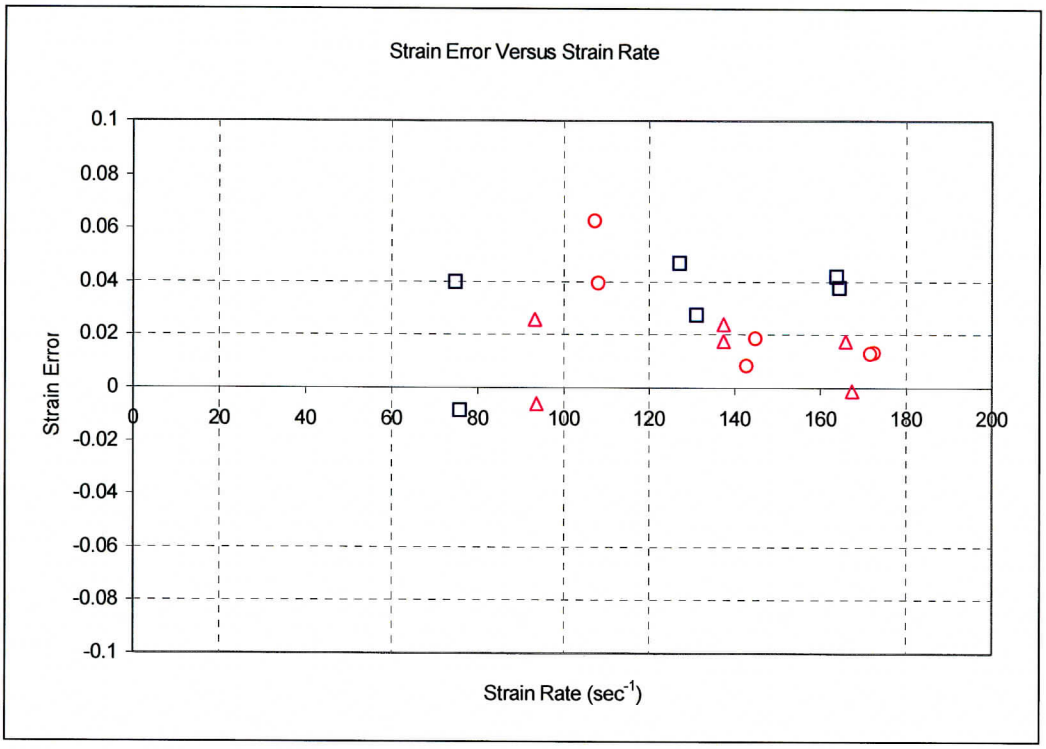

Figure 5-14 Stainless Steel 316L Failure Strain Error vs. Strain Rate and Temperature [57]

5.2 Titanium Alloy Grade 7

5.2.1 Initial Room Temperature Results for Titanium Alloy Grade 7

Fifteen tensile Titanium alloy Grade 7 specimens were initially tested at room temperature to acquire mechanical properties at low and moderate strain rates. These samples were procured from the Metal Samples Company of Mumford, AL. Figures 5-15 through 5-21 show the variation of the following mechanical properties with strain rate:

Figure 5-15 Yield Strength vs. Strain Rate
Figure 5-16 Ultimate Strength vs. Strain Rate
Figure 5-17 (Yield Strength)/(Ultimate Strength) vs. Strain Rate
Figure 5-18 Final Cross-Sectional Area Reduction vs. Strain Rate
Figure 5-19 Failure Strain vs. Strain Rate
Figure 5-20 Ultimate Strain vs. Strain Rate
Figure 5-21 Error Between Computed Failure Strain and Measured Failure Strain

Each of these figures shows the average results for the Titanium alloy Grade 7 as a solid green dot. The dots are fitted with a solid green power-law trendline and the equation is displayed on each figure. In addition, similar data were found in [9] for Titanium alloy Grade 6. This data was plotted as red diamonds and also fitted with a red dashed power-law trendline. This legend information is summarized in Table 5-3.

Table 5.3 Legend for Room Temperature Titanium Alloy Grade 7 Results Figures

Symbol	Presented Result
	Titanium Alloy 6Al-4V data points [9]
	Fitted Curve of Titanium Alloy 6Al-4V data points
	Titanium Alloy Grade 7 data points
	Average Values of Titanium Alloy Grade 7 data points
	Fitted Curve of Titanium Alloy Grade 7 average data points

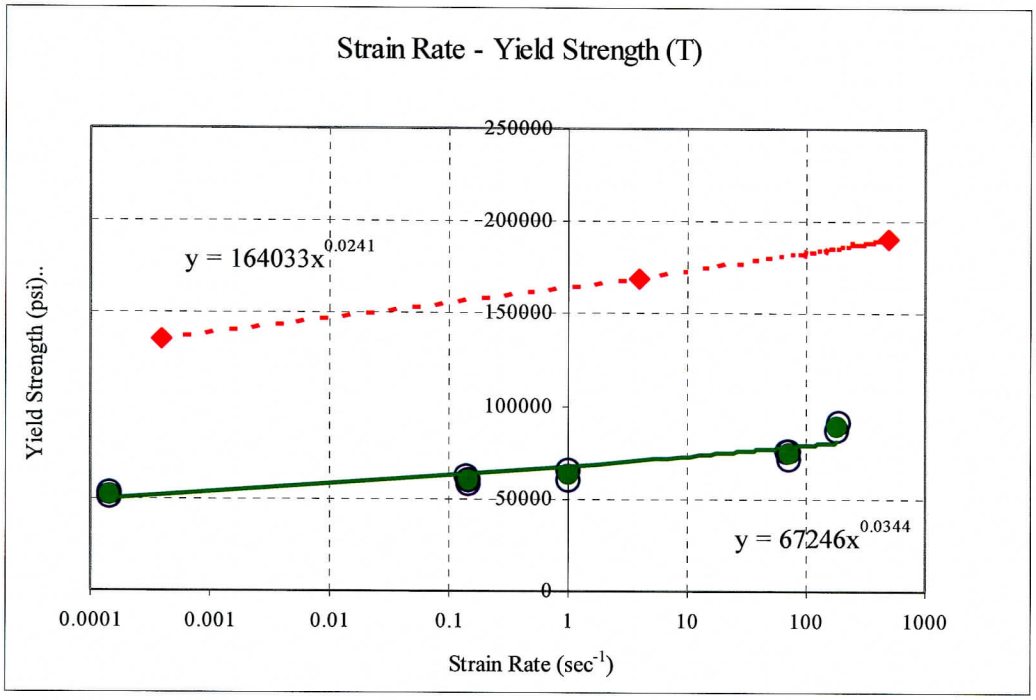

Figure 5-15 Room Temperature Titanium Yield Strength vs. Strain Rate [58-62]

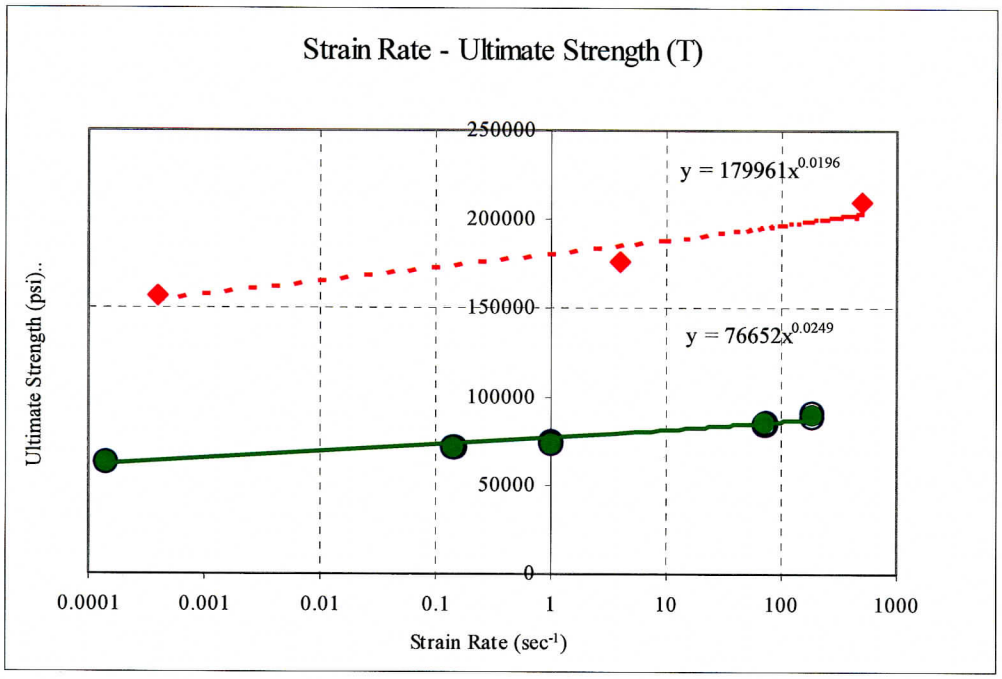

Figure 5-16 Room Temperature Titanium Ultimate Strength vs. Strain Rate [58-62]

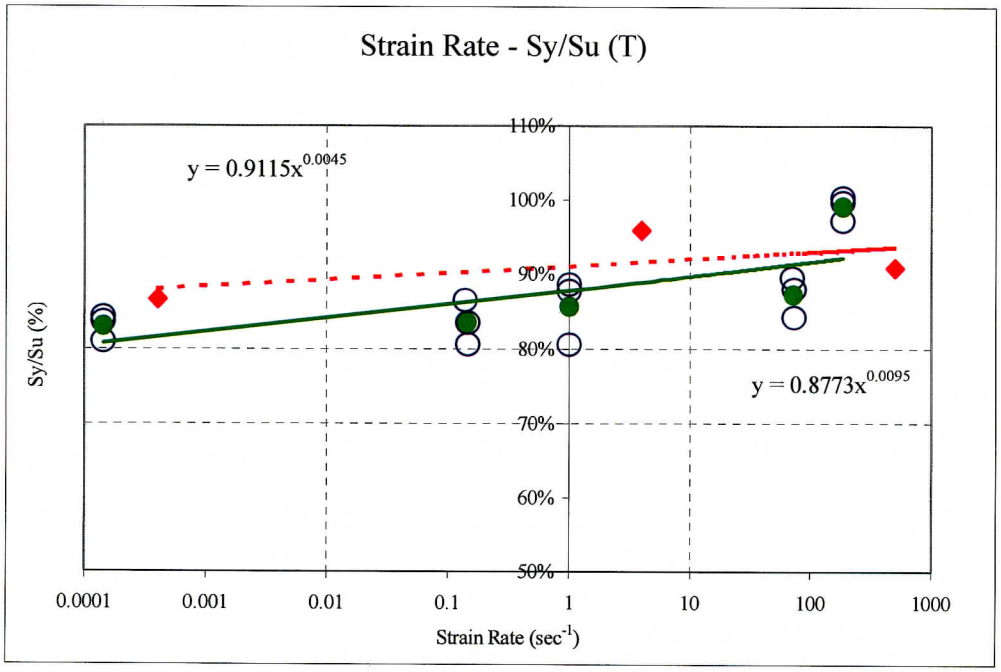

Figure 5-17 Room Temperature Titanium σ_y/σ_u Ratio vs. Strain Rate [58-62]

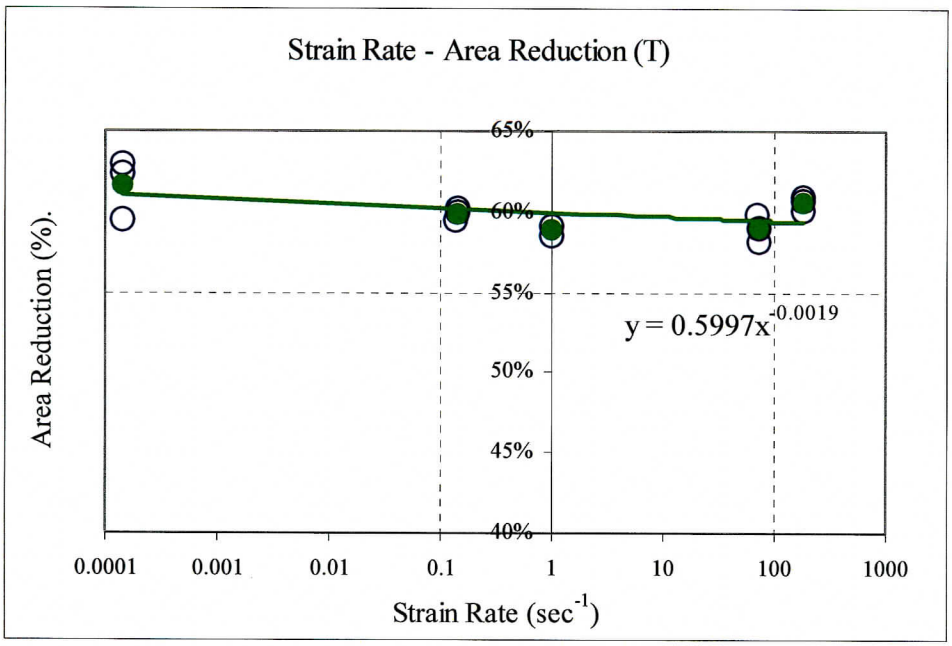

Figure 5-18 Room Temperature Titanium Final Area Reduction vs. Strain Rate [58-62]

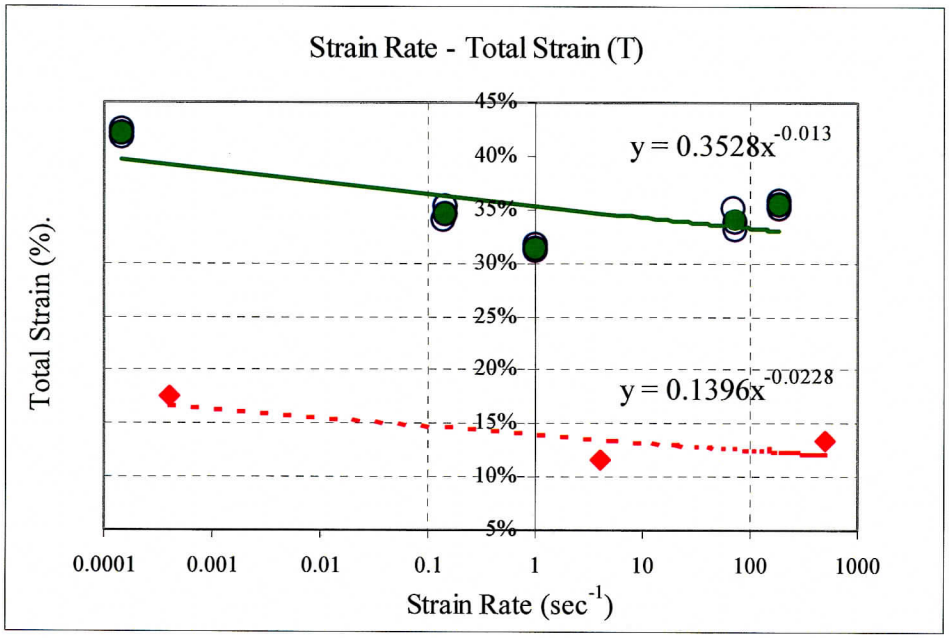

Figure 5-19 Room Temperature Titanium Failure Strain vs. Strain Rate [58-62]

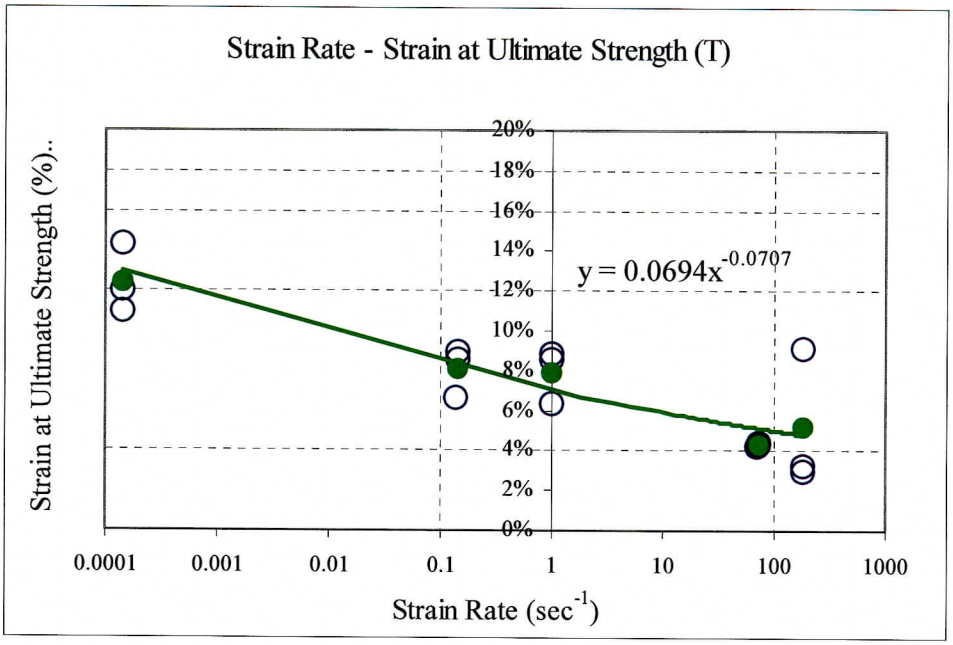

Figure 5-20 Room Temperature Titanium Ultimate Strain vs. Strain Rate [58-62]

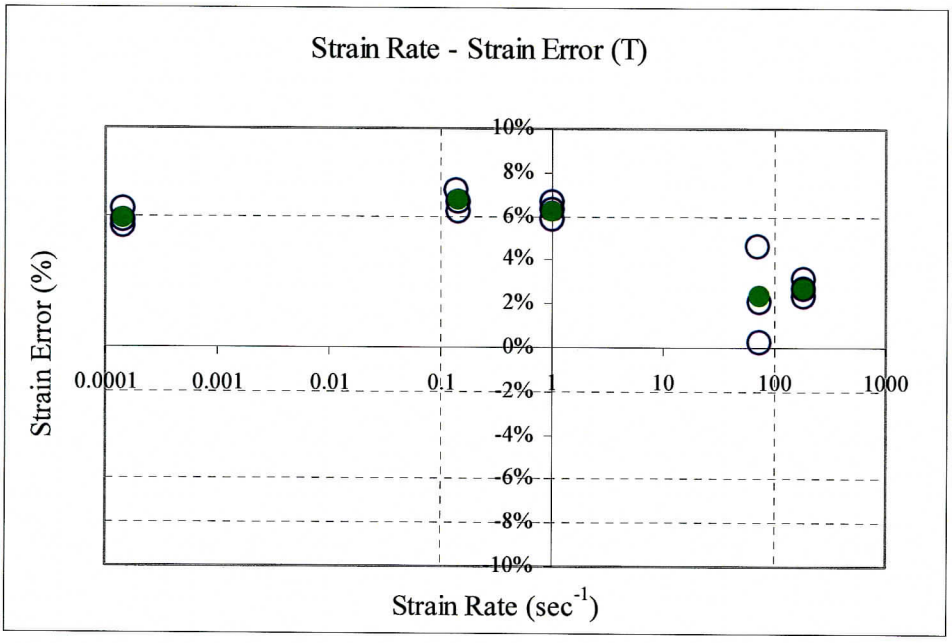

Figure 5-21 Room Temperature Titanium Failure Strain Error vs. Strain Rate [58-62]

5.2.2 Elevated Temperature Results for Titanium Alloy Grade 7

Eighteen tensile Titanium Alloy Grade 7 specimens were tested to acquire mechanical properties at various strain rates and temperatures. These samples were procured from Laboratory Testing incorporated of Hatfield, PA. Figures 5-22 through 5-28 show the variation of the following mechanical properties with strain rate and temperature:

Figure 5-22 Yield Strength vs. Strain Rate
Figure 5-23 Ultimate Strength vs. Strain Rate
Figure 5-24 (Yield Strength)/(Ultimate Strength) vs. Strain Rate
Figure 5-25 Final Cross-Sectional Area Reduction vs. Strain Rate
Figure 5-26 Failure Strain vs. Strain Rate
Figure 5-27 Ultimate Strain vs. Strain Rate
Figure 5-28 Error Between Computed Failure Strain and Measured Failure Strain

The legend information for these figures is summarized in Table 5-4.

Table 5-4 Legend for Elevated Temperature Titanium Alloy Grade 7 Results Figures

Symbol	Presented Result
■	Average Data Points of the Material at Room Temperature
▲	Average Data Points of the Material at 175 °F Temperature
◆	Average Data Points of the Material at 350 °F Temperature
□	Data Points of the Material at Room Temperature
△	Data Points of the Material at 175 °F Temperature
◇	Data Points of the Material at 350 °F Temperature
——	Fitted Curve of the Material Data Points at Room Temperature
——	Fitted Curve of the Material Data Points at 175 °F Temperature
——	Fitted Curve of the Material Data Points at 350 °F Temperature

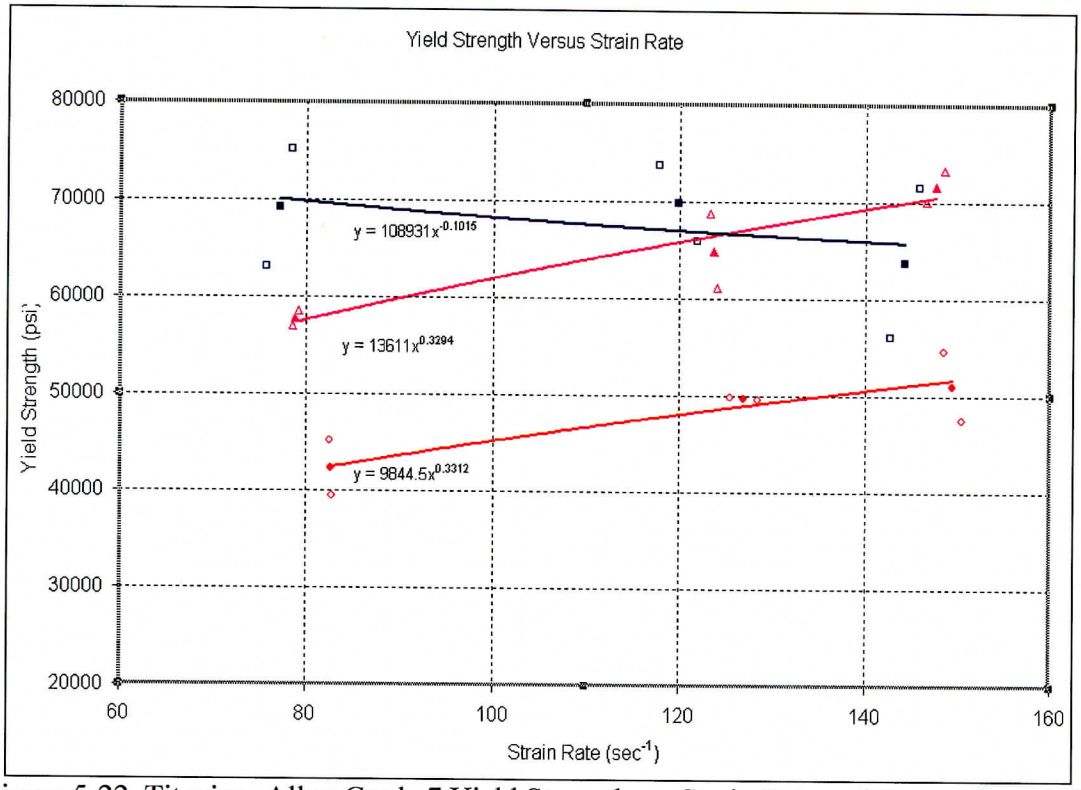

Figure 5-22 Titanium Alloy Grade 7 Yield Strength vs. Strain Rate and Temperature [63]

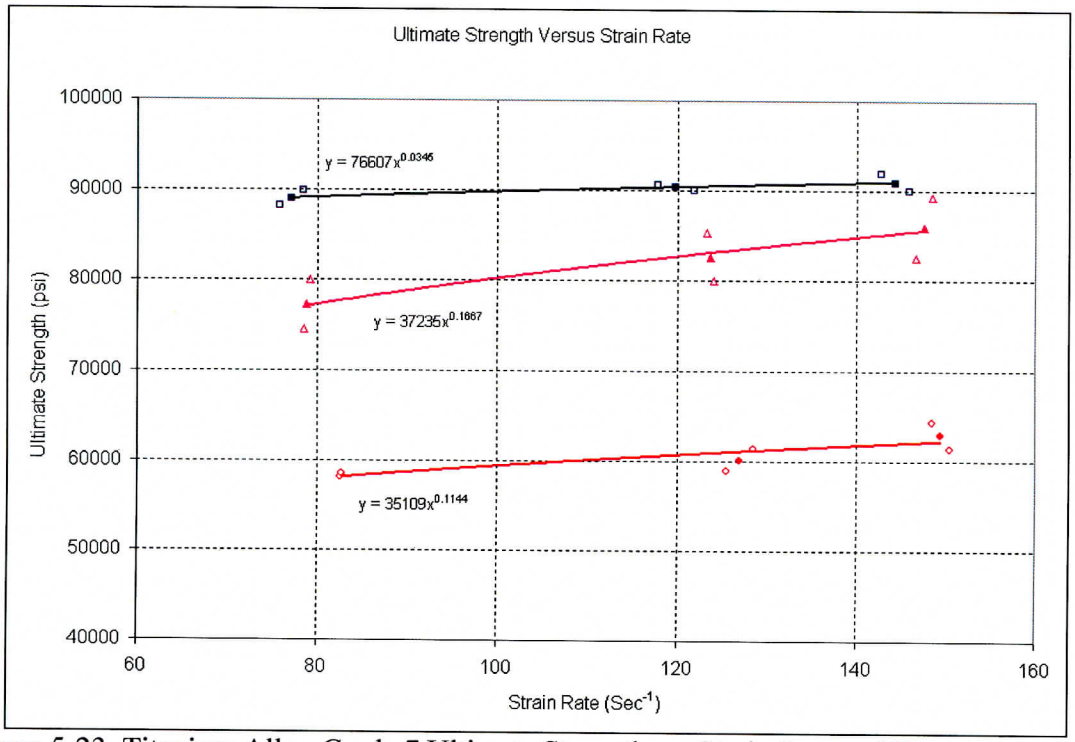

Figure 5-23 Titanium Alloy Grade 7 Ultimate Strength vs. Strain Rate and Temperature [63]

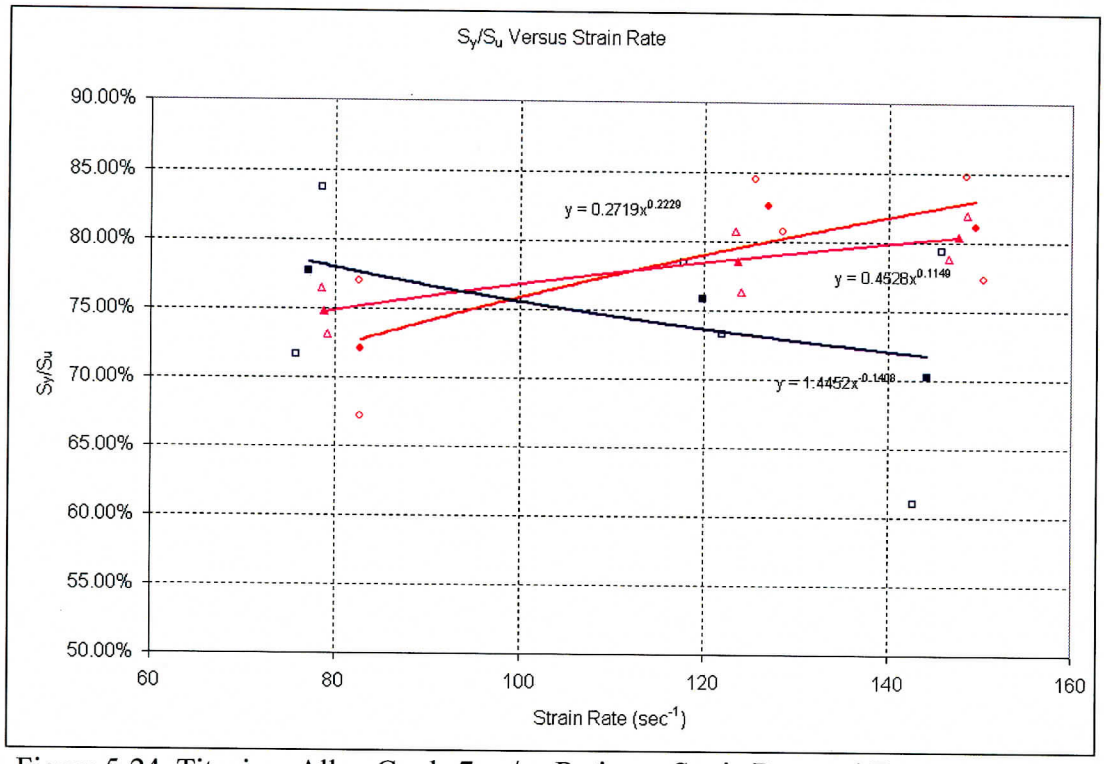

Figure 5-24 Titanium Alloy Grade 7 σ_y/σ_u Ratio vs. Strain Rate and Temperature [63]

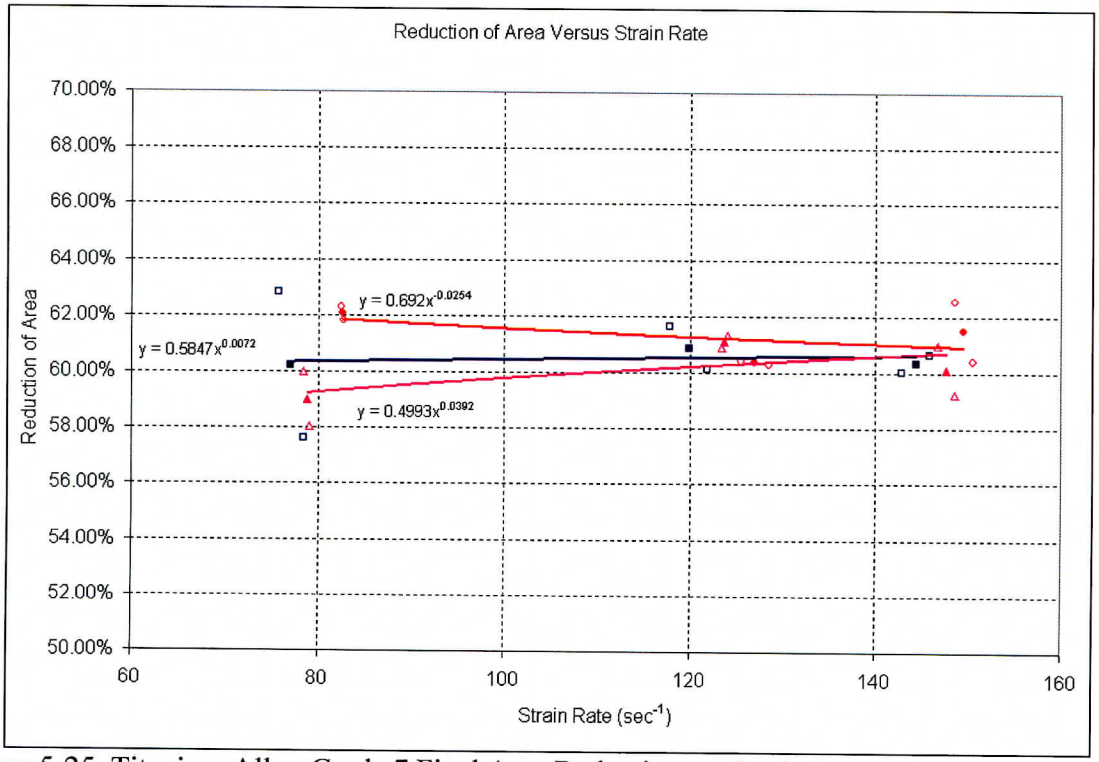

Figure 5-25 Titanium Alloy Grade 7 Final Area Reduction vs. Strain Rate and Temperature [63]

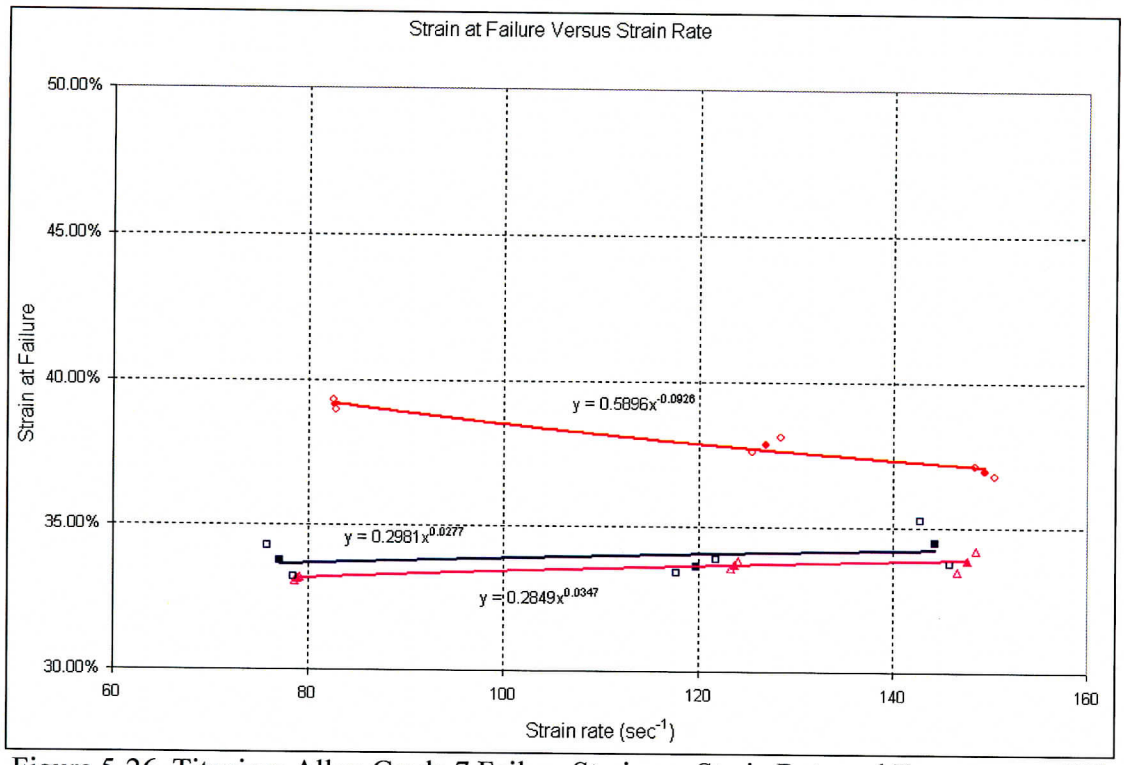

Figure 5-26 Titanium Alloy Grade 7 Failure Strain vs. Strain Rate and Temperature [63]

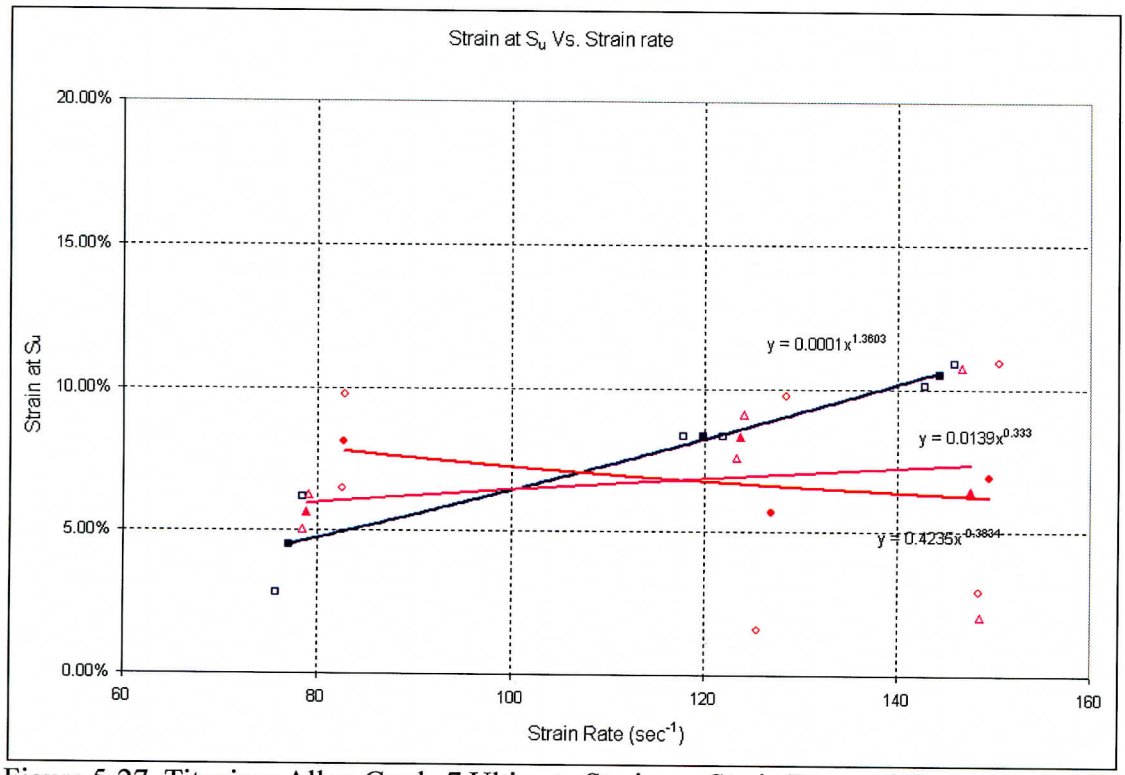

Figure 5-27 Titanium Alloy Grade 7 Ultimate Strain vs. Strain Rate and Temperature [63]

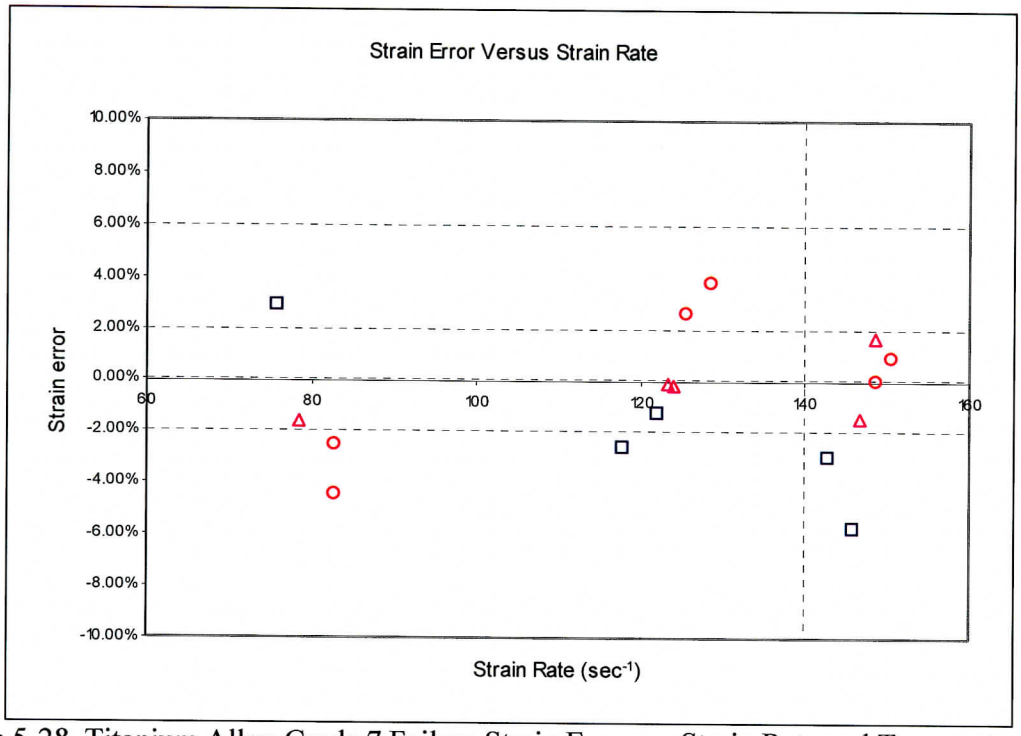

Figure 5-28 Titanium Alloy Grade 7 Failure Strain Error vs. Strain Rate and Temperature [63]

5.3 Alloy C22

5.3.1 Initial Room Temperature Results for Alloy C22

Eighteen tensile Alloy C22 specimens were initially tested at room temperature to acquire mechanical properties at low and moderate strain rates. These samples were procured from the Metal Samples Company of Mumford, AL. Figures 5-29 through 5-35 show the variation of the following mechanical properties with strain rate:

Figure 5-29 Yield Strength vs. Strain Rate
Figure 5-30 Ultimate Strength vs. Strain Rate
Figure 5-31 (Yield Strength)/(Ultimate Strength) vs. Strain Rate
Figure 5-32 Final Cross-Sectional Area Reduction vs. Strain Rate
Figure 5-33 Failure Strain vs. Strain Rate
Figure 5-34 Ultimate Strain vs. Strain Rate
Figure 5-35 Error Between Computed Failure Strain and Measured Failure Strain

Each of these figures shows the average results for the Alloy C22 as a solid green dot. The dots are fitted with a solid green power-law trendline and the equation is displayed on each figure. This legend information is summarized in Table 5-5.

Table 5-5 Legend for Alloy C22 Result Figures

Symbol	Presented Result
	Alloy C22 data points
	Average Values of Alloy C22 data points
	Fitted Curve of Alloy C22 average data points

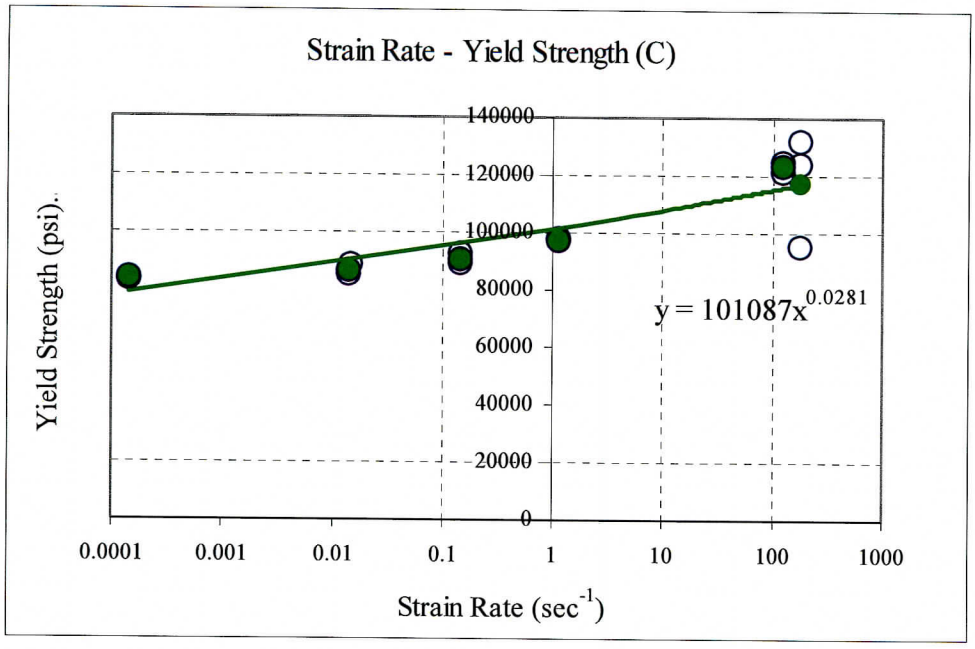

Figure 5-29 Room Temperature Alloy C22 Yield Strength vs. Strain Rate [64-69]

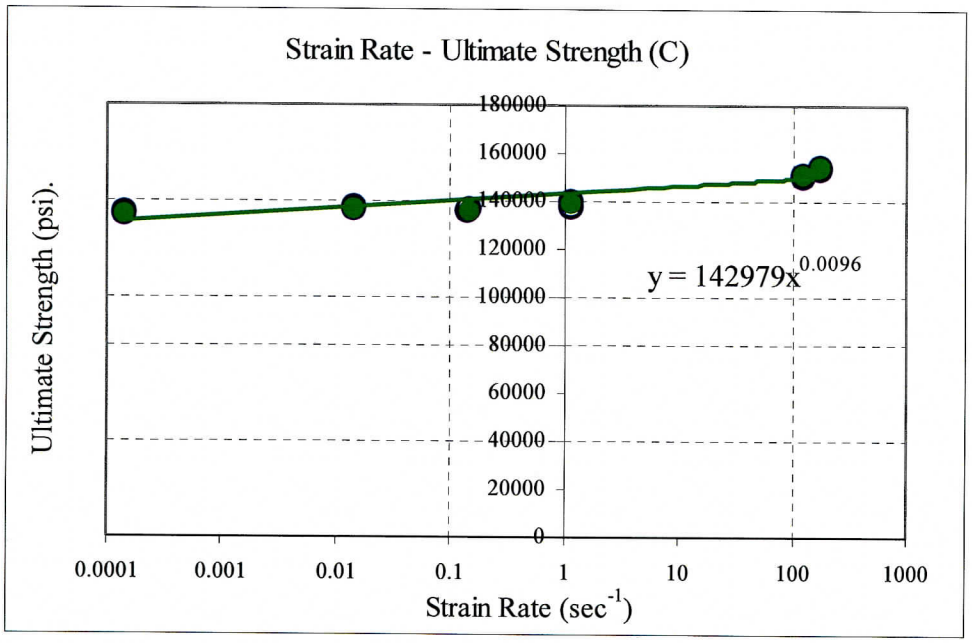

Figure 5-30 Room Temperature Alloy C22 Ultimate Strength vs. Strain Rate [64-69]

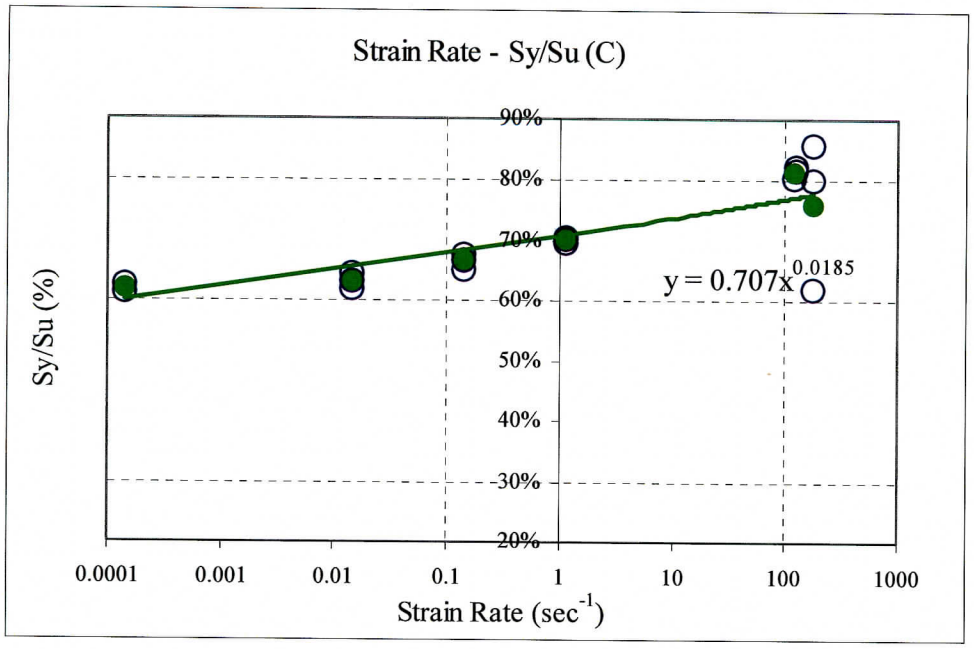

Figure 5-31 Room Temperature Alloy C22 σ_y/σ_u Ratio vs. Strain Rate [64-69]

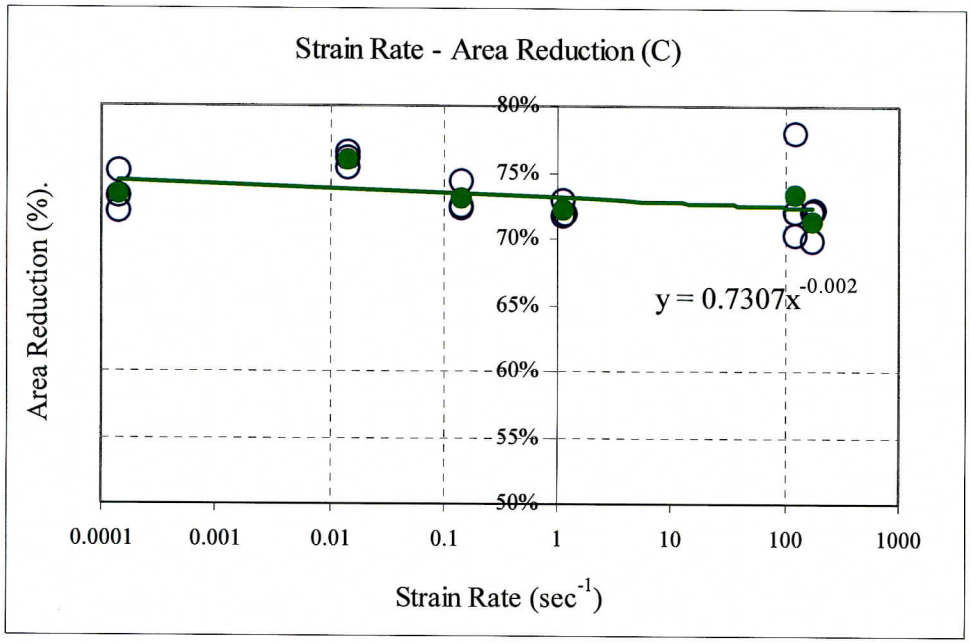

Figure 5-32 Room Temperature Alloy C22 Final Area Reduction vs. Strain Rate [64-69]

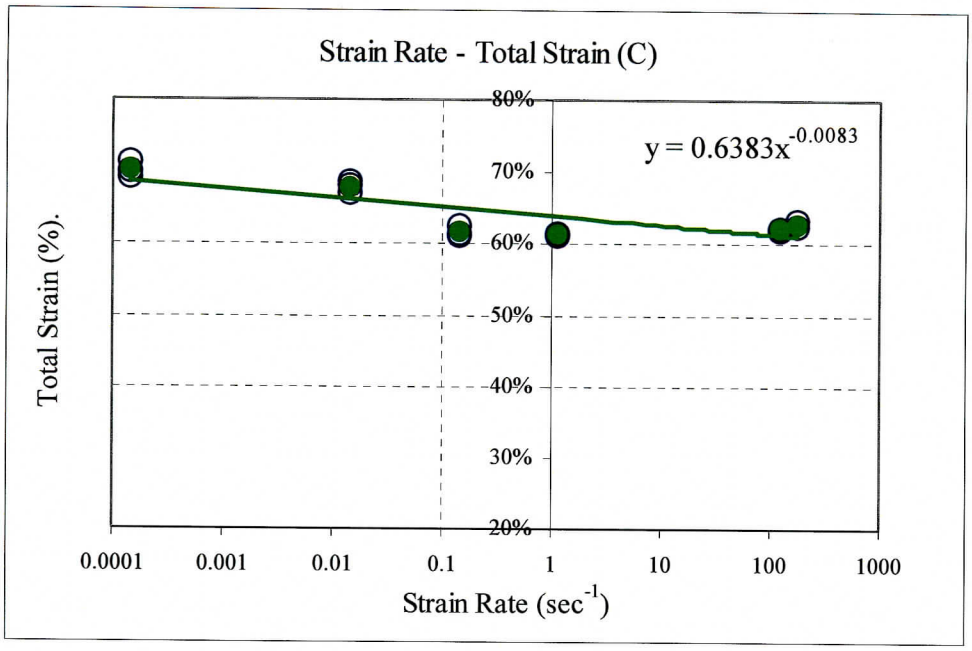

Figure 5-33 Room Temperature Alloy C22 Failure Strain vs. Strain Rate [64-69]

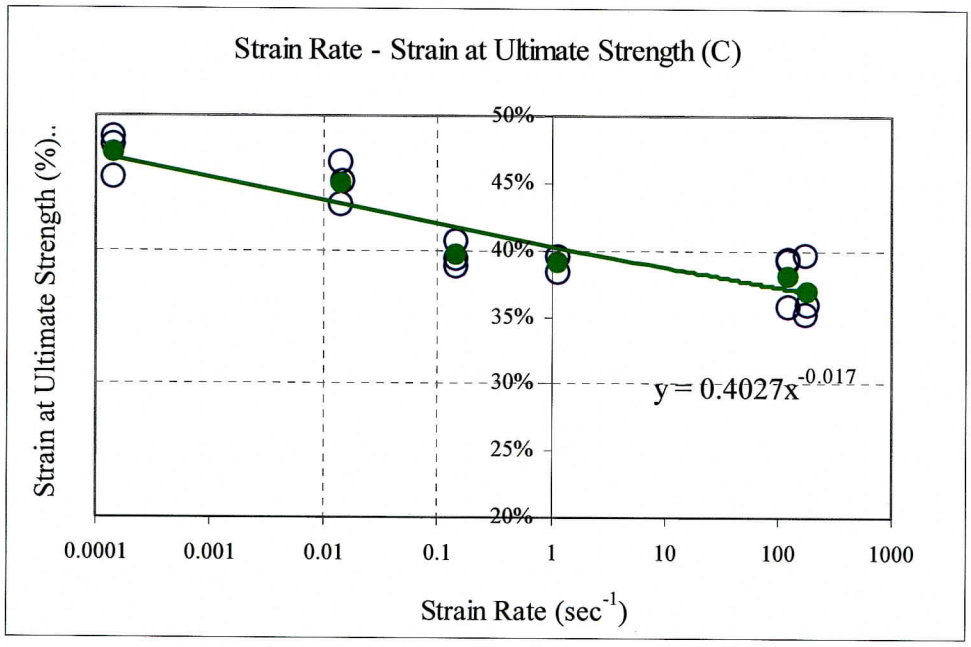

Figure 5-34 Room Temperature Alloy C22 Ultimate Strain vs. Strain Rate [64-69]

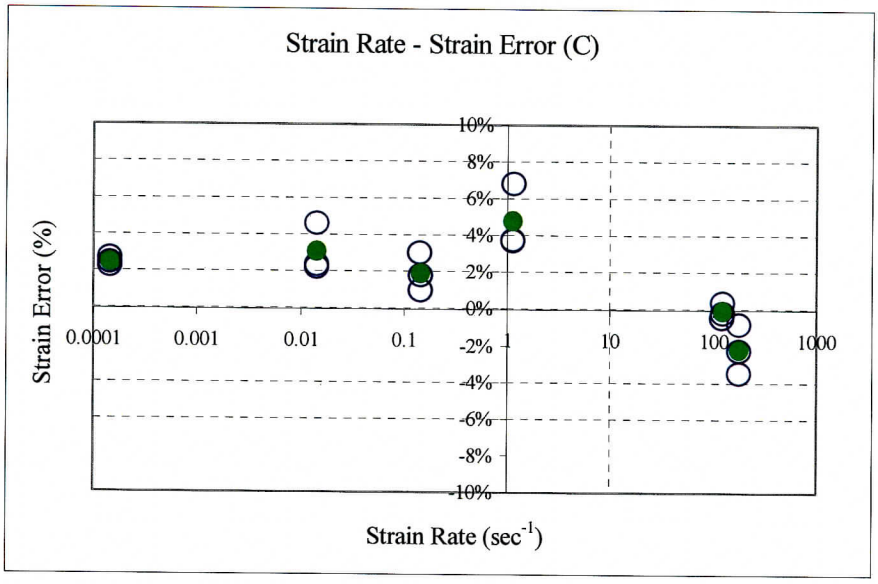

Figure 5-35 Room Temperature Alloy C22 Failure Strain Error vs. Strain Rate [64-69]

5.3.2 Elevated Temperature Results for Alloy C22

Eighteen tensile Alloy C22 specimens were tested to acquire mechanical properties at various strain rates and temperatures. These samples were procured from Laboratory Testing incorporated of Hatfield, PA. Figures 5-36 through 5-42 show the variation of the following mechanical properties with strain rate and temperature:

Figure 5-36 Yield Strength vs. Strain Rate
Figure 5-37 Ultimate Strength vs. Strain Rate
Figure 5-38 (Yield Strength)/(Ultimate Strength) vs. Strain Rate
Figure 5-39 Final Cross-Sectional Area Reduction vs. Strain Rate
Figure 5-40 Failure Strain vs. Strain Rate
Figure 5-41 Ultimate Strain vs. Strain Rate
Figure 5-42 Error Between Computed Failure Strain and Measured Failure Strain

The legend information for these figures is summarized in Table 5-6.

Table 5-6 Legend for Elevated Temperature Alloy C22 Results Figures

Symbol	Presented Result
■	Average Data Points of the Material at Room Temperature
▲	Average Data Points of the Material at 175 °F Temperature
◆	Average Data Points of the Material at 350 °F Temperature
□	Data Points of the Material at Room Temperature
△	Data Points of the Material at 175 °F Temperature
◇	Data Points of the Material at 350 °F Temperature
—	Fitted Curve of the Material Data Points at Room Temperature
—	Fitted Curve of the Material Data Points at 175 °F Temperature
—	Fitted Curve of the Material Data Points at 350 °F Temperature

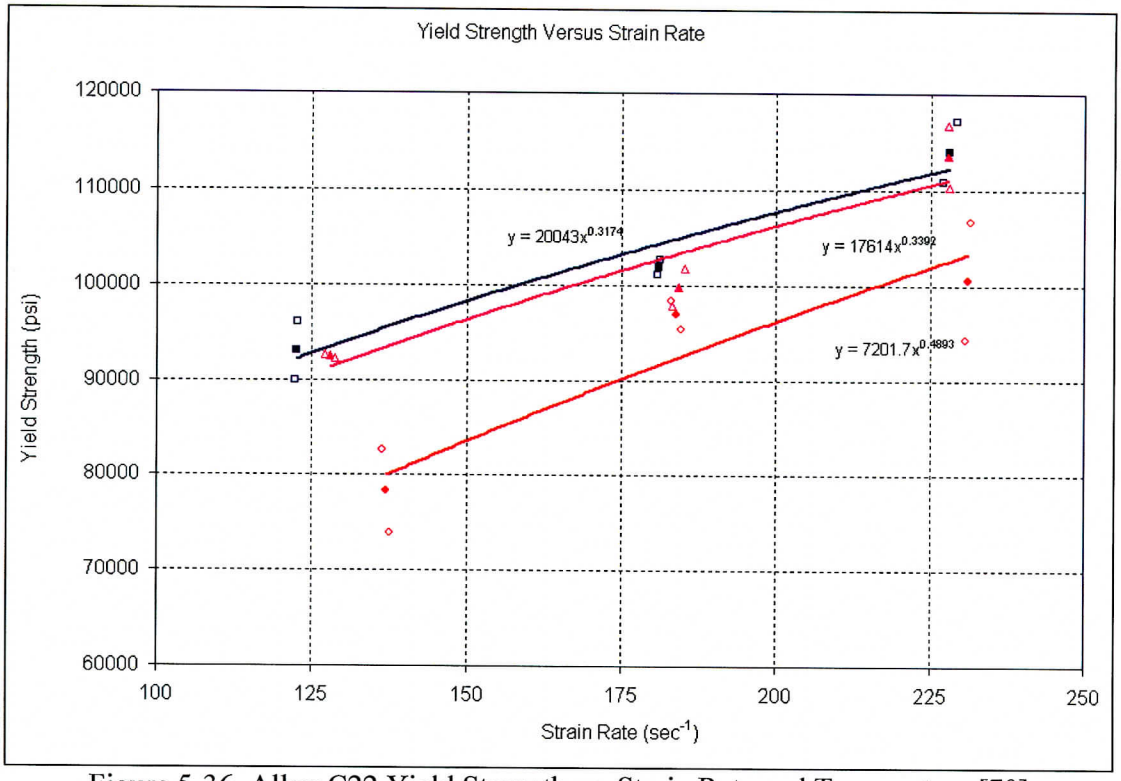

Figure 5-36 Alloy C22 Yield Strength vs. Strain Rate and Temperature [70]

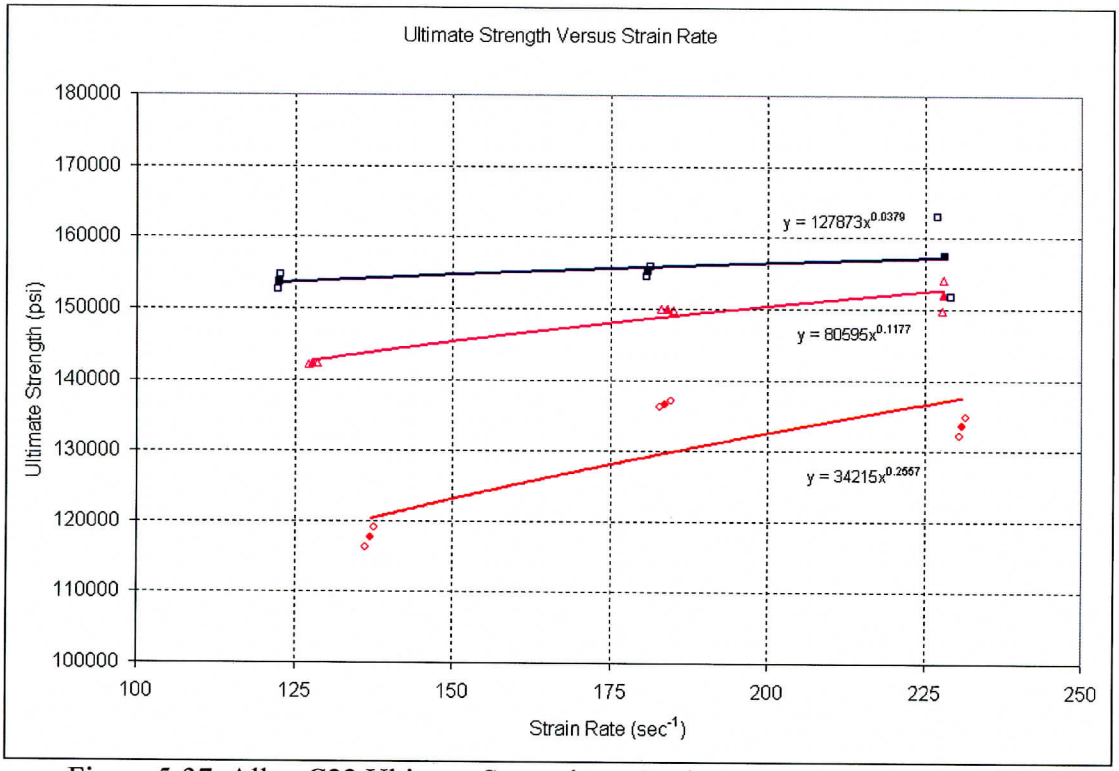

Figure 5-37 Alloy C22 Ultimate Strength vs. Strain Rate and Temperature [70]

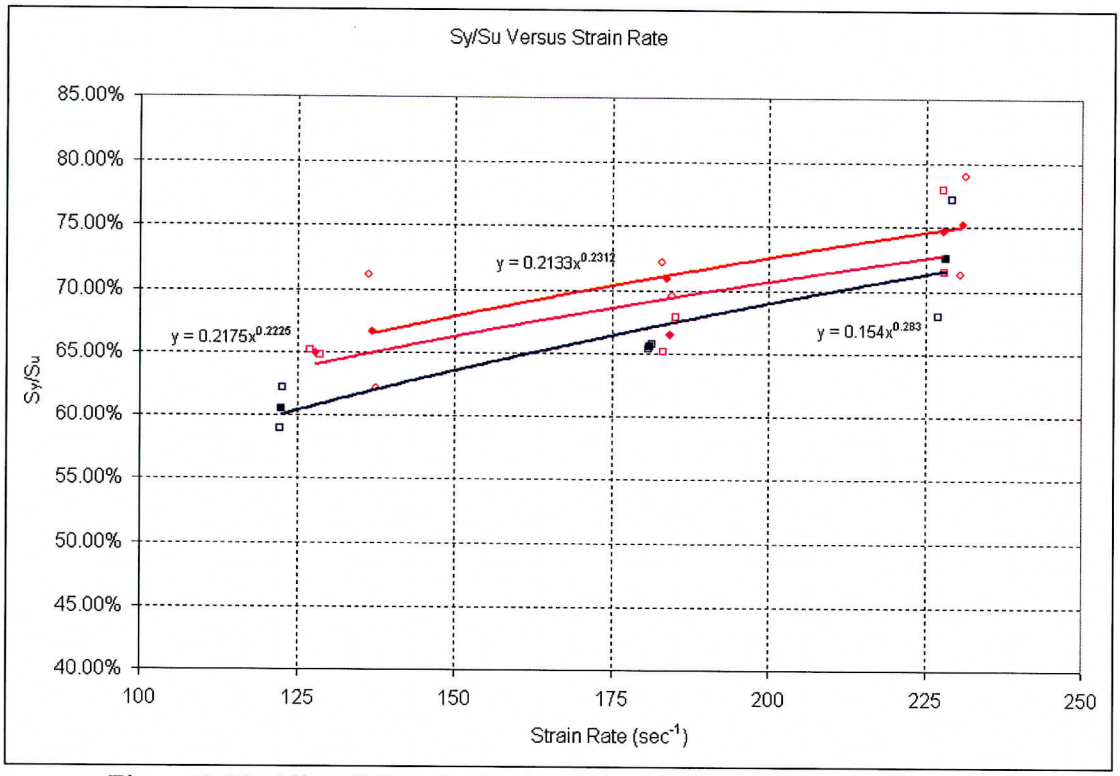

Figure 5-38 Alloy C22 σ_y/σ_u Ratio vs. Strain Rate and Temperature [70]

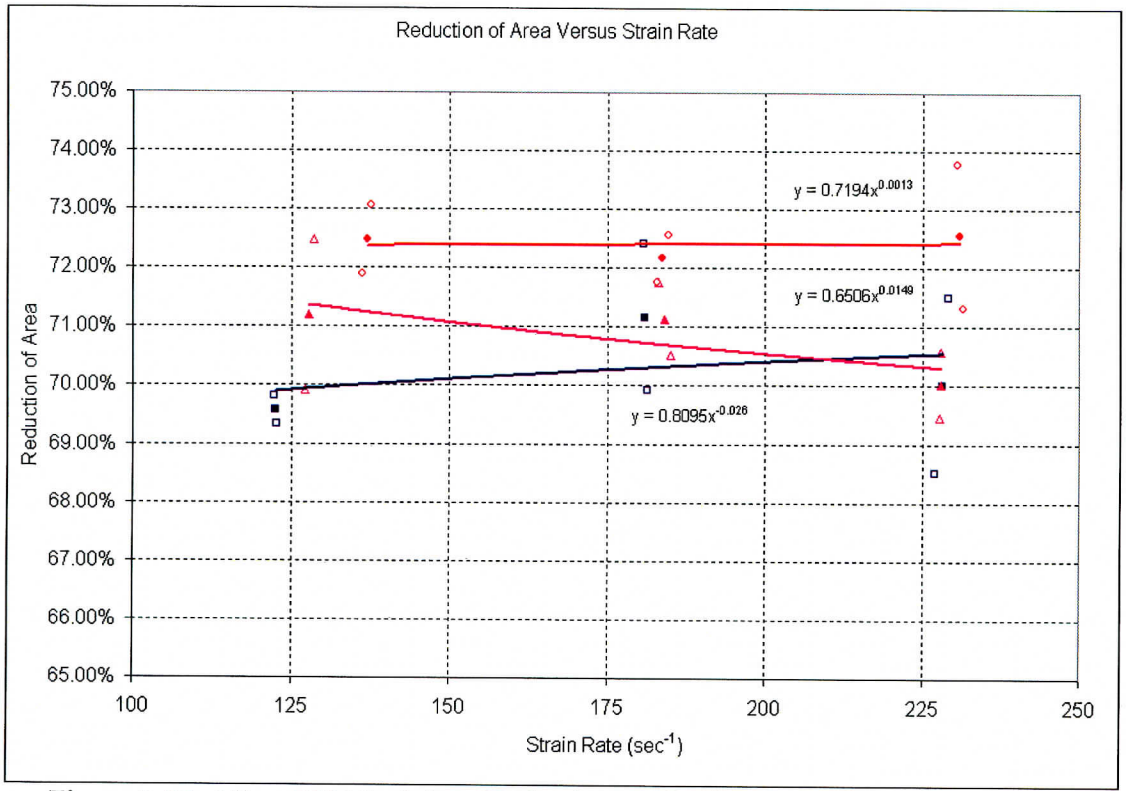

Figure 5-39 Alloy C22 Final Area Reduction vs. Strain Rate and Temperature [70]

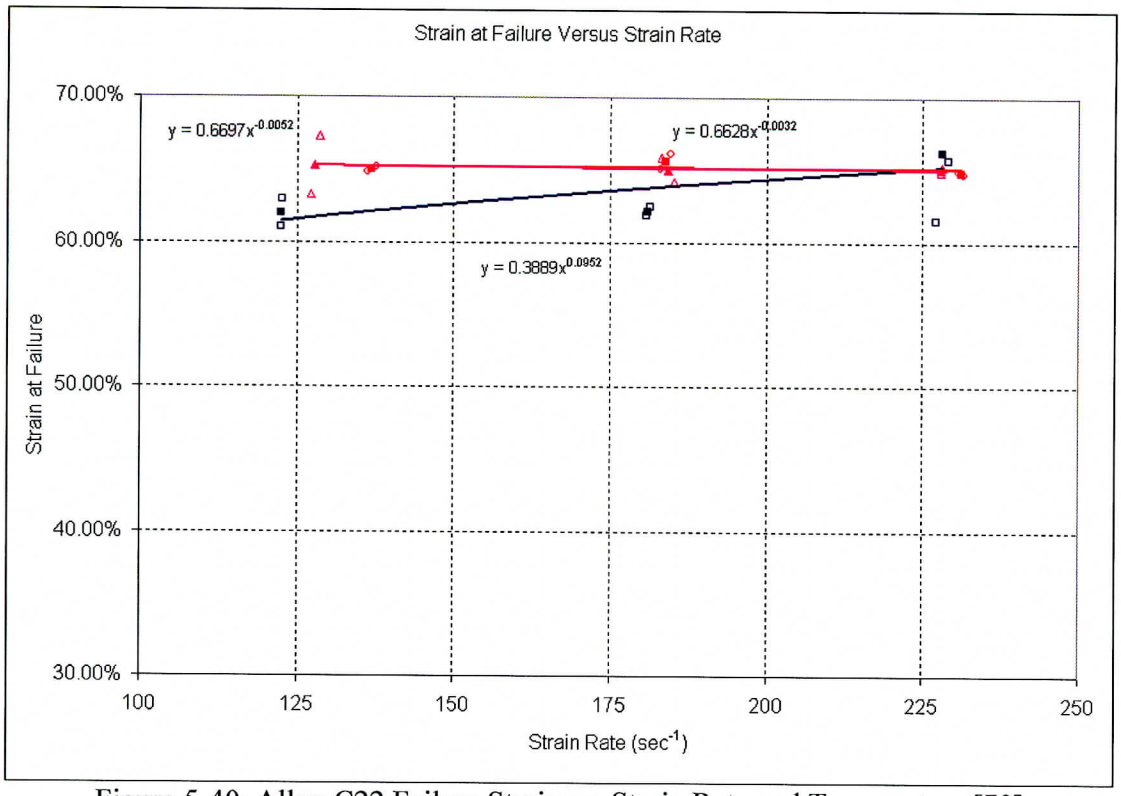

Figure 5-40 Alloy C22 Failure Strain vs. Strain Rate and Temperature [70]

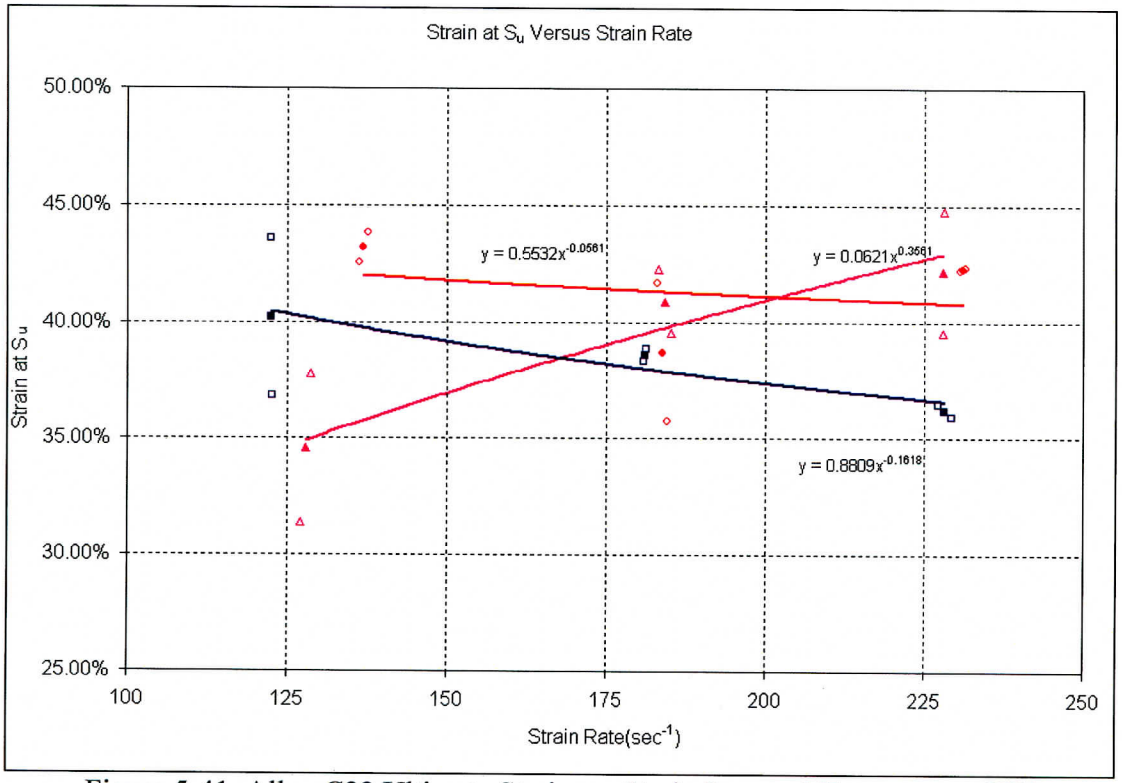

Figure 5-41 Alloy C22 Ultimate Strain vs. Strain Rate and Temperature [70]

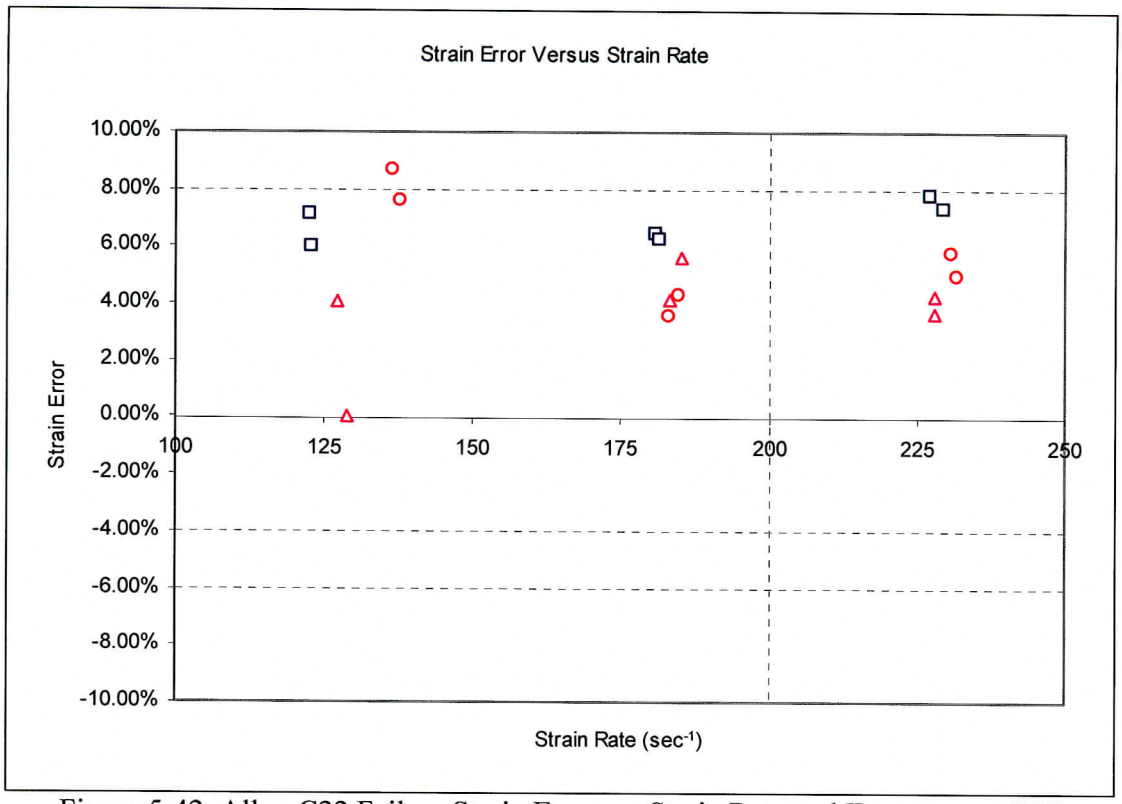

Figure 5-42 Alloy C22 Failure Strain Error vs. Strain Rate and Temperature [70]

CHAPTER 6

DISCUSSION OF RESULTS

6.1 General Observations for the Slow Strain Rate (MTS) Test Results

Materials were tested at strain rates in the range from 10^{-4} to 6 sec^{-1} during the initial stage of testing. These tests were conducted to finalize the procedure for material testing using the MTS test machine, define minimum and maximum strain rates obtainable for this testing procedure, and evaluate the accuracy of the results. During the initial stage of testing, a number of observations were made:

1. It was noticed that the average strain rates of the tests were proportional to the velocities of the actuator up to the strain rate of about 1 sec^{-1} for all of the materials tested. Further, at $\dot{\varepsilon} > 1$ sec^{-1}, the ratio of strain rate to velocity of the actuator began changing. It was also noticed that as the strain rate of testing increased, the smallest possible increment of data collection, 0.002 seconds, resulted in collecting only a few points. This provided an inadequate representation of the load-deflection response of the tested material and it was not possible to determine mechanical properties. The changing ratio between average strain rate and velocity of the actuator meant that the resistance of the material and slack in the test machine did not allow the actuator to reach specified velocity instantly, causing the strain rate to change significantly throughout the entire test. Based on the above-described observations, it was decided to limit the maximum strain rate of tensile testing to approximately 1 sec^{-1}.
2. The portion of the curve that represented plastic response of the material exhibited noise in the load signal (see Figure 4-1). This low magnitude noise differed slightly depending on the material and the strain rate of testing. Comparison of the consecutive local maximum and minimum of the load readings showed that the difference between those points was insignificant, reaching a few fractions of one percent. Also, comparing ultimate strengths of the material, as specified by the material suppliers, showed very close values with the ones computed using the maximum load readings of the MTS data acquisition software. Based on this finding, the processes of filtering the noise or curve fitting the data in the plastic range of material behavior became unnecessary.
3. The slope of the linear section of the engineering stress-strain curve that corresponds to the elastic behavior of the material was a few orders of magnitude less than the known values of modulus of elasticity. Existing slack in the drive mechanism of the MTS tensile machine as well as preloading of the machine and fixture components was responsible for a low slope value of the linear section of the curve that corresponded to the elastic region of material behavior. The final strain computed using the data collected by the LVDT of the MTS tensile machine was different from the actual final elongation found by measuring the specimen. The difference between the values of final elongation of the specimen and the values acquired by the data acquisition software varied with material and strain rate. The elastic region curve exhibited significantly lower slope than the actual modulus of elasticity.

A data handling procedure was designed to acquire accurate values of the mechanical properties of the tested materials taking into account these observations.

6.2 General Observations for the Moderate Strain Rate (Instron) Test Results

The objectives of the first round of experiments were to evaluate the procedure for moderate strain rate testing using the Instron Dynatup, identify the most suitable test fixture setup for the experiment, and to evaluate the accuracy of the results. During the initial stage of testing a number of observations were made:

1. It was noticed that load readings recorded by the data acquisition software of the Instron Dynatup impact machine showed two different types of noise.
   a. Single-peak wave that occurs at low stress values, usually took place before the portion of the curve representing elastic region.
   b. Wave-type noise that took place at higher values of stress and ran throughout the entire plastic range. The magnitude of this noise was dependent on the strain rate and material tested.

   Noise exhibited an increase in magnitude as the strain rate increased and had higher magnitudes for softer materials of lower strength and rigidity.

   Although wave propagation analysis is beyond the scope of this work, a simplified study shows that the noise in the signal may be attributed to the elastic wave propagation through components of the test machine and the fixture, Appendix B.
2. Similar to the MTS tensile test results, the slope of the linear portion of the curve representing the elastic region of material behavior appeared to be a few orders of magnitude lower than the known values of Young's Modulus for the tested material. This observation can be explained by the fact the data acquisition system measures some displacement in the fixture during the preloading stage of the test.
3. The total elongation, acquired by the data acquisition software, was also greater than the actual values based on measurements of the broken specimen. Similar to the MTS test results, unrealistic representation of the elastic region of material behavior affected the calculation of the total elongation.

6.3 Initial Room Temperature Mechanical Property Results

Results for the Stainless Steel 316L and Titanium Alloy Grade7 were presented along with mechanical properties of materials from the same material groups. Mechanical properties of Stainless Steel 304 [9] were plotted along side with the investigated Austenitic Stainless Steel 316L. Similarly; mechanical properties of Titanium Alloy 6Al-4V [9] were added to the charts with test results obtained by testing Titanium Alloy Grade 7. Although the two metals used in comparison have different chemical composition, heat treatment, and were manufactured from a different stock, the change of properties followed a similar pattern. This similarity serves as an additional way to verify the experimental procedure and results of this study.

Measurement inaccuracies within the elastic phase of the material behaviors did not allow the use of the standard methods for yield strength determination. In most cases, test results obtained at the same strain rates were generally consistent. Inconsistency in the results for the data obtained from MTS test machine could be due to the following factors:

1. Noise level in the signal at lower strain rates of testing had greater affect on the final results.
2. Proposed procedure for calculating yield strength showed some dependency on the noise level in the signal causing slight deviation in the results obtained from identical test setups.

Inconsistency in the results for the data obtained from Instron test machine could be due to the following factors:

1. Similar to the data obtained from MTS test machine, inaccurate representation of the elastic region of material had some contribution to the scatter pattern of the data.
2. Design of the Instron Dynatup drop weight impact test machine made it difficult to conduct identical tests, since lifting of the tup was controlled manually. Adding a software feature that would allow specifying desirable position of the tup in the test setup settings can eliminate this disadvantage.

6.4 Elevated Temperature Mechanical Property Results

After evaluating numerous tests, a data analysis procedure was developed which converts the raw data obtained from the data acquisition system to material characteristics (engineering stress-engineering strain curve) of the specimen material. Tests were done at several different strain rates at ambient, 175 °F and 350 °F temperatures for the three candidate materials. The following observations are made with the results obtained.

1. Titanium, for all the three temperatures, namely room, 175 °F and 350 °F, had an increase in the yield and ultimate strength values with strain rate. The strain at failure values also increased with strain rate, but not significantly. There was a significant decrease in yield and ultimate strength values with temperature for all the strain rates at 175 °F and 350 °F. The strain at failure increased with temperature for all the strain rates, but a significant increase was observed from 175 °F to 350 °F. In other words, the yield and ultimate strength of titanium is sensitive at 175 °F and 350 °F. The strain at failure is more sensitive at 350 °F than at 175 °F.
2. Stainless Steel, for all the three temperatures, had an increase in the yield and ultimate strength values with strain rate. The strain at failure values also increased with strain rate, but not significantly. There was a significant decrease in yield and ultimate strength values with temperature for all the strain rates especially from 175 °F to 350 °F. The strain at failure decreased with temperature for all the strain rates, but a significant decrease was observed from 175 °F to 350 °F. In other words, the yield strength of steel is more sensitive at 350 °F than at 175 F, but the ultimate strength is sensitive at 175 °F and 350 °F. The strain at failure is sensitive at 350 °F.
3. Alloy 22, for all the three temperatures had an increase in the yield and ultimate strength values with strain rate. The strain at failure values also increased with strain rate, but not significantly. There was a significant decrease in yield and ultimate strength values with temperature for all the strain rates especially from 175 °F to 350 °F. The strain at failure increased with temperature for all the strain rates, but a significant increase was observed at 175 °F. The values practically didn't change between 175 °F and 350 °F. In other words, the yield and ultimate strength of alloy 22 are more sensitive at 350 °F than at 175 °F, but the total strain is sensitive at 175 °F.

CHAPTER 7

CONCLUSIONS AND RECOMMENDATIONS

7.1 Conclusions

Results obtained in this work generally agree with the findings done by other researchers using materials with close composition on different experimental setups as described in Chapter 1. For example, several researchers studied behavior of several stainless steel alloys under varying strain rates, [15] and [9]. These results show that stainless steel 316L experienced an increase in yield and ultimate strengths with the increase of strain rate. Similarly, total elongation slightly decreased with increase of the strain rate. Literature review, [9], [13] and [16], showed that titanium alloy grade 7 experienced increase in yield and ultimate strengths. This current study confirms the conclusions of [9] and [13] by documenting a loss of ductility of titanium alloy grade 7 at higher strain rates. Obtaining comparable results for stainless steel and titanium alloy imply that the mechanical properties for alloy C22 are reliable. The literature search failed to yield any data obtained in previous studies regarding the behavior of a similar material. According to the results obtained in this work, nickel-based alloy C22 exhibited greater increase in yield strength than in ultimate strength with the increase in strain rate. It also showed decrease in the final elongation. Lack of the data corresponding to the same materials studied in this work made it impossible to have a comparison of mechanical properties obtained in this work with the results from other sources.

To summarize, the yield and ultimate strength of the three materials decrease with temperature. The possible explanation for this behavior is as temperature increases, the material becomes softer and thus loses its strength. Results also show that strain at failure increases with temperature for Titanium and Alloy 22 samples, but decreases with temperature for stainless steel 316L samples. This pattern is analogous to that of static tensile testing of similar materials shown in [2] and other related literature.

7.2 Recommendations

1. Additional experiments with the same materials should be conducted at slow strain rates on the MTS machine. The samples should have longer gage lengths (>1 inch) so that an extensometer can be used to measure strain directly.
2. Additional experiments with the same materials should be conducted at moderate strain rates on the Instron/Dynatup machine. An additional displacement sensor should be added to the system to measure the sample elongation directly. This should provide a more accurate measurement of strain during these experiments.
3. Wave 'shape pulsating' has been used successfully to minimize the noise in dynamic tests conducted on a split-Hopkinson bar apparatus. A similar method should be examined for the Instron Dynatup tensile fixture presented here. A possible pulse shaping mechanism may be the placement of a rigid foam, honeycomb, or elastomeric material between the striker and receiver.
4. A finite element analysis (FEA) of the dynamic experiments should be conducted to help understand the source of the noise in the load signal. It may be possible to incorporate a pulse-shaping device into the fixture to minimize the noise. Preliminary design of this device could be done using FEA.

5. Additional data acquisition channels should be added during the experiments to provide a more accurate measurement of strain, displacement, and force.
6. It is important to conduct additional series of testing using other materials. The fixture may work well for materials that are more brittle or have lower strength values.
7. The data generated in these experiments should be used to analyze a scale model of a container being impacted. Good correlation of analysis and experimental data would validate the accuracy of the data.

APPENDIX A: DEFINITIONS

1. Engineering Strain: Engineering Strain is defined as the ratio of the difference between original gage length and deformed gage length to the original gage length.

$$\varepsilon = \frac{l - l_0}{l} \cdot 100\%$$

2. Engineering Stress: Engineering Stress is defined, as the ratio of the load to the original cross sectional area it is applied to.

$$S = \frac{P}{A_0}$$

3. Average Strain Rate: Average strain rate is defined as the average value of the strain rate calculated for the entire duration of the test

$$\dot{\varepsilon}_a = \frac{\sum_{i=1}^{N} \dot{\varepsilon}_i}{N}$$

4. Velocity of the elastic wave propagation: Velocity of the elastic wave propagation is equal to square root of the Young's Modulus of the material to its density ratio.

$$c_o = (E/\rho)^{\frac{1}{2}}$$

5. True Stress [46]: The true stress is defined as the axial load in the specimen divided by the actual cross-sectional area. The cross-sectional area decreases as the material undergoes loading. Assuming a homogeneous strain distribution in the gage section up until the onset of necking, the true stress can be approximated as:

$$\sigma_T = \frac{P}{A_0}(1+\varepsilon)$$

The onset of necking generally occurs at the point of maximum load so this equation should not be used after maximum load. After the maximum load, the true stress should be determined from actual measurements of the load and cross-sectional area of the specimen.

6. True Strain [46]: The true strain is defined as the change in length of the gage section divided by the current length of the gage section. The true strain can be expressed as:

$$\varepsilon_T = \int_{L_o}^{L} \frac{dl}{l} = \ln\left(\frac{L}{L_o}\right) = \ln(1+\varepsilon).$$

This equation is also only good up until maximum load where necking occurs. Once necking occurs, the assumption of homogeneous strain in the gage section is no longer valid. After the maximum load, the true strain should be determined from actual measurements of the load and cross-sectional area of the specimen. Therefore, after maximum load, the true strain is defined as:

$$\varepsilon_T = \ln\left(\frac{A_o}{A}\right) = 2\ln\left(\frac{D_o}{D}\right).$$

APPENDIX B: WAVE PROPAGATION ANALYSIS

Elastic wave propagation through components of the fixture and elements of the test machine was analyzed comparing time periods of the wave-type noise in the signal with periods of elastic wave travel through the load gage.

Comparison of the signal peaks (shown in Figures B-1 and B-2) of the wave-type noise showed that the period of isolations was independent on the strain rate and had very slight dependency on the material tested. Table B-1 below presents time periods of isolations for three candidate materials tested.

Table B-1: Isolation Periods [37] (non-Q, for information only)

Stainless Steel 316L	Titanium Alloy Grade 7	Alloy C22
$1.53\ 10^{-4}$ sec	$1.70\ 10^{-4}$ sec	$1.63\ 10^{-4}$ sec

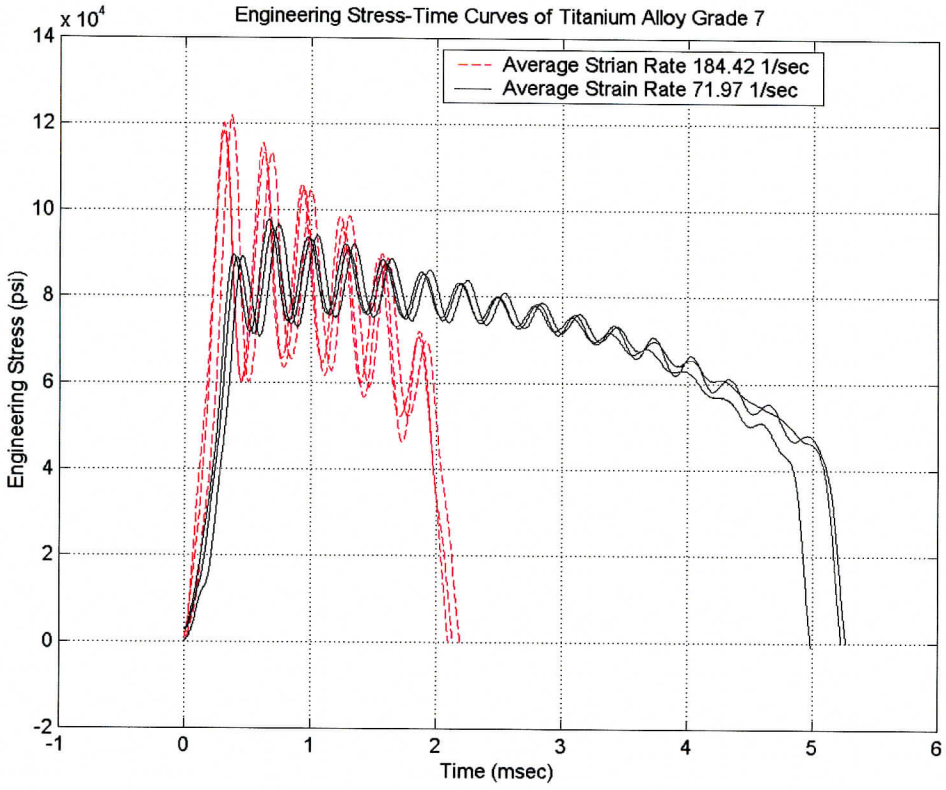

Figure B-1: Comparison of Dynamic Signals for Different Strain Rates [37] (non-Q, for information only)

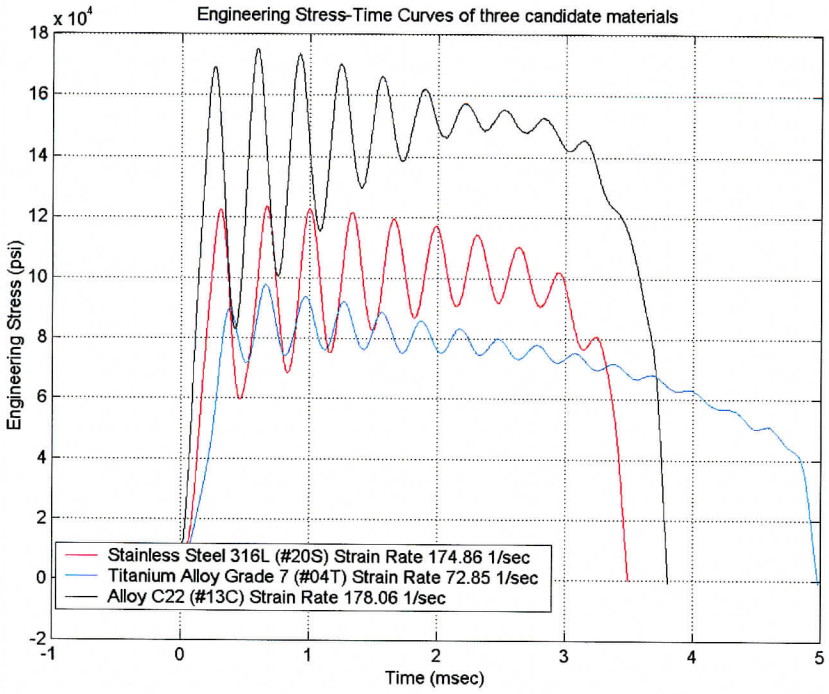

Figure B-2: Comparison of Dynamic Signals for Three Materials [37] (non-Q, for information only)

A number of metal plate tests conducted using a standard puncture test fixture also showed similar type of noise in the signal. These observations led to the conclusion that the source of the noise was an elastic wave propagating through the fixture and components of the test machine.

Since all of the components of the fixture and Instron/Dynatup test machine were made of steel, velocity of the elastic wave propagation was determined using its definition offered in Appendix A with Young's modulus and density of the construction steel. Position of the load cell gage and distances of wave travel through the elements of the machine were calculated. Using these known parameters, the time periods of the wave passing through the gage of the load cell were approximated. These values are presented in Table B-2.

Table B-2: Wave Travel Times [37] (non-Q, for information only)

Time travel through the mass block	Time travel through the fixture
$1.047\ 10^{-4}$ sec	$1.102\ 10^{-4}$ sec

As it is shown in the pictures below the major component of the wave originated at the surface of striker-transmitter contact propagated through the specimen to the holder through the insert and then reached the rigid base by passing through the columns. Having reached the base the wave reflected back passing through columns, holder, insert, specimen, transmitter, and striker, and then reached the load cell. A wave that reached load cell at the gage would cause a distortion in the signal reducing the measured values of the load. Having passed through the load cell the wave would continue moving through the massive tup until it reflected from the upper

wall of the mass blocks. A wave passing through the load cell on return would affect the measurements so that values of the load would be greater than actual.

Table B-3: Experimental Set-Up Dimensions [37] (non-Q, for information only)

Dimension	Value
A	10.400 in
B	5.500 in
C	1.980 in
D	2.40 in
E	1.065 in

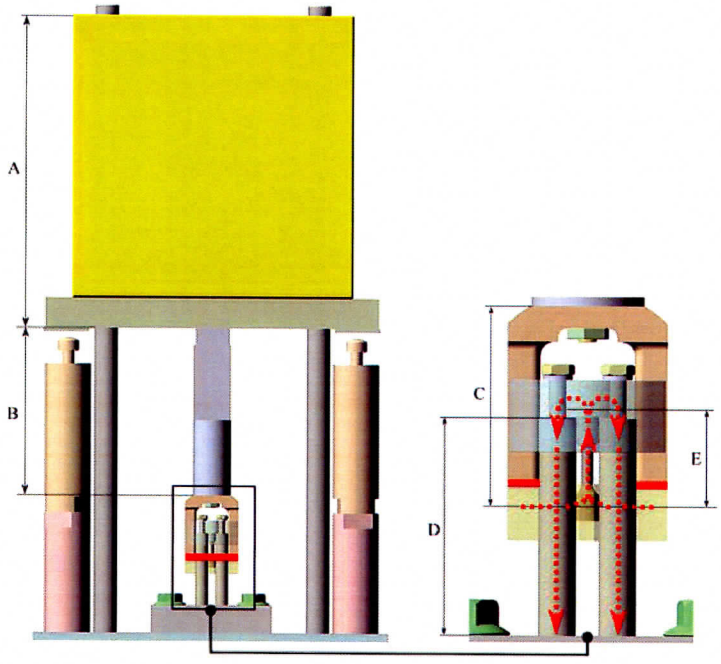

Figure B-3: Wave Travel Path Through Specimen and Fixtures [37]
(non-Q, for information only)

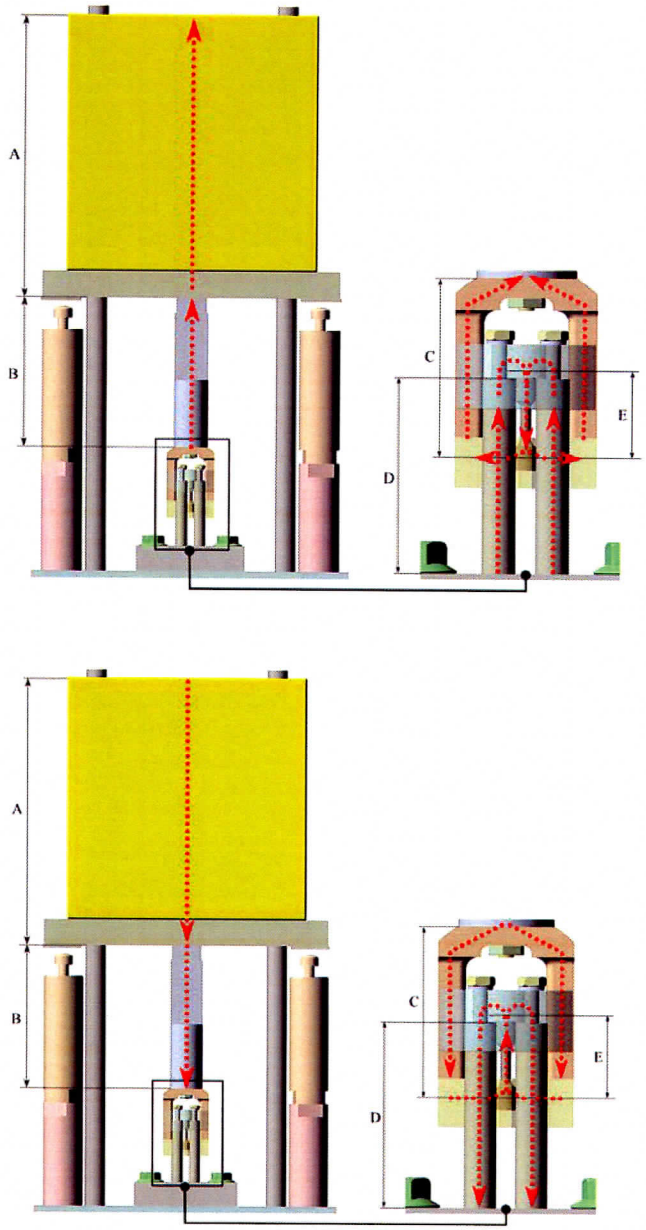

Figure B-4: Wave Travel Path Through Entire Test Apparatus [37]
(non-Q, for information only)

Taking into account the magnitude of the elastic wave propagation velocity, the slight difference between the values of the simplified model of wave propagation and the cycle periods of the waves that could be observed on stress-time curves could be justified by the fact that there was always a partial reflection of the waves at every part connection and/or change of components' cross section that would affect the time periods of isolations in the signal.

APPENDIX C: MATLAB FILE

This is the MATLAB file used to generate the curve fitting equations during the data reduction process [40].

```
% This file outputs three plots:
% 1 Engineering Stress-Strain Curve portion;
% 2 First Derivative of the Stress-Strain Curve Portion;
% 3 Second Derivative of the Stress-Strain Curve Portion;

% read stress-strain data from excel file

A=xlsread('YXXX.xls');%---------'YXXX.xls' excel file containing Stress-
Strain Curve portion data
n=X;%-------------------INPUT NUMBER OF ROWS HERE---------------[ ! ]

B=A(1:n,:);
p = polyfit(B(:,1),B(:,2),6);
f=polyval(p,B(:,1));
figure
plot(B(:,1),B(:,2),'r--');
hold on;
plot(B(:,1),f);
title('Engineering Stress-Strain Curve #XXX (Portion)');
xlabel('Engineering Strain (in/in)')
ylabel('Engineering Stress (psi)')
grid on;
sp=[p(1)*6,p(2)*5,p(3)*4,p(4)*3,p(5)*2,p(6)];
sf=polyval(sp,B(:,1));
figure
plot(B(:,1),sf)
grid on;
title('First Derivative of The Stress-Strain Curve Portion #XXX');
xlabel('Engineering Strain (in/in)');
ylabel('First Derivative Value');
s=polyfit(B(:,1),sf,6);
sk=polyval(s,B(:,1));
st=[s(1)*6,s(2)*5,s(3)*4,s(4)*3,s(5)*2,s(6)];
sn=polyval(st,B(:,1));
figure
plot(B(:,1),sn);
grid on
xlabel('Engineering Strain (in/in)');
ylabel('Second Derivative Value');
title('Second Derivative of the Stress-Strain Portion #XXX');
```

REFERENCES

1. Reference Design Description for a Geologic Repository, Rev 03 ICN, http://www.ymp.gov/documents/seda06m3_c/index.htm

2. American Society for Metals Handbook, Mechanical Testing and Evaluation, Vol. 8, ASM International, Ohio, 2000.

3. Harding, J., Wood, E. O., and Campbell, J. D., "Tensile Testing of Materials at Impact Rates of Strain", Journal of Mechanical Engineering Science, London, No. 2, pp. 88-96, 1960.

4. Sundararajan, S., Aekbote, K., Chou, C. C., Lim, G. G., Chickola, J., Walker, L. A., "High-Strain-Rate Tensile Testing of Door Trim Materials", Automotive Engineering, Vol. 105, No. 7, pp. 77, Jul. 2001.

5. Johnson, N. L. and Browne, A. L., "Conducting Dynamic Impact Tests Using a 'Free-Flight' drop tower facility Part II Practical Aspects", in 2001 ASME International Mechanical Engineering Congress and Exposition, New York, Nov. 2001.

6. Browne, A. L. and Johnson, N. L., "Conducting Dynamic Impact Tests Using a 'Free-Flight' drop tower facility Part I Drop Tower Facility", in 2001 ASME International Mechanical Engineering Congress and Exposition, New York, Nov. 2001.

7. Mouritz, A. P., "Failure Mechanics of Mild Steel Bolts Under Different Tensile Loading Rates", International Journal of Impact Engineering. Oxford, Vol. 15, No. 3, pp 311-324, 1983.

8. Hauser, F. E, Techniques for Measuring Stress-Strain Relations at High Strain Rates, Experimental Mechanics, Brookfield Center, No. 6, pp. 395-402, 1966.

9. Nicholas, T., "Dynamic Tensile Testing of Structural Materials using a Split Hopkinson Bar Apparatus", Technical Report AFWAL-TR-80-4053, Material Laboratory Air Force Wright Aeronautical Laboratories, Ohio, Oct. 1980.

10. Zukas, J. A., High Velocity Impact Dynamics, Computational Mechanical Associates, Towson, Maryland. 1992.

11. Al-Mousawi, M. M., Reid, S. R., and Deans, W. F. "The use of split Hopkinson Pressure Bar Technique in High Strain Rate Material Testing", in Proceedings in the Institution of Mechanics, Vol. 211, No. 4, pp 273-292, 1997.

12. Noble, J. P., Goldthorpe, B. D., Church, P., and Harding, J., "The Use of the Hopkinson Bar to Validate Constitutive Relations at High Rates of Strain", Journal of the mechanics and physics of solids, London, Vol. 47, No. 5, pp 1187-1206, 1999.

13. Steidel, R. F. and Makerov, C. E., "The Tensile Properties of Some Engineering Materials at Moderate Rates of Strain", ASTM bulletin, Philadelphia, No. 247, pp. 57-64, 1960.

14. El-Magd, E., "Simulation of the Material Behavior Under Impact Loading", Computational material science, Amsterdam, Vol. 1, No. 3, pp. 333-342, Jul. 1993.

15. Albertini, C. and Montagnani, M., Testing Techniques Based on the Split Hopkinson Bar, in Mechanical Properties at High Rates of Strain, The Institute of Physics, London, 1974.

16. Takeda, Kobayashi, "High Velocity Tensile Properties of Ti-15V-3Cr-3Al-3Sn Alloys", in Shock wave and high-strain-rate phenomena in materials, New York, pp. 99-101, 1992.

17. Lankford, J., "Temperature-strain rate dependence of compression strength and damage mechanisms in aluminum oxide", Journal of material science, v 16, pp.1567-1578, 1981.

18. Chiddister, J.L and Malvern, L.E., "Compression impact testing of aluminum at elevated temperatures", Experimental Mechanics, v 3, n 4, p81-90,1963.

19. Eleiche, A.M., Albertini, C., and Montagnani, M., "Response of AISI type 316L stainless steel to interrupted quasi-static to impact tension at elevated temperatures", Journal De Physique, v C5, pp. 495-498, 1985.

20. Gillat, A. and Wu, X. "Elevated temperature testing with the torsional split hopkinson bars", Experimental mechanics, v 34, pp.166-170, 1994.

21. Elwood, J. J. and Hillery, M.T., "High speed tensile testing at elevated temperatures - Machine design", Proceedings Of The International Matador Conference, Conf 31, Manchester, p383-388, April 1995.

22. Manjoine, M.J., "Influence of Rate of Strain and Temperature on Yield Stresses of Mild Steel", Journal of Applied Mechanics, v 11(A), pp.211-218, December 1944.

23. Manson, S. S. and Muralidharan, U.; Halford,G. R., "Tensile and Compressive Constitutive Response of 316 Stainless Steel at Elevated Temperatures", NASA Technical Memorandum, Lewis Research Cent, Cleveland, Ohio, USA, 1982.

24. Desisto, T.S. and Driscoll, D.E., "Effect of Strain Rate and Temperature on the true-stress true-strain properties of commercially pure Titanium", High Speed Testing, v 1, pp. 97, 1960.

25. Yuanxin Zhou and Yuanming Xia, "Tensile mechanical behavior of TiAl(FL) at high strain rate", Journal of materials science, v 35, n 4, pp. 925-929, February 2000.

26. Ward, C.H., Thompson, A.W., and Williams, J.C., "Elevated temperature tensile behavior of Ti-25Al-10Nb-3V-1Mo", Metallurgical and Materials Transactions A: Physical

Metallurgy and Materials Science, Sponsor: Wright Lab, Wright-Patterson AFB, OH, USA, v 26A, n 3, pp. 703-720.

27. Technical Data, Stainless Steels, Chromium-Nickel-Molybdenum: Types 316 (S31600), 316L (S31603), 317 (S31700), 317L (S31703), Allegheny Ludlum, http://www.alleghenyludlum/Ludlum/Documents/316_317.pdf

28. Technical Data, Corrosion-Resistant Titanium Alloys, Allegheny Ludlum, http://www.alleghenyludlum/Ludlum/Documents/titanium.pdf

29. Technical Data, Nickel-Base Alloy, AL 22, Allegheny Ludlum, http://www.alleghenyludlum/Ludlum/Documents/al22.pdf

30. "Standard Test Methods for Tension Testing of Metallic Materials", Annual Book of ASTM Standards, Vo. 03-01, E8-98, pp. 57-77, 1998.

31. Johnson, K. L., Contact Mechanics, Cambridge, pp. 341-344, 1985.

32. O'Toole, B. J., "Tensile Testing With the MTS Axial/Torsional Material Test System", IPLV-033, 2001. http://hrcweb.lv-hrc.nevada.edu/qa/ip.htm

33. "Instron Dynatup 8250 Drop Weight Impact Tester Operating Instructions", Instron Corporation, Revision A, 1999.

34. "Instron Dynatup EC Environmental Conditioning System User's Guide", Instron Corporation, Revision C, 1998.

35. ASM Handbook, Vol. 19, Fatigue and Fracture, The Materials Information Society., p 969, 1990.

36. Juvinall, C. R. and Marshek, K. M., Fundamentals of Machine Component Design, John Wiley & Sons, Inc., 2000

37. Zabotkin, K., Identification Of Dynamic Properties Of Materials For The Nuclear Waste Package At Room Temperature, University of Nevada Las Vegas Masters Thesis, 2002.

38. Dusi S., Identification Of Dynamic Properties Of Materials For The Nuclear Fuel Package At Elevated Temperatures, University of Nevada Las Vegas Masters Thesis, 2003.

39. Trabia, M., "Impact Testing of Tensile Specimens Using Dynatup 8250 with Model 930-I Operating Software", IPLV-031 2002. http://hrcweb.lv-hrc.nevada.edu/qa/iplv.htm

40. Dusi, S., "Determination of Mechanical Properties of Materials Under Dynamic Loading", IPLV-040, 2003.

http://hrcweb.lv-hrc.nevada.edu/qa/iplv.htm

41. Dusi, S., "Impact Testing of Tensile Specimens in the Environmental Chamber of Dynatup 8250 with Model 930-I Operating Software", IPLV-058, 2003. http://hrcweb.lv-hrc.nevada.edu/qa/iplv.htm

42. O'Toole, B. J., "Elevated Temperature Tensile Testing with the MTS Axial/Torsional Material Test System", IPLV-061, 2003. http://hrcweb.lv-hrc.nevada.edu/qa/iplv.htm

43. Penn Stainless Products, Inc., "Certificate of Test", Order 0432881/001, SON 51853, BOL 0116709, TAG 1429101, September 26, 2002.

44. Laboratory Testing Inc., "Certified Test Report ASP003-99-03-05649", March 26, 1999.

45. Laboratory Testing Inc., "Certified Test Report 20021115056", November 14, 2002.

46. Atlas of Stress-Strain Curves, 2nd Edition, ASM International,Materials Park, OH, page 5, 2002.

47. UCCSN Data ID No. 024MT.001, "Batch #1 MTS Test Results for Titanium Grade 7 under low strain rate tensile testing", Sample No 07T.DAT. http://hrcweb.nevada.edu/data/tda/

48. UCCSN Data ID No. 024MT.001, "Batch #1 MTS Test Results for Titanium Grade 7 under low strain rate tensile testing", Sample No 08T.DAT. http://hrcweb.nevada.edu/data/tda/

49. UCCSN Data ID No. 024MT.005, "Batch #5 Instron Dynatup Tensile Test Results for Titanium Grade 7 Under Impact Loading", file 04t.exp. http://hrcweb.nevada.edu/data/tda/

50. UCCSN Data ID No. 024MT.006, "MTS TEST RESULTS FOR STEEL 316L UNDER LOW STRAIN RATE TENSILE TESTING (BATCH #1)", files 'steel 01S.DAT', 'steel 02S.DAT', 'steel 03S.DAT'. http://hrcweb.nevada.edu/data/tda/

51. UCCSN Data ID No. 024MT.010, "MTS TEST RESULTS FOR STEEL 316L UNDER HIGH STRAIN RATE LOADING (BATCH #2)", files 'sample 04s.DAT', 'sample 05s.DAT', 'sample 06s.DAT'. http://hrcweb.nevada.edu/data/tda/

52. UCCSN Data ID No. 024MT.008, "MTS TEST RESULTS FOR STEEL 316L UNDER HIGH STRAIN RATE LOADING (BATCH #3)", files 'sample 07S.DAT', 'sample 08S.DAT', 'sample 09S.DAT'. http://hrcweb.nevada.edu/data/tda/

53. UCCSN Data ID No. 024MT.014, "INSTRON TENSILE TEST RESULTS FOR STAINLESS STEEL 316L UNDER MODERATE STRAIN RATE, SPECIMEN 10S". http://hrcweb.nevada.edu/data/tda/

54. UCCSN Data ID No. 024MT.015, "INSTRON TENSILE TEST RESULTS FOR STAINLESS STEEL 316L UNDER MODERATE STRAIN RATE, SPECIMEN 12S". http://hrcweb.nevada.edu/data/tda/

55. UCCSN Data ID No. 024MT.016, "INSTRON TENSILE TEST RESULTS FOR STAINLESS STEEL 316L UNDER MODERATE STRAIN RATE, SPECIMEN 15S". http://hrcweb.nevada.edu/data/tda/

56. UCCSN Data ID No. 024MT.017, "INSTRON TENSILE TEST RESULTS FOR STAINLESS STEEL 316L UNDER MODERATE STRAIN RATE, SPECIMEN 20S". http://hrcweb.nevada.edu/data/tda/

57. UCCSN Data ID No. 024SD.003, "Instron Dynatup tensile test results for stainless steel 316L specimens under impact loading in the machine environmental chamber under room and elevated temperatures (175 ^{O}F and 350 ^{O}F)", Each data point on the graph is taken from a separate ##SEnQA.exp file in this TDA. http://hrcweb.nevada.edu/data/tda/

58. UCCSN Data ID No. 024MT.001, "Batch #1 MTS Test Results for Titanium Grade 7 under low strain rate tensile testing", files 'Sample No 07T.DAT', 'Sample No 08T.DAT', 'Sample No 09T.DAT'. http://hrcweb.nevada.edu/data/tda/

59. UCCSN Data ID No. 024MT.002, "Batch #2 MTS Test Results for Titanium Grade 7 under low strain rate tensile testing", files 'Sample No 11T.DAT', 'Sample No 12T.DAT', 'Sample No 13T.DAT'. http://hrcweb.nevada.edu/data/tda/

60. UCCSN Data ID No. 024MT.003, "Batch #3 MTS Test Results for Titanium Grade 7 under low strain rate tensile testing", files 'Sample No 10T.DAT', 'Sample No 14T.DAT', 'Sample No 15T.DAT'. http://hrcweb.nevada.edu/data/tda/

61. UCCSN Data ID No. 024MT.004, "Batch #4 Instron Dynatup Test Results for Titanium Grade 7 under impact loading", files '01T.exp', '02T.exp', '03T.exp'. http://hrcweb.nevada.edu/data/tda/

62. UCCSN Data ID No. 024MT.005, "Batch #5 Instron Dynatup Test Results for Titanium Grade 7 under impact loading", files '04t.exp', '05t.exp', '06t.exp'. http://hrcweb.nevada.edu/data/tda/

63. UCCSN Data ID No. 024SD.001, "Instron Dynatup test results for titanium grade 7 under impact loading in the machine environmental chamber under room and elevated temperature", Each data point on the graph is taken from a separate ##TEnQA.exp file in this TDA.
http://hrcweb.nevada.edu/data/tda/

64. UCCSN Data ID No. 024MT.009, "MTS TENSILE TEST RESULTS OF ALLOY C22 UNDER LOW STRAIN RATE LOADING (BATCH #1)", files 'sample 01c.DAT', 'sample 02c.DAT', 'sample 03c.DAT'.
http://hrcweb.nevada.edu/data/tda/

65. UCCSN Data ID No. 024MT.007, "MTS TENSILE TEST RESULTS OF ALLOY C22 UNDER HIGH STRAIN RATE LOADING (BATCH #2)", files 'sample 04C.DAT', 'sample 05C.DAT', 'sample 06C.DAT'.
http://hrcweb.nevada.edu/data/tda/

66. UCCSN Data ID No. 024MT.011, "MTS TENSILE TEST RESULTS OF ALLOY C22 UNDER HIGH STRAIN RATE LOADING (BATCH #3)", files 'sample 07c.DAT', 'sample 08c.DAT', 'sample 09c.DAT'.
http://hrcweb.nevada.edu/data/tda/

67. UCCSN Data ID No. 024MT.012, "INSTRON TENSILE TEST RESULTS FOR ALLOY C22 UNDER MODERATE STRAIN RATE (BATCH #4)", files '10c.exp', '11c.exp', '12c.exp'.
http://hrcweb.nevada.edu/data/tda/

68. UCCSN Data ID No. 024MT.013, "INSTRON TENSILE TEST RESULTS FOR ALLOY C22 UNDER MODERATE STRAIN RATE (BATCH #5)", files '13c.exp', '14c.exp', '15c.exp'.
http://hrcweb.nevada.edu/data/tda/

69. UCCSN Data ID No. 024MT.018, "INSTRON TENSILE TEST RESULTS FOR ALLOY C22 UNDER MODERATE STRAIN RATE (BATCH #6)", files '16c.exp', '17c.exp', '18c.exp'.
http://hrcweb.nevada.edu/data/tda/

70. UCCSN Data ID No. 024SD.002, "Instron Dynatup tensile test results for alloy C22 specimens under impact loading in the machine environmental chamber under room and elevated temperatures (175 F and 350 F)", Each data point on the graph is taken from a separate ##QACEn.exp file in this TDA.
http://hrcweb.nevada.edu/data/tda/